# ELECTROCHEMICAL REDUCTION OF $CO_2$ TO METHANOL

A Thesis

Submitted to the Graduate Faculty of the
Louisiana State University and
Agricultural and Mechanical College
In partial fulfillment of the
Requirements for the degree of
Master of Science in Chemical Engineering

in

The Department of Chemical Engineering

by
Minh Tuyen H. Le
B.S., Louisiana State University, 2009
August 2011

## ACKNOWLEDGEMENTS

First of all, I would like to sincerely thank Dr. John C. Flake for being my advisor, for his full guidance, encouragement and inspiration, for supporting and sharing his endless knowledge and experience, and for making this study possible. I'm grateful to Dr. Maoming Ren for sharing all the insightful suggestions and help since the very first stage. I also wish to express my thanks to Dr. Gregory L. Griffin, and Dr. Richard L. Kurtz for serving on my examining committee.

Second, I would like to thank Dr. Gregory L. Griffin, Dr. Phillip T. Sprunger, Dr. Richard L. Kurtz, and Dr. Alvind Asthagiri for all the wonderful ideas, and guidance. Many thanks to Paul Rodriguez and Joe Bell who helped me with the single crystal reactor design. I greatly appreciate Dr. Eric Lamber from MIC, University of Florida who helped me perform the XPS experiment. I also would like to thank Frank Womack, Ziyu Zhang, and Fei Wang for helping with the working procedure and taking care of the ultra high vacuum chamber used for sample synthesis. My thanks to everyone in our research group; especially, I would like to thank Wanli Xu, Sri S. Vegunta, Punima Narayanan, Cheng-Chun Tsai, and Joel N. Bugayong for their help and friendship during the past two years. I gratefully acknowledge this study is financed by a grant from U.S. Department of Energy (DOE), Center for Atomic Level Catalyst Design.

Lastly, I specially thank my beloved family: my parents, my husband, my brother, and all my friends for their love, continuous support and encouragement.

## TABLE OF CONTENTS

## LIST OF TABLES

## LIST OF FIGURES

## ABSTRACT

An efficient method to convert $CO_2$ to fuels using renewable energy could displace crude oil without increasing $CO_2$ emission and provide high-density energy storage reservoirs similar to liquid fuels or batteries. Although photoelectrochemical conversion of $CO_2$ is possible, solar-to-fuel efficiencies are lower than the combination of conventional photovoltaics (up to 40% efficiency) and electrochemical cells (up to 80% Faradaic efficiency). In the electrochemical case, electrical energy from renewable sources may be converted to hydrocarbons or alcohols using electrocatalysts.

The direct reduction of $CO_2$ to $CH_3OH$ is known to occur at several types of electrocatalysts including oxidized Cu electrodes. In this thesis, we first examine the yield behavior of an electrodeposited cuprous oxide thin film and explore relationships between surface chemistry and reaction behavior relative to air-oxidized and anodized Cu electrodes. $CH_3OH$ yields and Faradaic efficiencies observed at cuprous oxide electrodes are remarkably higher than air-oxidized or anodized Cu electrodes suggesting Cu(I) species may play a critical role in selectivity to $CH_3OH$. Experimental results also show $CH_3OH$ yields are dynamic and the copper oxides are reduced to metallic Cu in a simultaneous process.

In order to improve $CH_3OH$ activity and electrode surface's stability, single crystal ZnO (10-10) is considered as a support since ZnO support are well known for methanol synthesis in an industrial hydrogenation reaction scale. Although experimental conditions pose challenging barriers to repeatability, Infrared Spectroscopy and yields suggest the oxide may provide stable surfaces with selectivity to $CH_3OH$. Yield behavior is discussed in comparison with photoelectrochemical and hydrogenation reactions where the improved stability of Cu(I) species may allow relatively constant $CH_3OH$ generation.

# CHAPTER 1. INTRODUCTION

## 1.1 Introduction

A rapidly growing population and industrialization has caused the world's natural resources difficulty in keeping up with demands. Today, fossil fuels such as coal, oil or natural gas (i.e., hydrocarbons) are burned in power plants to produce energy. Primarily 27 % of world energy comes from coal. From the International Energy Outlook 2010, with society's current level of energy consumption and high standards of living, world total energy consumption will increase by 49 % from 495 quadrillion Btu (2007) to 739 quadrillion Btu (2035) (Conti et al., 2010). Additionally, civilization and industrialization have brought not only technology, modern life, convenience to humanity but also pollution and emissions from factories, vehicles, and chemical plants, especially with an increase in atmospheric $CO_2$ concentration by 30 % from 300 ppm (1960) to 390 ppm (2009) (Tans, 2009). Carbon dioxide is one of the primary green house gases causing Earth's global warming effect. Finding solutions for energy and environmental crisis has become a challenge.

Methanol is a primary feedstock for many organic compounds, as well as a vital intermediate for various chemicals used in daily life products such as silicone, paint, and plastics. Being the perfect green chemical alternative with a volumetric energy density relatively similar to that of gasoline (methanol: 15.6 MJ/L; gasoline: 34.2 MJ/L), methanol is an ideal fuel for combustion, and transportation (Olah et al., 2006). Methanol is also currently used in Direct Methanol Fuel Cell, an electrochemical device that directly converts chemical energy of fuels into electrical energy. Most importantly, in its liquid form, methanol presents an excellent way to store energy conveniently and safely. Methanol is originally produced from synthetic gas (a mixture of carbon monoxide, carbon dioxide and hydrogen) in large scale industrial plants for

commercial purposes at millions of tons per year (Olah et al., 2006). Methanol can also be produced from methane conversion such as through selective oxidation of methane, catalytic gas phase oxidation of methane, liquid phase oxidation of methane, mono-halogenation of methane, and microbial or photochemical conversion of methane (Olah et al., 2006). Ultimately, methanol conversion from carbon dioxide reduction provides a highly attractive solution by recycling carbon dioxide from industrial exhaust into useful energy storage simultaneously with saving diminishing natural resources.

For over a century, electrochemical reduction of carbon dioxide has been studied due to its significant impact as a solution for both the energy and environmental issue. Using carbon dioxide as a feedstock is a way to maintain $CO_2$ levels in atmosphere. In this method, electricity generated from renewable energy sources such as solar, wind, hydro, nuclear, wave, tides, and geothermal serves as an external power supply for electron transport. With highly efficient electrocatalyst designs, carbon dioxide reduction reaction to valuable compounds and alternative fuels can displace the conventional fuels and ease the world's dependence on fossil fuels.

From the early 1900's to the 1980's, electrochemical carbon dioxide reduction studies focused on several types of metal electrodes such as amalgamated zinc, amalgamated copper, lead, mercury with formic acid as the main product (Coehn et al., 1904; Fischer et al., 1914; Teeter et al., 1954; Paik et al., 1969). In the mid of 1980's, Frese et al. investigated methanol formation from carbon dioxide at several metals and semiconductors such as ruthenium, molybdenum, GaAs, InP with promising results; however, current densities were lower than 1mA $cm^{-2}$ (Canfield et al., 1983; Frese et al., 1985; Summers et al., 1986). In 1985, Hori et al. discovered metallic copper can electrochemically reduce carbon dioxide to hydrocarbons (methane, ethylene, etc.) at high rates and efficiencies (Hori et al., 1985). This served as a basis

for a larger focus on copper electrodes as the rational catalyst in the hope of finding the ideal electrocatalysts for $CO_2$ reduction. Figure 1.1 is the Pourbaix diagram for carbon dioxide showing the equilibrium reduction potentials as a function of pH. Reduction reactions of carbon dioxide at metallic copper are listed below with standard potentials $E_o$.

$$2H^+ + 2e^- \rightleftharpoons H_2 \qquad E_o = 0.0 \text{ V vs. SHE} \qquad (1.1)$$

$$CO_2 + 12H^+ + 12e^- \rightleftharpoons C_2H_4 + H_2O \qquad E_o = 0.079 \text{ V vs. SHE} \qquad (1.2)$$

$$CO_2 + 8H^+ + 8e^- \rightleftharpoons CH_4 + H_2O \qquad E_o = 0.169 \text{ V vs. SHE} \qquad (1.3)$$

$$CO_2 + 2H^+ + 2e^- \rightleftharpoons CO + H_2O \qquad E_o = -0.103 \text{ V vs. SHE} \qquad (1.4)$$

$$CO_2 + H^+ + 2e^- \rightleftharpoons HCOO^- + H_2O \qquad E_o = -0.225 \text{ V vs. SHE} \qquad (1.5)$$

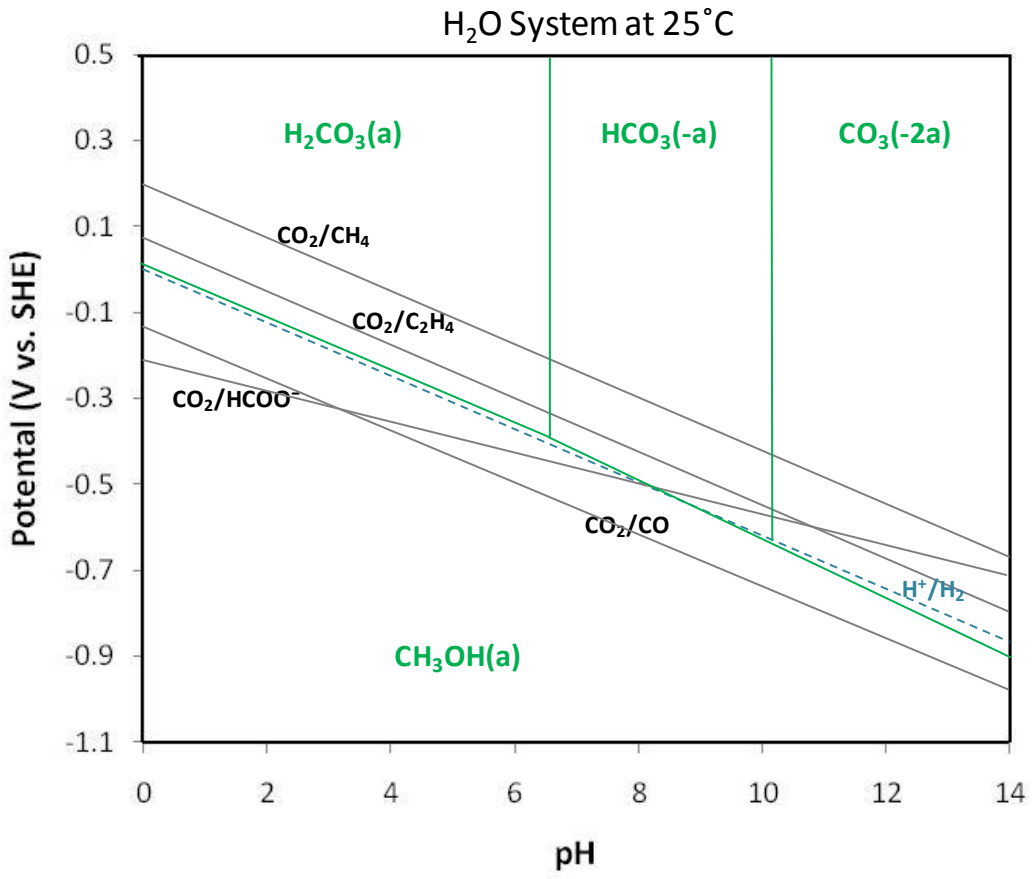


Figure 1.1. Pourbaix diagram for carbon dioxide reduction reaction at 25˚C

This study focuses on the electrochemical reduction of carbon dioxide to methanol and more specifically relating surface properties with yield and selectivity. The overall reaction of methanol formation (Equation 1.8) is a combination of the reduction reaction at the cathode (Equation 1.6) and the oxidation reaction at the anode (Equation 1.7).

Cathode: $CO_2 + 6H^+ + 6e^- \rightleftharpoons CH_3OH + H_2O$ $E_o = 0.02$ V vs. SHE (1.6)

Anode: $3H_2O \rightleftharpoons 1.5O_2 + 6H^+ + 6e^-$ $E_o = 1.23$ V vs. SHE (1.7)

Overall: $CO_2 + 2H_2O \rightleftharpoons CH_3OH + 1.5O_2$ $E_o = 1.21$ V vs. SHE (1.8)

Thermodynamically, it is possible to electrochemically reduce carbon dioxide to methanol; however, carbon dioxide's reduction potential is only 20 mV positive of water reduction, which results in hydrogen generation. Therefore, an ideal catalyst should have a high hydrogen overpotential which allows the reduction reaction of carbon dioxide to achieve high selectivity and rates well before water reduction occurs. Copper oxides, specifically Cu(I), and copper based zinc oxide (10-10) are chosen as working electrodes in this work. Results with oxidized copper show methanol yields are directly related with Cu(I) intensities; however, the reaction is dynamic and the electrodes loose activity during reaction indicating unstable electrodes. Copper and copper oxides supported on zinc oxide electrodes show relatively more stable results over longer reaction time as well as reusable catalyst's surface; however, reproducible methanol yields are difficult to establish. While surface structure and morphology are crucial in determining methanol yields, there are many challenge barriers such as the operating conditions of temperature, pressure, and local pH near the electrode surface (Hori, 2008).

**1.2 Overview**

The ultimate goal of this study is to gain a fundamental understanding of $CO_2$ reduction at the molecular level to create catalyst design with high selectivity and yields.

Chapter 2 introduces several carbon dioxide reduction pathways such as hydrogenation, photoelectrochemical reduction and electrochemical reduction. Catalytic hydrogenation reaction for methanol synthesis requires high temperature and pressure conditions, whereas photoelectrochemical and electrochemical reduction processes offer convenient ways to reduce carbon dioxide to hydrocarbons and oxygenates at mild conditions.

While carbon dioxide electrochemical reduction has been proven to primarily yield methane and ethylene at metallic copper, Chapter 3 focuses on the experimental details of electrochemical reduction of carbon dioxide to methanol at copper oxide electrodes. Chapter 3 also describes the relationship between surface chemistry and catalyst performance via characterization. Although copper oxides show promising results in methanol formation, the reactions are dynamic, and copper oxides are reduced to metallic copper in a simultaneous process. It is essential to construct a better catalyst design which allows a stable reaction with high catalytic activity and selectivity, as well as reproducible results.

Chapter 4 describes the experimental work for electrochemical reduction reaction of $CO_2$ at copper, copper oxide based zinc oxide electrodes. Infrared spectra and yields confirm $CO_2$ reduction activity toward methanol formation. In the future, fundamental theory and leveraging DFT will help explain the effects of surface chemistry on yields, selectivity, and stability at the molecular level to form a basis for $CO_2$ reduction electrocatalysts.

Possible mechanism pathways for direct electrochemical reduction of carbon dioxide to methanol are discussed in Chapter 5, as well as major conclusions and future recommendations.

# CHAPTER 2. LITERATURE REVIEW

## 2.1 $CO_2$ Reduction Pathway

In the past century, researchers have focused on investigating different pathways to convert carbon dioxide to valuable products such as hydrocarbons and alcohols. Hydrogenation of carbon dioxide has been intensively studied and has shown promising results in pilot plants; however, high temperature and high pressure conditions, in addition to high consumption of hydrogen, make this process less efficient. The conversion of carbon dioxide at room temperature and atmospheric pressure using solar light or electrical energy are more attractive routes. Photocatalysis uses semiconductor to promote reactions in the presence of light radiation. Formic acid, methane, methanol, and ethanol are common products of the photoelectrochemical reduction of carbon dioxide at metal/oxide electrodes; however, the quantum efficiency and production rate are very low. A recent innovation in conversion of carbon dioxide has been developed via aqueous electrocatalytic reduction (Hori, 2008).

## 2.2 $CO/CO_2$ Hydrogenation

The effort to convert carbon dioxide to hydrocarbons has been studied for over a century. In 1920, Franz Fischer and Hans Tropsch invented the Fischer-Tropsch process with two main steps. The first step is the partial oxidation of coal or natural gas to hydrogen gas and carbon dioxide. The carbon dioxide and hydrogen are then converted into alternate fuel sources such as formic acid, methanol, and ethanol. Commercially, methanol has been produced from synthetic gas, which contains mostly carbon monoxide, hydrogen, and a small amount of carbon dioxide. The combination of synthetic gas is demonstrated by a stoichiometric number S whish is shown in Equation 2.1 below.

$$S = \frac{molH_2 - molCO_2}{molCO + molCO_2} \tag{2.1}$$

Ideal S for methanol formation is slightly below 2. Excess hydrogen increases S leading the reaction to produce ammonia. The presence of carbon dioxide will lower S and improve productivity. Moreover, some studies have shown that a mixture with proper combination of carbon dioxide and carbon monoxide not only can increase the yield of methanol but also decrease the activation energy of the reaction (Klier et al., 1982; Lee et al., 1993; King et al., 1996). Production of methanol from synthetic gas under high temperature (300-400 ˚C) and high pressure (250-350 atm) was first brought to an industrial scale by BASF in the 1920s using zinc chromite catalyst. Until the end of World War II, coal-derived synthetic gas was the main reactant for methanol production. Synthetic gas can be produced from coal by gasification, a process which combines partial oxidation and steam treatment. Coal was then replaced by natural gas, which had a lower cost and fewer impurities.

Methanol production via catalytic hydrogenation of carbon dioxide is an exothermic reaction (Equation 2.2). The technical method has been applied in many pilot plants using a two step approach: the reverse water gas shift (RWGS) with the conventional methanol synthesis process.

$CO_2 + 3H_2 \rightarrow CH_3OH + H_2O$ $\Delta H_{298} = -49.5$ kJ/mol ; $\Delta G_{298} = 3.30$ kJ/mol (2.2)

$CO_2 + H_2 \rightarrow CO + H_2O$ $\Delta H_{298} = 41.2$ kJ/mol ; $\Delta G_{298} = 28.6$ kJ/mol (2.3)

$CO + 2H_2 \rightarrow CH_3OH$ $\Delta H_{298} = -91$ kJ/mol ; $\Delta G_{298} = -25.34$ kJ/mol (2.4)

Water formation from the RWGS (equation 2.2) is a critical issue. Besides playing a vital role in initially accelerating the conversion of $H_2$ and $CO_2$ to CO and $H_2O$, water acts as an inhibitor on the catalyst and slows down the consecutive step of methanol synthesis (equation 2.3). Catalysts for carbon dioxide hydrogenation to methanol should be able to overcome water intolerance, as well as improve activity, selectivity, and stability.

Although different catalyst combinations and preparations have been thoroughly studied over the past few decades, copper – zinc oxides containing various promoters such as $ZrO_2$, $Ga_2O_3$, and $SiO_2$ remain important catalysts (Liu et al., 2003). Because methanol synthesis using copper based catalyst is a highly surface sensitive reaction, the activity and selectivity strongly depend on the catalyst's surface structure and stability. The roles of the catalyst active sites have attracted many researchers' interests. Several researchers (Pan et al., 1988; Rasmussen et al., 1994; Rasmussen et al., 1994; Askgaard et al., 1995; Deng et al., 1996) suggested methanol is formed on a metallic copper surface of a copper based catalyst, and the activity of the catalyst is directly proportional to the surface area of metallic copper. Chinchen et al. found that the catalytic activity for methanol synthesis is independent of the $Cu^O$ surface area (Chinchen et al., 1987), while Herman et al. claimed $Cu^+$ sites are the active sites in methanol synthesis (Herman et al., 1979). A comparison of clean Cu (100) with oxidized Cu (100) showed increased methanol formation in oxidized Cu (100) by an order of magnitude (Szanyi et al., 1991). The formation of Cu(I) sites from oxidation of Cu particles was proven to stabilize reaction intermediates (carbonate, formate, and methoxy species) during methanol synthesis (Bailey et al., 1995). Similar observation was found by using near-infrared-visible absorption spectrum, dissolved Cu(I) on ZnO matrix forming $Cu^+$-O-Zn was believed to be the active site (Klier, 1982).

In addition to the active sites, an appropriate support is crucial in improving the yield and activity. Metal oxides are common supports for preparing catalysts used in methanol synthesis. In 1979, Herman and colleagues showed that at 250 ˚C and 75 atm, pure Cu metal yielded less than $10^{-8}$ kg of methanol per square meter of the catalyst per hour, while a supported copper based catalyst copper/zinc oxide with 30/70 composition by weight yielded $3.63x10^{-5}$ kg of

methanol per square meter of the catalyst per hour (Herman et al., 1979). ZnO is a wurtzite, n-type semiconductor. Besides oxygen vacancies, ZnO contains an electron pair which may serve as an active site for methanol synthesis. According to Herman et al., the electron pair in $Zn^{+}$ may create cation and anion lattice vacancies which can improve the adsorption and transformation of the reactant, as well as enhance copper dispersion. Consequently, while optimizing the dispersion of the copper particles, ZnO creates a copper – zinc active site on the catalyst. As shown in Figure 2.1, formate intermediate may adsorb at the interface between Cu and ZnO or Cu-O-Zn (Nakamura et al., 2003). Ultimately, migrating ZnO onto Cu particles provides an active site for methanol synthesis. Using mixtures of $Cu/SiO_2$ + $ZnO/SiO_2$ to examine the role of ZnO in Cu/ZnO methanol synthesis, Choi et al. concluded that ZnO created Cu-Zn active sites for methanol synthesis and the morphology of Cu was not changed (Figure 2.2.) (Choi et al., 2001).

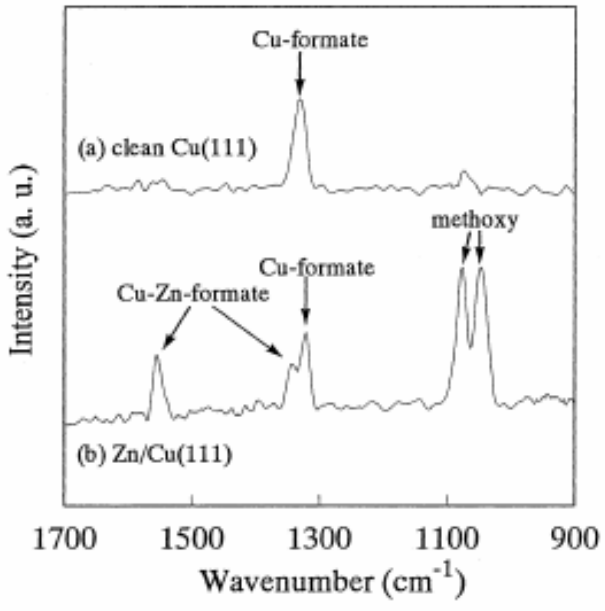


Figure 2.1. In situ IR absorption spectra of formate species and methoxy species on clean Cu(111) and Zn/Cu(111) during $CO_2$ hydrogenation at 343 K and 760 torr (reprinted from (Nakamura et al., 2003)).

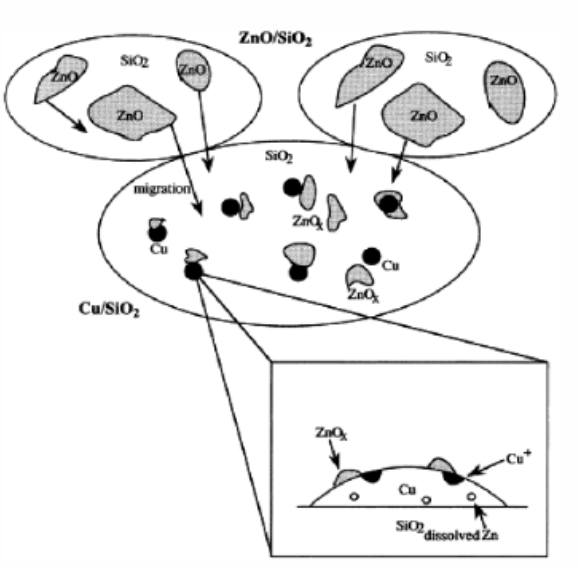


Figure 2.2. Model of the active site for methanol synthesis over a physical mixture of $Cu/SiO_2$ + $ZnO/SiO_2$ (reprinted from (Choi et al., 2001))

Most importantly, ZnO is believed to stabilize many active sites after extensive operating and increases catalyst's life time by absorbing the impurities presenting in the synthetic gas stream (Twigg et al., 2001). Since copper is very sensitive, and a low level of sulfur can poison the catalyst causing deactivation, ZnO acts as a support which can efficiently remove the poisons.

Apart from catalyst selection, an optimal reaction condition is also essential in maximizing the product yield, as well as the catalyst life time. Since hydrogenation of carbon monoxide and carbon dioxide in methanol synthesis is an exothermic reaction, according to Le Chatelier's principle, methanol conversion is favored by increasing pressure and decreasing temperature. The equilibrium constant decreases with an increase in temperature; hence, methanol synthesis would prefer a low temperature condition. On the other hand, increasing temperature may improve the reaction rate for carbon monoxide and carbon dioxide hydrogenation. Methanol synthesis exhibits various optimal temperature ranges when different catalysts are used; therefore, temperature control is extremely important. Overheating the catalyst can rapidly reduce its activity and shorten its lifetime. Heating can cause sintering and

agglomeration of copper based catalysts. Also, the catalyst life is very sensitive to operating pressure. Catalysts tend to deactivate faster at high pressures. A search for ideal catalysts to be used at low pressure and still achieve high activity in the long run is still in the research phase.

In the near future, finite and non-renewable natural feed stocks should be replaced by renewable resources. Carbon dioxide necessary for methanol production can be obtained from various emissions and the atmosphere. The recovery of fossil fuel burning sources and carbon dioxide extracted from air could provide a sufficient amount of carbon dioxide for the hydrogenation procedure. The capture of carbon dioxide is not a difficult task compared to the formation of hydrogen. One draw-back with hydrogenation of carbon dioxide is high energy consuming of hydrogen generation. The water electrolysis to produce hydrogen occurs by applying an electric current between electrodes inserted into the water. The process requires more hydrogen per consumption then hydrocarbon and alcohols being produced. Other ways to overcome these difficulties are photochemical and electrochemical reduction of carbon dioxide. These methods can produce methanol, formaldehyde, formic acid, methane, and ethylene at relatively high selectivity with minimal energy input.

### 2.3 Photoelectrochemical Reduction of $CO_2$

Photoelectrochemical reduction of carbon dioxide or photocatalysis generally uses semiconductors to promote reaction in the presence of sun light. The semiconductor is used as a catalyst to absorb solar energy and generate electrons and protons needed for the reduction of carbon dioxide. While hydrogenation of carbon dioxide requires high temperature and high pressure conditions ((400-800 K, 2-12 MPa) (Chinchen et al., 1987; Joo et al., 1999; Wu et al., 2001; Saito et al., 2004), photocatalysis occurs under relatively mild conditions with advantageous energy input – sun light – a continuous and readily available source. Photocatalytic

method not only can reduce carbon dioxide emissions, but also can produce very useful chemicals such as formic acid, formaldehyde, methanol, methane, etc. Figure 2.3 shows a model of the $CO_2$ photocatalytic reduction mechanism on $Cu/TiO_2$. With the assistant of light radiation, an electron hole pair ($e^-$ and $h^+$) is generated per absorbed photon. While OH radicals and $O_2$ are formed from the scavenging holes on titania ($TiO_2$), $CO_2$ and $H_2O$ molecules interact with the trapped electrons on the Cu clusters to produce methanol.

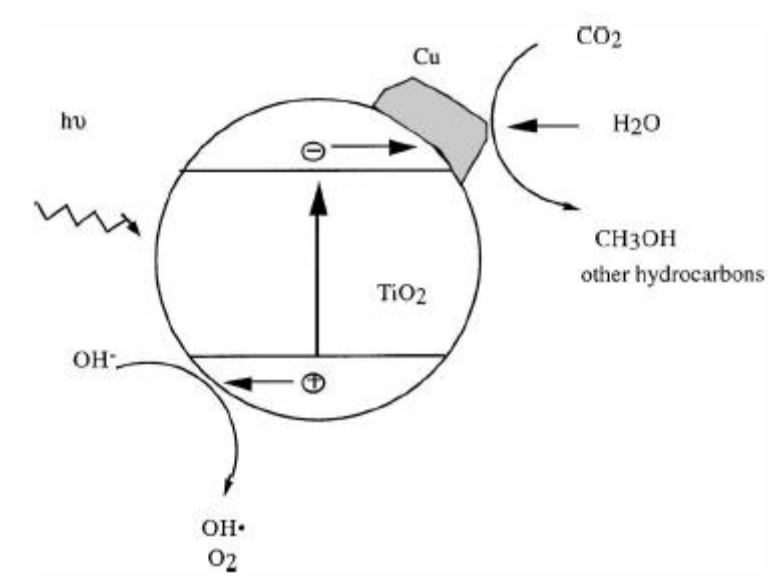


Figure 2.3. Mechanism of $CO_2$ photocatalytic reduction on $Cu/TiO_2$ (reprinted from (Tseng et al., 2002))

Intensive research on photochemical reduction of carbon dioxide has been conducted during the past four decades. In 1975, the first photoelectrochemical cell, which consisted of a $TiO_2$ single crystal anode and a platinum cathode, was invented (Fujishima et al., 1975). This photocell, when irradiated by light, generated oxygen at the anode and hydrogen at the cathode. The reactor could produce 1.1 liters of hydrogen per day or 6.6 liters of hydrogen per square meter of $TiO_2$. While metals have continuum electronic states, semiconductors have a band gap that extends from the top of the fully filled valance band to the bottom of the vacant conduction band (Figure 2.4.). When being exposed to light radiation, the generation of electron hole pairs

($e^-$ and $h^+$) promotes the reduced – oxidized reaction. The semiconductor electrode immersed in the electrolyte is connected to the counter-electrode through an external circuit.

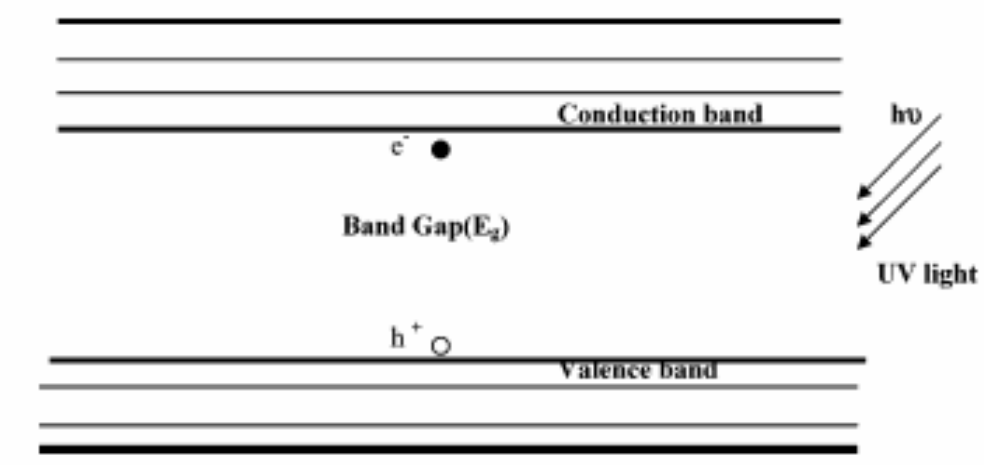


Figure 2.4. Band-gap diagram (formation of holes ($h^+$) and electrons ($e^-$) upon UV irradiation of semiconductor surface) ( reprinted from(Kabra et al., 2004))

In 1978, a photoelectrode consisting of a single crystal p-gallium phosphide was used for the photoelectrochemical reaction (Halmann, 1978). Unlike the reduction of carbon dioxide on metal cathodes which stops essentially after two electron transfer because of the high overpotential for formic acid reduction, the photo-electrolysis on p-gallium phosphide proceeds further to yield formaldehyde and methanol. After 90 hours of irradiation, product concentration was as follows: formic acid $5x10^{-2}$ M, formaldehyde $2.8x10^{-4}$ M, and methanol $8.1x10^{-4}$ M.

The active solid surface for photoelectrochemical reduction of carbon dioxide has also been under intense study. Hemminger et al. introduced the four distinct processes taking place at the active solid surface: i) photoelectron – hole pair generation, charge separation and trapping, ii) oxidation and reduction reactions of the adsorbates, iii) rearrangement and other surface reactions of intermediates, and iv) removal of the products and regeneration of the surface (Hemminger et al., 1978). Using $TiO_2$ and $SrTiO_3$ crystal surfaces, they discovered the importance of $Ti^{3+}$ surface ions for the dissociative adsorption of water and the importance of the

band gap illumination for $Ti^{3+}$ regeneration after being oxidized in the presence of water. Various semiconductor photoelectrocatalysts such as $WO_3$, $TiO_2$, ZnO, CdS, GaP, and SiC (99.5-99.9999% purity) have been studied to form organic compounds such as formic acid, formaldehyde, methanol, and methane (Inoue et al., 1979). They concluded that when estimating charge transfer for semiconductor electrodes, photo excited electrons in the more negative conduction band reduce carbon dioxide more efficiently.

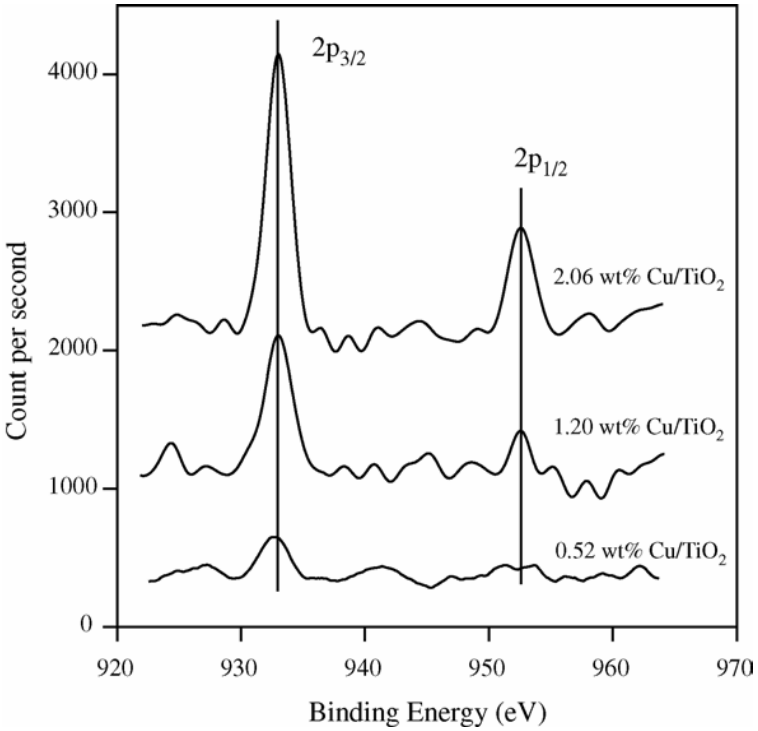


Figure 2.5. XPS of Cu 2p on $Cu/TiO_2$ catalysts (reprinted from (Wu et al., 2005))

One of the most challenging tasks for photoelectrochemical reduction of carbon dioxide to methanol is enhancement efficiencies. From a thermodynamic perspective, converting one mole of carbon dioxide to methanol requires 228 kJ of energy. Six electrons are required to reduce $C^{+4}$ of $CO_2$ to $C^{-2}$ of $CH_3OH$ as discussed from equation 1.6. The reaction mechanism in the photoreduction of carbon dioxide involves two main radicals H• and $\bullet CO_2^-$. These radicals

are produced by electron transfer from the valence band to the conducting band in the semiconductor by photon absorption having an energy equal to or greater than the band gap of the semiconductor. With a band gap of 3.2 eV, $TiO_2$ is ideal to promote the carbon dioxide reduction using UV illumination. Several researchers have investigated the efficiency and selectivity of the processes by modifying the photocatalyst surface with metal. In 1992, photocatalytic reduction of carbon dioxide in an aqueous $TiO_2$ suspension mixed with copper powder was introduced (Hirano et al., 1992); however, $TiO_2$ by itself is an inefficient catalyst for the photochemical reduction of carbon dioxide because of low product yields. The presence of copper particles on the $TiO_2$ surface not only offers reaction sites for carbon dioxide with an excited electron but also helps the reducing species react with positive holes on the semiconductor site. By adding potassium bicarbonate (0.01 M $KHCO_3$) into the $CO_2$ saturated aqueous solution containing $TiO_2$ suspension mixed with copper powder, methanol yield was doubled as compared with the bicarbonate-free solution (Hirano et al., 1992). Tseng et al. used titania and titania supported copper catalysts prepared by an improved sol-gel, a homogeneous hydrolysis technique, to improve the photoelectrochemical reduction efficiency (Tseng et al., 2002). Concentration of catalyst and copper loading were also investigated. Energy Dispersive X-ray Spectroscopy (EDX) and X-ray Photoelectron Spectroscopy (XPS) analyses revealed that Cu $2p_{3/2}$ is 933.4 eV, which indicated primary $Cu_2O$ species on the $TiO_2$ supports and most copper clusters were on the $TiO_2$ surface. In addition, Wu and colleagues experienced a maximum yield of methanol at 0.45 mmole/g catalysts/hr using 1.2 wt % $Cu/TiO_2$ catalyst under a light intensity of 16 $W/cm^2$ (Wu et al., 2005). XPS spectra of $Cu/TiO_2$ with different copper loadings showed copper on $TiO_2$ exist in multiple oxidation states; however, Cu(I) was the primary species (Figure 2.5.). $Cu_2O$ serves as an electron trap to reduce the recombination rate of

electron hole pairs during excitation of the photocatalyst. The 2.0 wt% Cu/TiO2 achieved highest dispersion among different copper loading catalysts. The methanol yield for this composition was 118 µmol/g catalysts after 6 hours of 254 nm UV irradiation (Figure 2.6.).

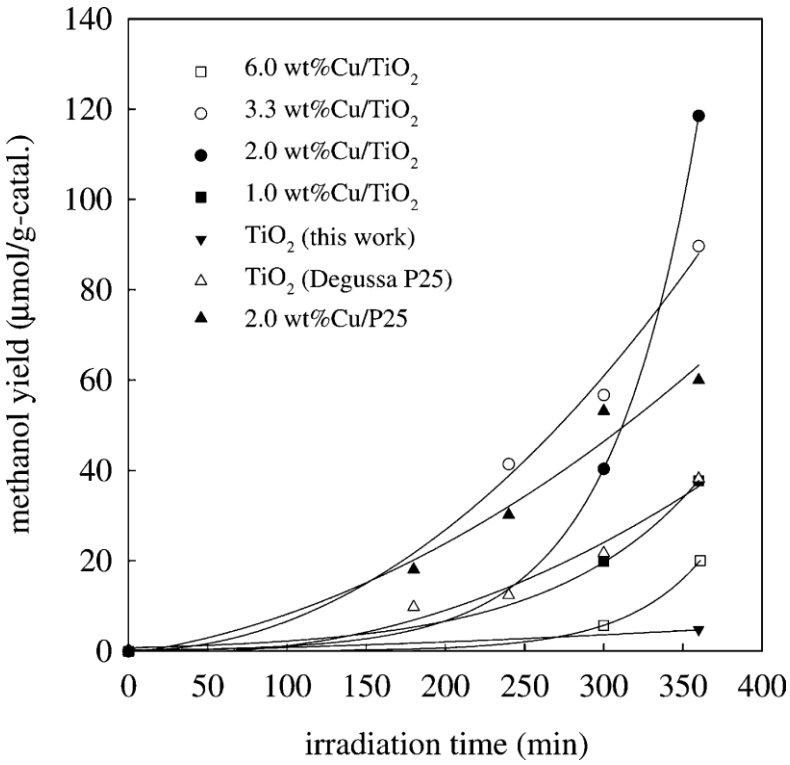


Figure 2.6. Time dependence on the methanol yields of various catalysts (reprinted from (Tseng et al., 2002))

The electron positive hole recombination leading to limited product formation on the catalyst surface lowers the photocatalysis process's efficiencies. Product efficiency and selectivity depend primarily on the type of catalyst. Even though copper based titanium oxide has been known to be the best catalyst for methanol production in the photoelectrochemical process, in order to upgrade to an industrial scale, methanol yields need to be improved significantly. In addition, with an extremely low light intensity, a large surface area would be needed to provide enough energy for the reaction to occur efficiently (Wu et al., 2005). Therefore, another alternative solution for carbon dioxide reduction is necessary.

## 2.4 Electrochemical Reduction of $CO_2$

The foundations of electrochemistry in the late $18^{th}$ century were marked by the investigation of Galvani and Volta. They established the relationship between chemical reactions and electricity. Electrochemistry studies chemical reactions occurring at the interface of an electron conductor (the working electrode) and an ionic conductor (the electrolyte). Electrons are transferred between the electrode and the electrolyte in the solution. It is called an electrochemical reaction when an external voltage drives the reaction or a voltage is created by a chemical reaction. Since electrons are transferred between molecules, this reaction is also called an oxidation - reduction (redox) reaction. An electrochemical reaction mechanism is a step by step sequence of electron transfer. An electrocatalytic process involves oxidation and reduction through direct transfer of electrons. Researches and applications in this area have attracted many scientists from all over the world during the past century.

One of the most practical recent electrocatalytic applications is the electrochemical reduction of carbon dioxide to hydrocarbons and alcohols. This method uses electricity produced from renewable energy source including hydro, solar, wind, geothermal, wave and tides for generation of electrons. The direct electrochemical reduction of $CO_2$ to $CH_3OH$ presents an attractive method to produce liquid fuels such as dimethyl ether (DME), synthetic gasoline, and feedstock for several organic compounds (Lee et al., 1995; Jayamurthy et al., 1996). Although $CH_3OH$ is typically produced in hydrogenation reactions using syngas and $CO_2$ feeds (400-800 K, 2-12 MPa) (Chinchen et al., 1986; Chinchen et al., 1987; Joo et al., 1999; Wu et al., 2001; Saito et al., 2004), the aqueous electrochemical process operates at room temperature and offers a convenient means for storing electrical energy without increasing $CO_2$ emissions. Similar to photocatalysis, electrocatalysis is an electron transfer sequence procedure. Theoretically, water is

oxidized at the anode and releases electrons followed by reduction of carbon dioxide at the cathode to hydrocarbons and alcohols. Unfortunately, the reduction potential of carbon dioxide is very closed to water reduction. We would like to utilize all the potential to achieve the highest yield; however, increasing the reduction rate of carbon dioxide may also lead to the reduction potential of water, which will result in hydrogen formation. The key to this process is to find a stable catalyst with a high overpotential for hydrogen reduction, allowing further $H^+$ transfer steps selectively towards forming methanol.

Studies on the electrochemical reduction of carbon dioxide began more than a century ago with high hydrogen overpotential metals and amalgams. In 1904, Coehn and Jahn used zinc, amalgamated zinc and amalgamated copper cathode to electrolytically reduce carbon dioxide in aqueous $NaHCO_3$ and $K_2SO_4$ solutions, in which formic acid was the only product (Coehn et al., 1904). Fischer and Prziza ran electrolytic reduction reactions of carbon dioxide that had been dissolved under pressure (Fischer et al., 1914). Once again, formic acid was the only product and copper plated with amalgamated zinc electrodes were reported to be the most efficient. Finally, minimal amounts of methanol were obtained with Pb electrodes in $K_2SO_4$ and $(NH_4)_2SO_4$ electrolyte. Truman and Pierre conducted experiments for carbon dioxide reduction on mercury cathodes and yielded only formic acid at 100 % current efficiency (Teeter et al., 1954). In 1969, Paik et al. reduced carbon dioxide on the mercury electrode in buffered neutral and acidic aqueous solutions by means of steady state polarization techniques, cathodic galvanostatic charging techniques, and current efficiency determinations (Paik et al., 1969). The only reduction product in neutral solution was formic acid; while in the acid solution, both formic acid and hydrogen were formed. However, these early papers show that with mercury as the cathode, the current efficiency was high at initial stages, and then fell rapidly with time. Ultimately, Udupa et

al. investigated the electrolytic reduction of carbon dioxide at a rotating amalgamated cathode to improve and maintain high current efficiency so that formate could be built up without loss in current efficiency (Udupa et al., 1971). In 1977, Russell et al. attempted to electrochemically reduce carbon dioxide to methanol through intermediate reactions because conditions for a direct conversion could not be achieved (Russell et al., 1977). Formic acid was reduced from carbon dioxide in a neutral electrolyte on a mercury electrode; however, it could not be further reduced to methanol due to the limited potential region. Fortunately, formaldehyde could be reduced to methanol at a current density of 10 mA $cm^{-2}$. In 1982, Hori et al. studied the effect of electrolyte in carbon dioxide electrolytic reduction on a mercury electrode by investigating different aqueous solutions of $NaHCO_3$, $NaH_2PO_4$-$Na_2HPO_4$, NaCl, $NaClO_4$, $Na_2SO_4$, $LiHCO_3$, and $KHCO_3$ as well as their combination (Hori et al., 1982).

Similar studies were continued on different metal electrodes with the hope of finding the optimal catalysts for the process. In 1983, as part of a program to study the conversion of inorganic substances into fuels, Canfield and Frese investigated the reduction of carbon dioxide to methanol, formaldehyde and methane on n and p-GaAs, and p-InP semiconductor electrodes (Canfield et al., 1983). The highest current achieved was around 400 μA $cm^{-2}$. In 1985, Frese and Leach chose ruthenium electrode because ruthenium was known at that time for being active in the gas phase conversion of carbon dioxide to methane at low temperature (Frese et al., 1985). The reaction yielded carbon monoxide, methane, and a small amount of methanol. Even though the reaction was stable, current density was less than 0.4 mA $cm^{-2}$. Frese et. al. also tried molybdenum electrodes in 0.2 M $Na_2SO_4$ electrolyte (pH = 4.2) to convert carbon dioxide to methanol at good selectivity and yield under appropriate conditions (Summers et al., 1986). It was shown that the Faradaic efficiency depends on several factors such as chemical surface

pretreatment and voltage cycling pretreatment. In voltage cycled electrodes, carbon dioxide rapidly converted to methanol at up to 370 % Faradaic efficiency; however, cycled electrodes were also subject to molybdenum corrosion. During the same period, Hori et. al. succeeded in electrochemically reducing carbon dioxide to hydrocarbons at several metal electrodes in an aqueous bicarbonate solution (0.5-1.0 M $KHCO_3$) with a high current density (5.0-5.5 mA $cm^{-2}$) (Hori et al., 1985). Cd, In, Sn, and Pb electrodes mainly produced formate. Ag and Au yielded majority of CO. Ni and Fe exclusively produced $H_2$, with trace amount of CO and $CH_4$. Only Cu

Table 2.1. Typical current efficiencies (%) for $CO_2$ reduction products at -2.2 V vs. SCE (193˚C) in a $CO_2$ saturated 0.05M $KHCO_3$ aqueous. (reprinted from (Azuma et al., 1990))

| Metal | T °C | $CH_4$ | CO | $C_2H_4$ | $C_2H_6$ | HCOOH | $H_2$ | Sum |
|---|---|---|---|---|---|---|---|---|
| Cd[a] | 0 | 0.015 | 3.7 | 0.002 | 0.00056 | 55.9 | 35.7 | 95 |
| | 20 | 0.0073 | 1.8 | 0.001 | 0.00040 | 35.5 | 63.2 | 100 |
| In[a] | 0 | 0.001 | 3.0 | 0.00035 | 0.0006 | 70.0 | 25.0 | 98 |
| | 20 | 0.050 | 14.7 | 0.0046 | 0.0067 | 33.3 | 56.5 | 105 |
| Sn | 0 | 0.65 | 1.4 | 0.068 | 0.44 | 28.5 | 67.5 | 99 |
| | 0 | 0.84 | 0.35 | 0.95 | 0.69 | 5.2 | 94.9 | 102 |
| Pb[a] | 0 | 0.39 | 0.12 | 0.008 | 0.0014 | 16.5 | 82.9 | 100 |
| | 20 | 0.06 | 0.10 | 0.001 | 0.0003 | 9.9 | 93.3 | 103 |
| Tl | 0 | 0.20 | 0.16 | 0.003 | 0.0010 | 53.4 | 46.2 | 100 |
| Hg | 0 | 0.0004 | 0.20 | t | t | 90.2 | 9.5 | 100 |
| | 20 | 0.0035 | 0.64 | 0.0002 | 0.00006 | 87.6 | 7.9 | 96 |
| Zn | 0 | 0.23 | 9.8 | t | nm | 19.5 | 68.1 | 98 |
| Pd[a] | 0 | 0.083 | 11.6 | 0.011 | 0.014 | 16.1 | 73.3 | 101 |
| | 20 | 0.31 | 3.2 | 0.061 | 0.078 | 8.6 | 90.3 | 103 |
| Ti | 0 | t | 13.5 | t | nm | 5.2 | 69.4 | 83 |
| Ni | 0 | 0.71 | 21.0 | 0.069 | 0.18 | 13.7 | 61.7 | 97 |
| | 20 | 0.13 | 0.60 | 0.010 | 0.021 | 0.10 | 98.8 | 100 |
| Ag | 0 | 1.4 | 40.7 | 0.0052 | 0.013 | 20.5 | 32.6 | 95 |
| | 20 | 1.1 | 30.0 | 0.0090 | 0.0027 | 16.0 | 50.0 | 98 |
| Au | 0 | t | 16.9 | t | nm | 10.3 | 73.4 | 101 |
| Cu | 0 | 24.7 | 16.5 | 6.5 | 0.015 | 3.0 | 49.3 | 100 |
| | 20 | 17.8 | 5.4 | 12.7 | 0.039 | 10.2 | 52.0 | 98 |
| C | 0 | 0.11 | t | 0.0064 | 0.0070 | 0.31 | 92.5 | 93 |
| Al | 0 | 0.012 | t | 0.00022 | 0.00040 | 0.78 | 95.7 | 96 |
| Si | 0 | 0.025 | 0.08 | t | t | 1.6 | 102.2 | 104 |
| V | 0 | 0.02 | 1.3 | t | nm | 2.6 | 91.9 | 96 |
| Cr | 0 | 0.74 | 0.49 | 0.050 | 0.18 | 0.15 | 92.2 | 94 |
| Mn | 0 | 1.5 | 0.34 | 0.093 | 0.29 | 0.03 | 90.9 | 93 |
| Fe | 0 | 0.07 | 2.2 | t | nm | 1.1 | 89.8 | 93 |
| Co | 0 | 0.13 | 0.47 | 0.0057 | 0.032 | 0.85 | 92.9 | 94 |
| Zr | 0 | 0.49 | 0.42 | 0.021 | 0.055 | t | 99.9 | 101 |
| Nb | 0 | 0.16 | 0.46 | 0.0088 | 0.042 | 0.03 | 97.3 | 98 |
| Mo[a] | 0 | 0.010 | t | 0.00028 | 0.0015 | 0.21 | 99.9 | 100 |
| | 20 | 0.031 | 0.02 | 0.00077 | 0.0057 | 0.19 | 98.6 | 99 |
| Ru | 0 | 0.043 | 0.65 | t | t | 0.08 | 99.1 | 100 |
| Rh | 0 | 0.031 | 2.5 | 0.00067 | 0.0036 | 1.35 | 99.3 | 103 |
| | 20 | 0.053 | 0.66 | 0.0030 | 0.011 | 2.4 | 99.3 | 103 |
| Hf | 0 | 0.0046 | 1.14 | 0.00027 | 0.0010 | 0.35 | 99.2 | 101 |
| | 20 | 0.0073 | 0.08 | 0.00057 | 0.0005 | 0.21 | 100.9 | 101 |
| Ta[b] | 0 | 0.0015 | 0.09 | 0.0015 | 0.0002 | t | 100.7 | 101 |
| | 20 | 0.0039 | t | 0.0039 | 0.0001 | t | 102.2 | 102 |
| W[a] | 0 | 0.015 | 0.06 | 0.0043 | 0.0022 | 1.3 | 96.3 | 98 |
| | 20 | 0.055 | 0.21 | 0.0022 | 0.010 | 2.6 | 96.9 | 100 |
| Re[a] | 0 | 0.044 | t | 0.00022 | 0.0056 | 2.0 | 99.0 | 101 |
| | 20 | 0.038 | t | 0.00024 | 0.0048 | 1.4 | 95.3 | 97 |
| Ir | 0 | 0.051 | 0.53 | 0.0035 | 0.0072 | 1.0 | 98.8 | 100 |
| | 20 | 0.086 | t | 0.0057 | 0.015 | 0.58 | 100.3 | 101 |
| Pt | 0 | 0.29 | 1.2 | t | nm | 5.5 | 92.6 | 100 |

[a] At −2.0V *vs.* SCE.
[b] At −2.8V *vs.* SCE.
t : trace.
nm: not measured.

Table 2.2. Typical current efficiencies (%) for hydrogen evolution ($\eta[H_2]$) and total $CO_2$ ($\eta[CO_2]$) on various metal electrodes and the distribution (%) into CO ($F_{CO}$) and HCOOH ($F_{HCOOH}$) and hydrocarbons ($F_{CxHy}$) at 0.05M $KHCO_3$, 0˚C, -2.2 V. vs. SCE. (reprinted from (Azuma et al., 1990))

| Electrodes | $\eta(H_2)$ | $\eta$(red-$CO_2$) | $F_{CO}$ | $F_{HCOOH}$ | $F_{CxHy}$ | Note |
|---|---|---|---|---|---|---|
| Cd | 35.7 | 59.6 | 6.2 | 93.8 | t | −2.0V |
| In | 25.0 | 73.0 | 4.1 | 95.9 | t | −2.0V |
| Sn | 67.5 | 31.1 | 4.5 | 91.8 | 3.7 | |
| Pb | 82.9 | 17.0 | 0.7 | 96.9 | 2.4 | −2.0V |
| Tl | 46.2 | 53.8 | t | 99.8 | t | |
| Hg | 9.5 | 90.4 | 0.2 | 99.8 | t | |
| Zn | 68.1 | 29.5 | 33.2 | 66.0 | 0.8 | |
| Pd | 73.3 | 27.8 | 41.7 | 57.9 | 0.4 | −2.0V |
| Ti | 69.4 | 18.7 | 72.2 | 27.8 | t | |
| Ni | 61.7 | 35.7 | 58.9 | 38.4 | 2.7 | |
| Ag | 32.6 | 62.6 | 65.0 | 32.7 | 2.2 | |
| Au | 73.4 | 27.2 | 62.1 | 37.9 | t | |
| Cu | 49.3 | 50.7 | 32.5 | 5.9 | 61.5 | |
| C | 92.5 | 0.43 | t | 71.5 | 28.5 | |
| Al | 95.7 | 0.79 | t | 98.4 | 1.6 | |
| Si | 102.2 | 1.7 | 4.77 | 93.8 | 1.5 | |
| V | 91.9 | 3.9 | 33.2 | 66.3 | 0.5 | |
| Cr | 92.2 | 1.6 | 30.4 | 9.3 | 60.2 | |
| Mn | 90.9 | 2.3 | 15.1 | 1.3 | 83.6 | |
| Fe | 89.8 | 3.4 | 65.3 | 32.6 | 2.1 | |
| Co | 92.9 | 1.5 | 31.6 | 57.1 | 11.3 | |
| Zr | 99.9 | 0.99 | 42.6 | t | 57.4 | |
| Nb | 97.3 | 0.70 | 65.6 | 4.3 | 30.1 | |
| Mo | 99.9 | 0.22 | t | 94.7 | 5.3 | −2.0V |
| Ru | 99.1 | 0.77 | 84.1 | 10.4 | 5.6 | |
| Rh | 99.3 | 3.9 | 64.3 | 34.7 | 0.9 | |
| Hf | 99.2 | 1.5 | 76.2 | 23.4 | 0.4 | |
| Ta | 100.7 | 0.30 | 29.7 | t | 70.3 | −2.8V |
| W | 96.3 | 1.4 | 4.3 | 94.1 | 1.6 | −2.0V |
| Re | 99.0 | 2.0 | t | 97.6 | 2.4 | −2.0V |
| Ir | 98.8 | 1.6 | 33.3 | 62.8 | 3.9 | |
| Pt | 92.6 | 7.0 | 17.2 | 78.7 | 4.1 | |

t: trace.

cathode produced significant amount of $CH_4$. The copper electrodes were also pretreated by etching in 7% $HNO_3$ aqueous solution; however, little difference in Faradaic efficiency of $CH_4$ formation was observed. In addition, the presence of oxygen in the electrolyte remarkably enhances the $CH_4$ production. After successfully producing methane from copper electrodes, in 1986, Hori et al. continued their studies using copper electrode in an aqueous bicarbonate solution at a low temperature with a current density of 5 mA $cm^{-2}$ (Hori et al., 1986). The Faradaic efficiency of methane formation was about 65 % at 0 ˚C and dropped with an increase in temperature, whereas that of ethylene formation rose up to 20 % at 40 ˚C. By 1987, Cook et al. were able to improve the efficiency of methane and ethylene production using in situ electrodeposited copper layers on a glassy carbon electrode (Cook et al., 1987). At 8.3 mA $cm^{-2}$, the carbon dioxide reduction reached almost 100 % current efficiency. At 25 mA $cm^{-2}$, the

overall current efficiency for carbon dioxide reduction was 79 %. These yields were by far the highest Faradaic efficiency and current density yet reported for the carbon dioxide reduction reaction.

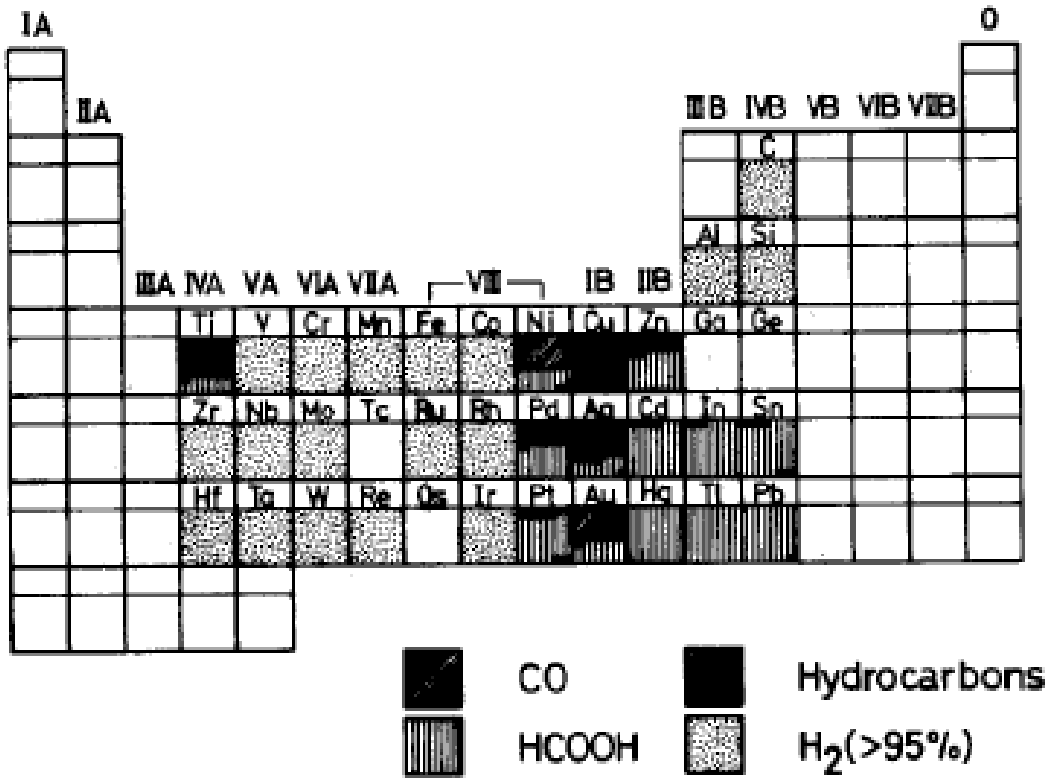


Figure 2.7. Periodic table for $CO_2$ reduction products at -2.2V vs. SCE in low temperature 0.05M $KHCO_3$ solution reprinted from (Azuma et al., 1990))

A systematic rule for the electrocatalytic reduction of carbon dioxide on metal surfaces was suggested. Azuma and colleagues measured the reduction products on 32 types of metals in aqueous $KHCO_3$ solution at low temperature (0˚C) and discussed the reduction mechanism (Azuma et al., 1990) (Table 2.1 and Table 2.2). Out of 32 metals (including Cd, In, Sn, Pb, Tl, Hg, Zn, Pd, Ti, Ni, Ag, and Au) Cu showed relatively high total current efficiencies for carbon dioxide reduction. Only copper was able to produce hydrocarbon efficiently, while other metals yield primarily formic acid. Based on this dependence of reduction products on various metals, a

periodic table for carbon dioxide reduction was developed which suggested a systematic rule for the electrochemical reduction of carbon dioxide on transition metal surfaces (Figure 2.7.). Heavy transition metals in the IIB, IIIB, and IVB groups reduced carbon dioxide to formate. Some of VIII and IB metals are effective for carbon monoxide production. Copper is located between these two groups and is selectively active toward carbon dioxide reduction to hydrocarbons. Similarly, in 1976, Broden et al. had already discovered a relationship between the metals' positions in the periodic table and their ability to chemisorb carbon monoxide dissociatively, the initial step for hydrogenation to methanol (Broden et al., 1976). However, at present, there is no consensus on the molecular mechanism of the metal electrodes and their properties toward electrocatalytic activities and selectivities for carbon dioxide reduction.

With the discovery of copper as an active catalyst for carbon dioxide reduction to hydrocarbons, electrocatalytic research has moved to an upper stage. Kaneco and coworkers have done a series of experiment in this field using copper in different solvents to produce formic acid, methane, ethylene and carbon monoxide with increasing Faradaic efficiency (Kaneco et al., 1999; Kaneco et al., 1999; Kaneco et al., 2003; Kaneco et al., 2006; Ohya et al., 2009). Frese et. al. studied the electrochemical reduction of carbon dioxide to methane on copper foil electrodes in 0.5 M $KHCO_3$, pH 7.6. The highest methane formation rates at 22 ˚C and 0 ˚C were $8x10^{-5}$ and $1.1x10^{-4}$ mol $cm^{-2}$ $h^{-1}$ at current densities of 17 and 23 mA $cm^{-2}$, respectively (Kim et al., 1988). The results showed that the catalytic properties of copper depended on its physical form and method of preparation. Polishing the copper surface helped achieve the highest methane formation rates. Cleaning copper with HCl was preferred over $HNO_3$ cleaning. In this experiment, copper foil was oxidized by oxygen in air prior to carbon dioxide reduction to form a visible layer of CuO and $Cu_2O$ on copper surface. After HCl cleaning, all the oxides were

dissolved to form cuprous chloride complex ions. The $Cu^{+}$ in the $Cu_2O$ was stabilized and prevented from disproportionating to $Cu^{0}$ and $Cu^{2+}$. It was concluded that HCl removed the oxides without precipitation of metallic copper, which was known to deactivate the catalyst surface.

Understanding the characteristics of metal surfaces would be beneficial to recognizing the carbon dioxide reduction reaction mechanism. Even though it is known that copper is the vital active catalyst component, the active sites and orientation are still a topic of debate. Carbon dioxide was electrochemically reduced at Cu (100), Cu(110) and Cu (111) electrodes at constant current density of 5 mA $cm^{-2}$ in 0.1 M $KHCO_3$ at ambient temperature (Hori et al., 1995). Ethylene was favorably produced on Cu (100), while Cu (111) yielded mostly methane. Cu (110) showed intermediate products of both. Terunuma and colleagues studied the relationship between hydrocarbon production in the electrochemical reduction of carbon dioxide and the characteristics of the copper electrode by conducting various pretreatment methods on copper (Terunuma et al., 1997). A copper metal surface is easily contaminated with organic compounds due to its high affinity for absorbed oxygen. Surfaces with copper oxide to some extent demonstrated much higher activity for hydrocarbon production. The $Cu_2O$ site has a stronger activity for the reduction of protons than the Cu site. In the experiment, the Cu site was responsible for the physical adsorption of carbon dioxide to form carbon monoxide as a first step. The heat of adsorption of carbon monoxide on $Cu_2O$ is larger than that on metallic Cu, and the $Cu_2O$ site is more favorable to the adsorption of carbon monoxide than the Cu site. Therefore, controlling the number of Cu (I) sites is very important in enhancing the selectivity and productivity towards methanol formation.

There are good reasons to expect $Cu^{+}$ ions in the $Cu_2O$ to be the active site for methanol

production from electrochemical reduction of carbon dioxide. Recently, Chang et al. (Chang et al., 2009) have investigated the electrochemical reduction of carbon dioxide by $Cu_2O$ – catalyzed carbon cloths and concluded that methanol was the only product. It was indicated that $Cu^+$ is directly involved in the catalytic actions to promote carbon dioxide compositions. Frese et al. have observed the carbon dioxide reduction to methanol at several oxidized copper electrodes including anodized copper foil, copper foil thermally oxidized in air, and air oxidized copper electrodeposited on anodized or air oxidized Ti foil at 22 ˚C (Frese, 1991). The highest methanol rate obtained was $1x10^{-4}$ mol $cm^{-2}$ $h^{-1}$ from anodized copper foil in 0.5 M $KHCO_3$. The current density was as high as 33 mA $cm^{-2}$. While copper oxides show the greatest yields and efficiencies, a more fundamental question regarding oxidized Cu electrodes centers on their formal reduction potentials relative to $CO_2$. The formal potential for $CO_2$ reduction to $CH_3OH$ occurs 20mV positive of the SHE, while copper oxides are reduced at more positive potentials. Further, several $CO_2$ reduction studies suggest an initial step requiring CO which has a formal potential of –0.103 V (SHE). (Hori et al., 1989; Hori et al., 1991; Gattrell et al., 2006; Hori, 2008). Figure 2.8 shows polarization data from carbon dioxide electrochemical reduction at metallic copper electrodes (Hori et al., 1989). Copper is considered unique among metals with both intermediate hydrogen overpotentials and carbon monoxide adsorption allowing further reduction to hydrocarbons. The first pathway in the system is the formation of both formate and carbon monoxide. As the potentials become more negative, carbon monoxide and formate suppress hydrogen evolution. At potentials more negative than –1.25 V (SHE), carbon monoxide is further converted to ethylene at first, and methane becomes dominant after –1.35 V (SHE). Understanding how equilibrium potentials affect the activity and selectivity of the reaction might be helpful in determining the reaction mechanism.

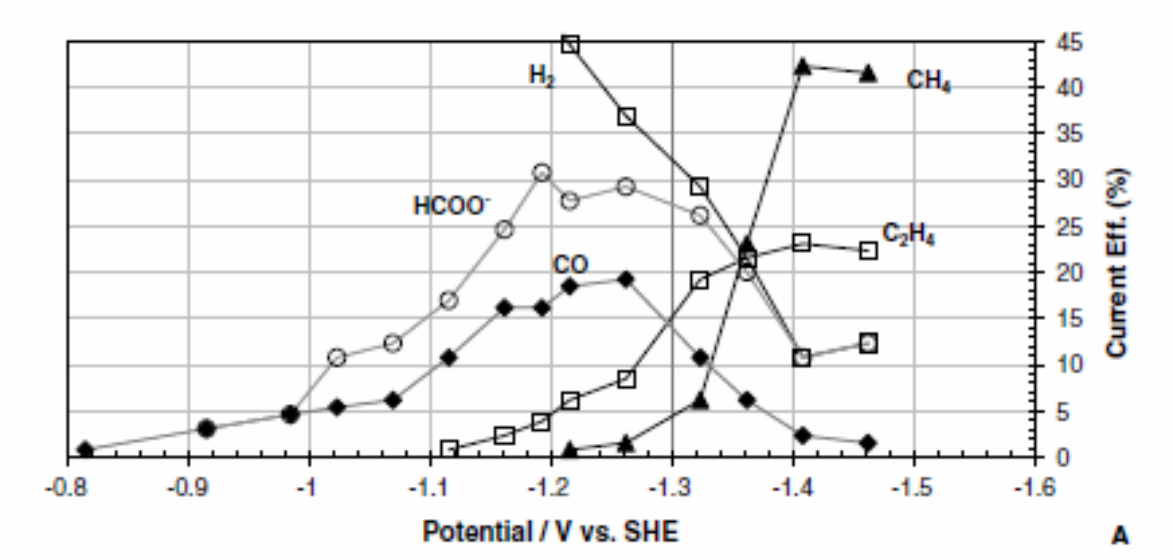


Figure 2.8. Current efficiencies at different potentials (0.1 M $KHCO_3$, $CO_2$ bubbled) reprinted from (Hori et al., 1989))

Theoretically, copper oxides should be reduced before $CO_2$ reduction reactions take place since the formal potentials for $Cu^+$ and $Cu^{2+}$ reduction occur well positive of $CO_2$ reduction as shown in Figure 2.9. Furthermore, even though the reduction of $Cu^+$ to metallic Cu occurs at less positive potential than reduction of $Cu^{2+}$ to Cu (Equation 2.4 and Equation 2.5), $Cu^+$ was more difficult to be reduced to metallic Cu than $Cu^{2+}$ at the same operating conditions via Temperature-Programmed Reduction (TPR) method (Wang et al., 2004; Estrella et al., 2009).

$$Cu_2O + 2H^+ + 2e^- \rightleftharpoons 2Cu + H_2O \qquad E_o = 0.471 \text{ V vs. SHE} \qquad (2.4)$$

$$CuO + 2H^+ + 2e^- \rightleftharpoons Cu + H_2O \qquad E_o = 0.570 \text{ V vs. SHE} \qquad (2.5)$$

$$2CuO + 2H^+ + 2e^- \rightleftharpoons Cu_2O + H_2O \qquad E_o = 0.669 \text{ V vs. SHE} \qquad (2.6)$$

It is believed that the electronic properties of $Cu_2O$, a p-type semiconductor with a band gap of 2.14 eV play an important role in the adsorption of carbon dioxide and carbon monoxide. The oxygen on copper oxides increases the number of defect electrons so that carbon dioxide can be adsorbed easily onto the catalyst surface (Chang et al., 2009). It is also suggested by Frese et al. that carbon dioxide would initially be chemisorbed on the oxidized copper surface (most

likely p-$Cu_2O$ sites) to form $CO_{ad}$ and $O_{ad}$. $Cu_2O$ has the $O_2$ anions in a body center and the $Cu^+$ cations in a face centered lattice. The valence band states in $Cu^+$ are sources of electrons for chemisorption. Recently, experiments on Cu (I) halide compounds at the three phase interface have shown significant results on hydrocarbon production (Ogura et al., 2003; Yano et al., 2004; Ogura et al., 2005). Carbon monoxide, after being reduced from carbon dioxide, adsorbs on $Cu^+$ with its p-bond perpendicular to the surface and results in the formation of methane and ethylene. Cu(I) halides not only adsorb CO much more strongly than Cu does but also help stabilize HCOO and $CH_2$=CH intermediates; thus, enhancing $C_2H_4$ formation. Therefore, $Cu^+$ species is promising candidate for carbon dioxide reduction reactions on its surface.

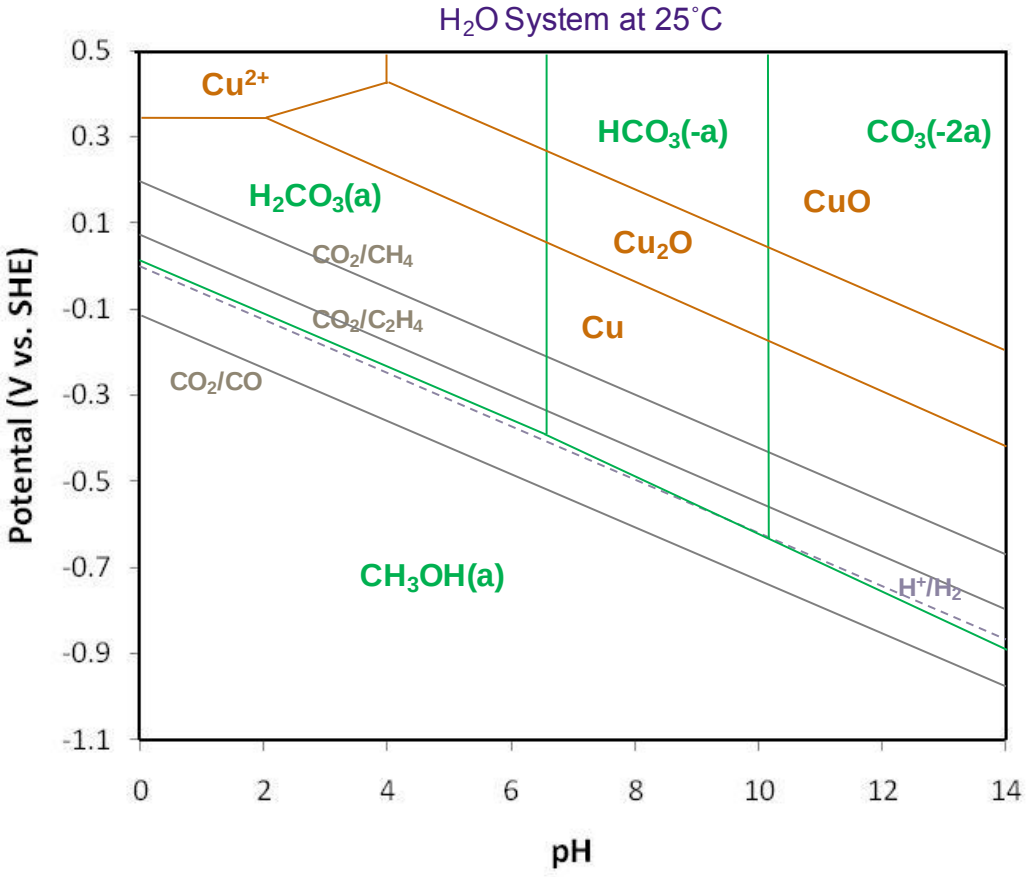


Figure 2.9. The equilibrium potentials as a function of pH for copper and carbon dioxide reduction reaction

Further investigation has been focused on the role of the substrate and its surface orientation. Among many oxides, zinc oxide with its wurtzitic crystal structure has been chosen as an industrial catalyst because of its effective methanol synthesis at low temperature and pressure. Klier suggested that the basal (0001) ZnO planes tend to accumulate more of the solute copper atoms than the prism (101-0) planes (Klier, 1982). Moreover, copper solute sites on the zinc oxide surface are the active site for carbon monoxide adsorption. It was demonstrated by Ohya et al. that the Faradaic efficiencies of methane and ethylene were much higher in copper oxide/zinc particle-press electrode than in metallic copper electrode (Ohya et al., 2009). Maximum efficiencies were achieved from the electrode consisting of $Cu_2O$/Zn. Therefore, ZnO does more than just provide a surface for the copper. It probably helps stabilize $Cu^+$ atoms or promotes $Cu^{2+}$ to behave like $Cu^+$. In the hydrogenation case, ZnO has shown its significant role as a support for the copper-zinc catalyst not only by stabilizing the $Cu^+$ species but also forming a copper-zinc active site and removing impurities which can deactivate the catalyst in the long run. Similar effects are believed to take place in the electrochemical reduction case.

The ideal composition of copper/zinc oxide for effective methanol production is still not clear. Klier has done several experiments on catalytic hydrogenation of carbon monoxide and carbon dioxide by varying the copper/zinc oxide composition from 0/100 to 100/0 (Klier, 1982). Of those compositions, the 67/33 Cu/ZnO on the (0001) basal ZnO planes and the 30/70 Cu/ZnO on the (101-0) prism ZnO planes demonstrated an effective irreversible adsorption of carbon monoxide and achieved the highest activity among the catalysts studied. On the other hand, Wayne Goodman's group has investigated the carbon monoxide oxidation over Au/$TiO_2$ prepared from metal-organic gold complexes (Yan et al., 2006). Even though gold has been known to be an inefficient catalyst, a monolayer of gold on an oxide surface led to strong

performance of carbon monoxide oxidation. The oxygen in the oxide may utilize some of the electrons from gold and change its chemistry to make it behave like an active catalyst. As a result, whether the copper physical state should be a monolayer, bilayer, atom, bulk or cluster and how the oxide takes role in the reaction mechanism are still under investigation.

Because of all the advantages methanol offers: a convenient and safe means of storing energy, excellent fuels for combustion engines, electricity generator, intermediate substances for a diverse array of chemical products and materials, methanol formation has become a very attractive research route. In particular, methanol conversion from carbon dioxide can simultaneously solve the energy and environmental crisis by recycling carbon dioxide to fuels. Catalytic hydrogenation with hydrogen, photoelectrochemical reduction and electrochemical reduction in an aqueous solution are the most common pathways to convert carbon dioxide into methanol. The goal is to maximize methanol yield and efficiency with minimal energy input. The most promising approach is to convert carbon dioxide electrochemically, which shows higher production rate and conversion at mild reaction conditions. However, methanol is preferred in the photoelectrochemical reduction and hydrogenation to the electrochemical reaction as seen in previous papers. Therefore, an optimal electrocatalyst needs to be designed which must have high selectivity toward methanol instead of other hydrocarbons such as methane, and ethylene. The material properties and catalyst behavior such as the active sites, the geometries, the compositions, the substrate effects as well as the electron transfer step mechanism have to be thoroughly understood. A cycle of learning should be developed to incorporate computational work with synthesis, and characterization work. Once computational work is done, the results can be compared to experimental work to develop theoretical models. Synthesis will well design the catalysts, and with the help of characterization, the results can be analyzed, evaluated and

improved. Even though the effort to put everything together is still tremendous and requires substantial time commitment, with human intelligence, electrochemical reduction of carbon dioxide at industrial scale will no longer be an unrealistic dream.

# CHAPTER 3. REDUCTION OF $CO_2$ AT COPPER OXIDE SURFACES*

## 3.1 Introduction

As described by Hori, electrochemical product selectivity and efficiency of $CO_2$ reduction reactions are highly dependent on the electrocatalysts and operating conditions (Hori, 2008). Direct $CO_2$ to $CH_3OH$ electrochemical reduction reactions in aqueous electrolytes were first reported by Frese et al. using III-V semiconductor electrodes (GaAs and InP); however, maximum current densities were lower than 1 mA $cm^{-2}$ (Canfield et al., 1983). Similar works have also demonstrated $CH_3OH$ as a direct product of electrochemical $CO_2$ reduction reactions on Mo (Summers et al., 1986), and several types of Ru electrodes (Frese et al., 1985; Bandi, 1990; Popic et al., 1997; Spataru et al., 2003; Qu et al., 2005) at current densities less than 2 mA $cm^{-2}$ with Faradaic efficiencies up to 60%. At present, the greatest reported current densities and Faradaic efficiencies towards $CH_3OH$ production are associated with oxidized Cu electrodes with current densities up to 33 mA $cm^{-2}$ and Faradaic efficiencies greater than 100% (Frese, 1991). It is important to note Faradaic efficiencies are based on a six-electron reduction reaction and efficiencies greater than unity indicate electrochemical-chemical (EC or CE) mechanisms (Frese, 1991; Gattrell et al., 2006; Hori, 2008).

Although the oxidation states and electrode stability were not explicitly considered in previous electrocatalytic reduction studies, copper oxide catalysts are known to favor $CH_3OH$ in both photoelectrochemical and hydrogenation systems. Photoelectrochemical $CO_2$ reduction reactions are typically performed on Cu-loaded titania surfaces; however, quantum efficiencies for $CO_2$ reduction under UV or solar radiation conditions are typically very low (Tseng et al., 2002; Wu et al., 2005). As with Cu-based electrodes, $CH_3OH$ formation at photoelectrodes is associated with oxidized Cu species, particularly Cu/Cu(I) interfaces (Nakatsuji et al., 2000;



*Reprinted by permission of "Electrochemical Reduction of $CO_2$ to Methanol at Copper Oxide Surfaces"

Slamet et al., 2009). Likewise, several works suggest copper oxides, Cu cations, or oxide interfaces provide active reduction sites and ZnO stabilizes oxidized Cu in hydrogenation reactions (Fujitani et al., 2000; Wu et al., 2001; Yang et al., 2010). In this work, we examine the surface chemistry and $CH_3OH$ formation behavior of several electrocatalysts with Cu(I) surface sites and consider the possible pathways for the direct electrochemical reduction of $CO_2$ to $CH_3OH$.

## 3.2 Experimental

### 3.2.1 Fabrication of Electrodes

Electrodes for $CO_2$ reduction were fabricated via oxidization of Cu foils (99.99%, ESPI Metals) or thin film electrodeposition. Air-oxidized electrodes were prepared by first cleaning the foil in 0.1 M hydrochloric acid (HCl) (36.5-38.0%, Sigma-Aldrich) for 20 seconds followed by oxidation in an air furnace at 403 K for 17 hours. Anodized electrodes were created by electrochemically oxidizing Cu foil in 0.5 M potassium bicarbonate ($KHCO_3$) (99.7%, Sigma-Aldrich) at a constant potential of 1.25 V (SCE) for 3 minutes. Cuprous oxide thin films ($Cu_2O$) were electrodeposited on stainless steel substrates at –0.555 V (SCE) and 333 K for 30 minutes in a lactate solution including 0.4 M copper sulfate ($CuSO_4$) (> 99%, Sigma-Aldrich) and 3 M lactic acid (Sigma-Aldrich) at pH 9.0 with Cu foil as the anode (Golden et al., 1996; Mahalingam et al., 2002). All electrodes were rinsed with deionized water and dried under $N_2$ before use as cathodes. An Ag/AgCl electrode saturated with NaCl was selected as the reference electrode along with a Pt wire as the counter electrode. A Princeton Applied Research Model 263A potentiostat was used in all electrochemical experiments.

### 3.2.2 Electrochemical Reduction Reaction and Electrode Characterization

The $CO_2$ reduction experiments were performed in a typical three - electrode cell (30 mL

volume) at potentials ranging from –1.0 V to –1.9 V (SCE). Typical cathode areas ranged from 1.0 to 2.0 $cm^2$. An aqueous electrolyte (0.5 M $KHCO_3$) was saturated with ultrapure $CO_2$ (99.9999%, Airgas, USA) by bubbling for 30 minutes (298 K, pH 7.6). Faradaic efficiencies were calculated assuming six electrons are required per $CH_3OH$ molecule. Liquid phase samples were taken from the sealed reactor via a syringe septum and reaction products were analyzed by Gas Chromatography-Flame Ionization Detector (GC-FID) (Agilent, GC5890). Electrolytes were purified prior to the reaction by pre-electrolysis at 0.025 mA $cm^{-2}$ for 24 hours with Pt wires as both cathode and anode (Hori et al., 2005). Before pre-electrolysis, $Zn^{2+}$ concentrations were approximately 0.2 ppm and $Fe^{2+}$ concentrations were less than 0.02 ppm as determined by Inductively Coupled Plasma - Mass Spectrometry (ICP-MS). After pre-electrolysis, ion contamination levels were below detectable limits (0.02 ppm).

The electrochemical behavior of copper oxide electrodes were evaluated using cyclic voltammetry at a scan rate of 10 mV $s^{-1}$ in the same $CO_2$ saturated 0.5 M $KHCO_3$ electrolyte used in reduction studies. Microstructure and morphology were analyzed using Hitachi S-3600N Variable Pressure Scanning Electron Microscope (VP-SEM). Near-Edge X-ray absorption fine structure (NEXAFS) measurements were performed at the LSU Center for Advanced Microstructures and Devices (CAMD) synchrotron's varied-line-space plane-grating-monochromator (VLSPGM) beamline. The photon energy scale was calibrated with Cu standard samples (CuO, Cu and $Cu_2O$). The incident beam intensity was concurrently monitored by an Au mesh placed in the incident beam before sample. The measured sample spectrum $I_0$ (total electron yield mode) was normalized by the total electron yield of the Au mesh. Reproducibility of the spectra was carefully monitored and verified by multiple scanning (typically four times). NEXAFS spectra were acquired at room temperature at both the O K-edge and the Cu L-edge

regions. Auger electron spectra were obtained using an Ultra-high Vacuum X-ray photoelectron spectroscopy (UHV XPS), a Perkin-Elmer PHI 5100 system using Al Kα X-ray source, at the Major Analytical Instrumentation Center (MAIC) at University of Florida including sputter depth profiling. Crystal orientations of copper oxides were analyzed by X-ray Diffraction (XRD) using a Cr-K$\alpha$ ($\lambda$ = 2.291 Å) source at a scanning rate of 3˚ min$^{-1}$.

### 3.3 Results

#### 3.3.1 Electrochemical Reduction Reaction

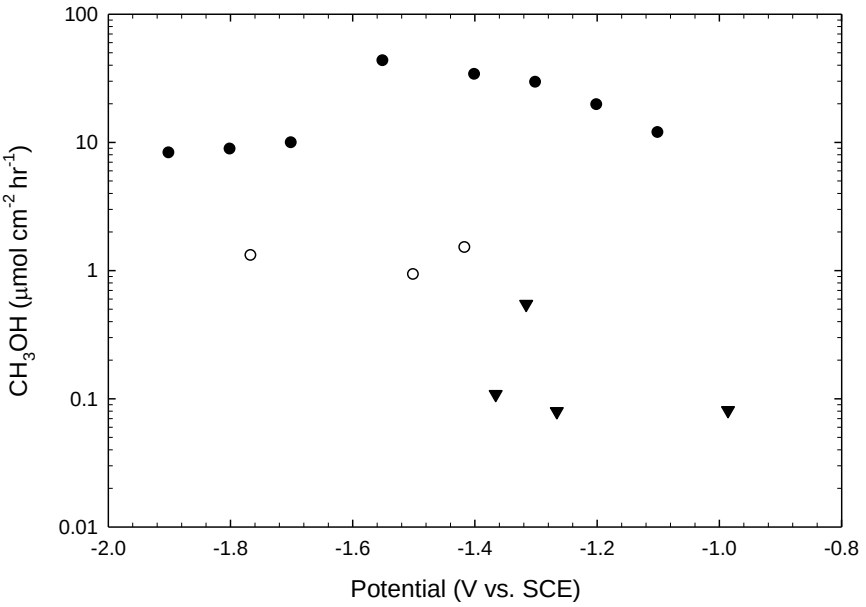


Figure 3.1. $CH_3OH$ formation rate versus potential of ▼, air-oxidized Cu; ○, anodized Cu; ●, electrodeposited cuprous oxide film.

As shown in Figure 3.1, $CH_3OH$ formation rates at electrodeposited cuprous oxide electrodes are quite high ranging from 10 to 43 μmol cm$^{-2}$ hr$^{-1}$; yields from anodized Cu electrodes ranged from 0.9 to 1.5 μmol cm$^{-2}$ hr$^{-1}$; and yields from air-oxidized Cu electrodes ranged from 0.08 to 0.9 μmol cm$^{-2}$ hr$^{-1}$ (all based on geometric electrode areas). Formation rates typically increase with potential from –1.1 V (SCE) and reach a maxima near -1.55 V (SCE), then decrease dramatically at potentials more cathodic than -1.55 V (SCE) accompanied with

significant hydrogen evolution. Figure 3.2 shows electrodeposited cuprous oxide electrodes allow significantly higher Faradaic effeciencies relative to anodized Cu and air-oxidized Cu electrodes. The greatest Faradaic efficiency (38%) was also observed using electrodeposited cuprous oxide electrodes at -1.1 V (SCE). No liquid phase products other than $CH_3OH$ were detected and gas phase analysis showed predominantly $H_2$ and trace amounts of CO.

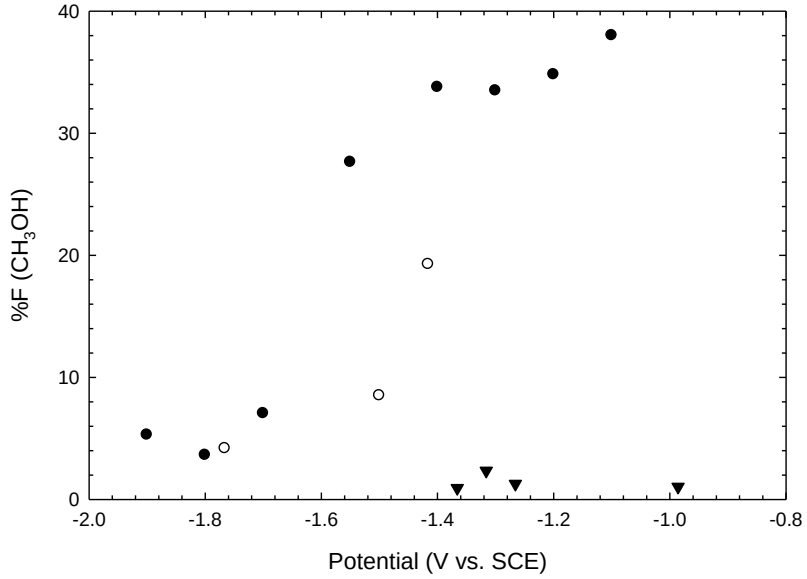


Figure 3.2. Faradaic efficiencies versus potential of ▼, air-oxidized Cu; ○, anodized Cu; ●, electrodeposited cuprous oxide film.

Initial experiments also showed product distribution is dynamic at all oxidized Cu electrodes; $CH_3OH$ formation rates tend to diminish at longer reaction times (>30 minutes) and are accompanied with $CH_4$ generation. As described by Hori, $CH_4$ is the primary reduction product at Cu electrodes which suggests these oxides are reduced during the reaction. In this case, a potential of -1.5V (SCE) was used with a batch reaction time of 10 minutes to maximize product detectability without significant loss in activity. While the primary loss of activity may be associated with reduction of the active copper oxides, losses may also be affectd by contamination from the impurities in the electrolyte or $CH_3OH$ oxidation at counter electrode (Hori, 2008).

### 3.3.2 Scanning Electron Microscope (SEM)

In efforts to understand the dynamic reaction behavior at copper oxide electrodes, we examined the surface morphology, composition and structure of the electrodes before and after 10 minute reduction reactions. Figure 3.3 shows SEM images of the electrodes before and after the 10 minute $CO_2$ reduction reaction at –1.5 V (SCE). Dispersed crystallites approximately 1 µm in size with 2 µm spacing are seen on the air-oxidized Cu electrode in Figure 3.3(a). The microcrystals are absent after the 10 minute reaction at –1.5 V (SCE) as shown in Figure 3.3(b). As seen in Figure 3.3(c), anodized Cu electrodes show a porous layer (approximately 200 nm thick) with copper oxide nodules approximately 2 µm in diameter before the reaction and smaller nodules after the reaction as seen in Figure 3.3(d). Figure 3.3(e) reveals electrodeposited cuprous oxide crystals with well-defined four-sided pyramid geometry with a strong (100) orientation; crystal dimensions are approximately 2 µm on edge and the film is approximately 2 µm thick. As with the anodized electrode, average crystal dimensions are reduced to less than 1 µm after the reaction as shown in Figure 3.3(f).

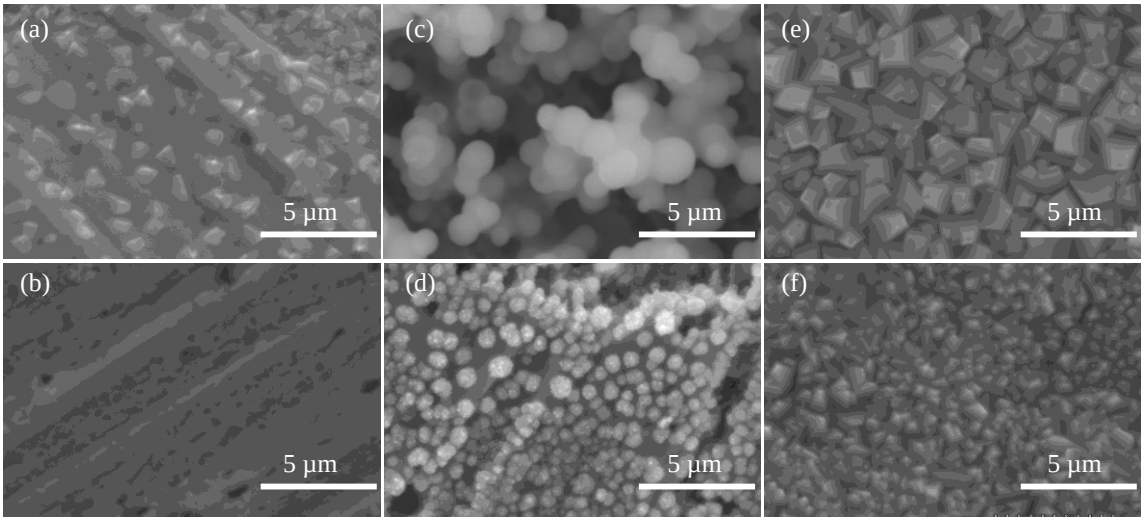


Figure 3.3. SEM images of (a), air-oxidized Cu before reaction; (b), after reaction; (c), anodized Cu before reaction; (d), after reaction; (e), electrodeposited cuprous oxide film before reaction; (f), after reaction.

$CH_3OH$ yields from the cuprous oxide thin film electrodes are remarkable, at least one order of magnitude greater than the anodized electrode and two orders of magnitude greater than the air-oxidized electrode based on apparent (geometric) electrode area. Actual areas of the electrodes relative to the apparent areas were estimated as 1.3x greater for the air-oxidized sample, 3.0x greater for the anodized sample and 1.7x greater for the cuprous oxide film based on SEM analysis. If yields are normalized to actual (estimated) surface areas, the anodized Cu yield results are comparable to the air-oxidized electrode while yields from the cuprous oxide film remain approximately two orders of magnitude greater than either the air-oxidized or anodized electrodes. The dramatic increase in $CH_3OH$ yields associated with the cuprous oxide thin film suggests Cu(I) species may play a key role in reducing $CO_2$ to $CH_3OH$.

### 3.3.3 X-Ray Diffraction (XRD)

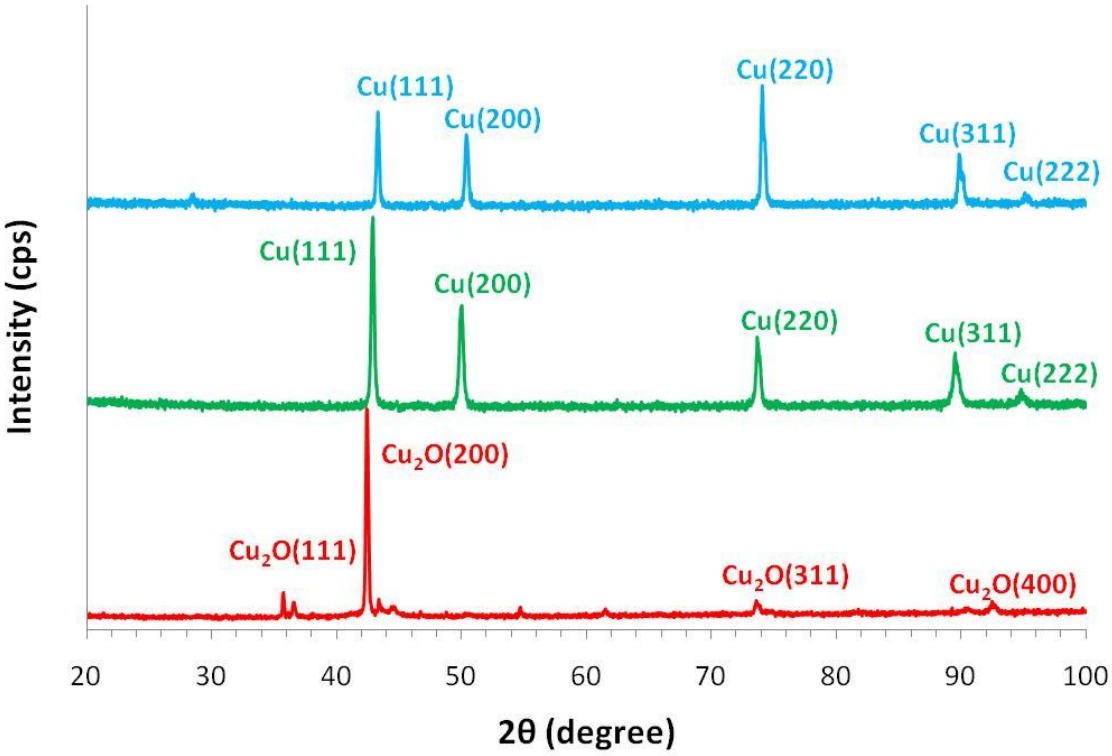


Figure 3.4. XRD spectra of (a), air-oxidized Cu; (b), anodized Cu; (c), electrodeposited cuprous oxide film before reaction.

An XRD pattern from the electrodeposited cuprous oxide film prior to the reduction reaction is presented in Figure 3.4. A strong signal at $2\theta = 42.2^{\circ}$ associated with $Cu_2O$ (200) orientation. This is consistent with Golden et al. and Wang et al. work using similar electrodeposition techniques (Golden et al., 1996; Mahalingam et al., 2002). XRD patterns of air-oxidized Cu and anodized Cu samples show spectra typical of polycrystalline Cu substrates (Chow et al., 1997).

### 3.3.4 Near Edge X-Ray Absorption Fine Structure (NEXAFS)

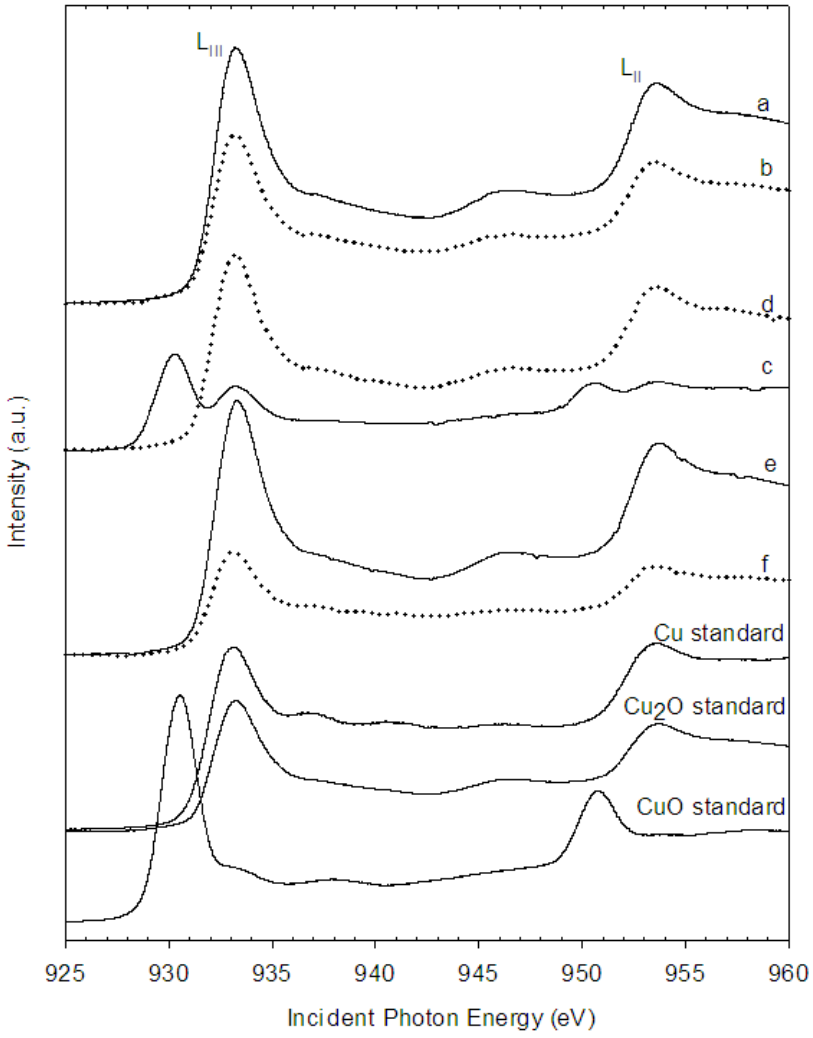


Figure 3.5. NEXAFS spectra of Cu L-edge regions of (a), air-oxidized Cu before reaction; (b), after reaction; (c) anodized Cu before reaction; (d), after reaction; (e), electrodeposited cuprous oxide film before reaction; (f), after reaction.

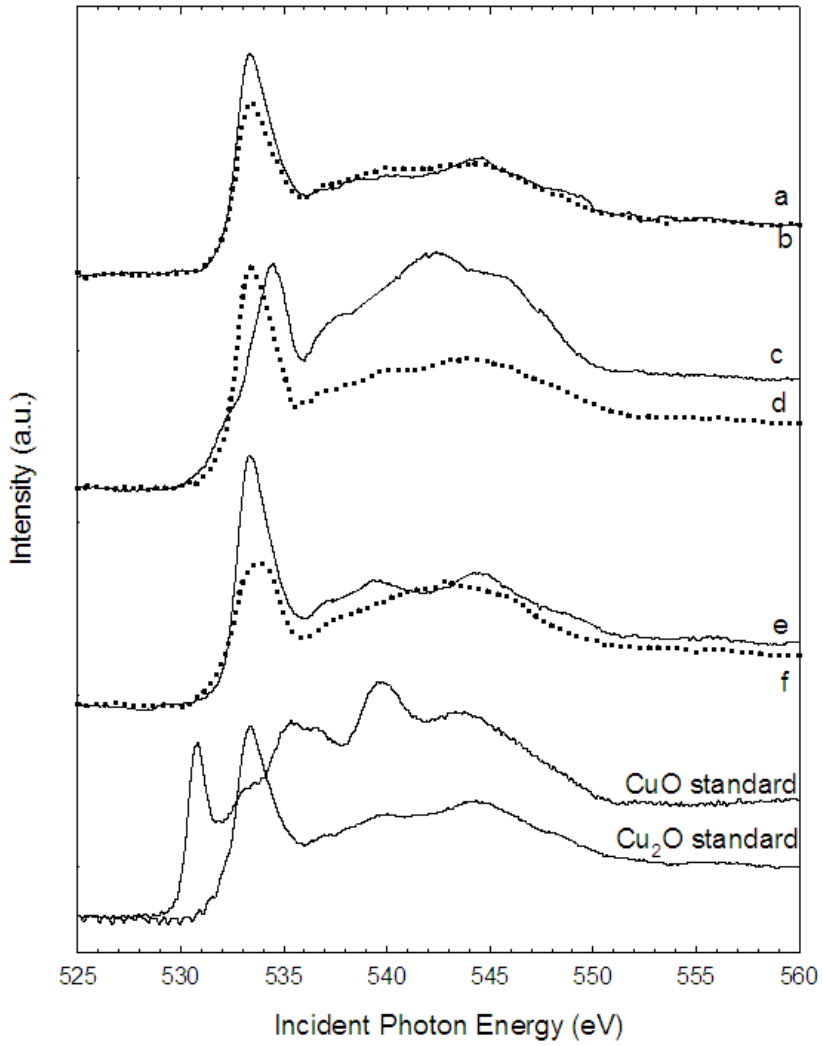


Figure 3.6. NEXAFS spectra of O K-edge regions of (a), air-oxidized Cu before reaction; (b), after reaction; (c) anodized Cu before reaction; (d), after reaction; (e), electrodeposited cuprous oxide film before reaction; (f), after reaction.

Cu L-edge NEXAFS spectra of the air-oxidized, the anodized, and electrodeposited samples, before and after the 10 minute reaction at -1.5V (SCE) are shown in Figure 3.5, along with three standards: Cu(0), Cu(I), and Cu(II). The CuO standard is characterized by two relatively intense features at 930.5 eV and 950.5 eV. They arise from the dipole transitions of the Cu $2p_{3/2}$ ($L_{III}$) and Cu $2p_{1/2}$ ($L_{II}$) into the empty d-states. The smaller peak at ~938 eV is a shake-up (multielectron excitation) satellite. Similarly, the Cu and $Cu_2O$ standards show intense features at ~933 eV and ~953.5 eV, indicating Cu(0) and/or Cu(I) with differing satellite

structure. As seen in Figure 5, the air-oxidized Cu and electrodeposited cuprous oxide film shows a Cu(I) peak at 933.3 eV, with a similar satellite structure as compared with the $Cu_2O$ standard. This peak decreases intensity after the $CO_2$ reduction reaction. Oxide reduction is also confirmed by the O-K edge of air-oxidized Cu and electrodeposited cuprous oxide films with a peak at 533.5 eV and similar satellite structure as $Cu_2O$ standard as shown in Figure 3.6. As for anodized Cu, the $L_{III}$ peak at 930.3 eV attenuates upon reaction and the Cu(I) at 933.3 eV decreases as metallic Cu(0) appears at 933 eV. The O-K edge of the anodized Cu shows a small shoulder at ~530.8 eV and extends to a peak at ~534.5 eV suggesting the anodized Cu electrode surface includes a mixture of CuO, $Cu_2O$ and $Cu_4O_3$ (Schedel-Niedrig et al., 2000).

### 3.3.5 X-Ray Photoelectron Spectroscopy (Auger)

Auger spectra are shown in Figure 3.7 before and after the 10 minute reduction reaction at –1.5 V (SCE). The electrodes were sputter cleaned using $Ar^+$ to remove organic contamination prior to analysis. Results for the air-oxidized electrode show a Cu(I) peak at 917.5 eV prior to the reduction reaction and a well defined Cu(0) peak at 919 eV after the reaction. Likewise, the anodized Cu sample shows a broad peak at 918 eV before the reaction and a Cu(0) peak at 919 eV after the reaction. The electrodeposited cuprous oxide film shows a dominant Cu(I) peak at 917.5 eV before the reaction with a small Cu(0) shoulder at 919 eV. Auger spectra of the electrodeposited cuprous oxide sample after the reaction was inconclusive due to delamination from the support.

Qualitatively, $CH_3OH$ yield trends follow Cu(I) intensities prior to the reaction as determined by NEXAFS and Auger analysis. Electrodeposited cuprous oxide films showed $CH_3OH$ formation rates up to 43 μmol $cm^{-2}$ $hr^{-1}$ and Faradaic efficiencies up to 38%, while air-oxidized and anodized electrodes showed rates at least one order of magnitude lower. Both

Auger and NEXAFS data indicate all oxides electrodes are partially reduced during the 10 minute reaction at –1.5 V (SCE), which is consistent with the observation of decreased $CH_3OH$ yields and the simultaneous increase in $CH_4$ production in longer experiments (>30 minutes). The results suggest $CH_3OH$ production may be primarily associated with Cu(I) surface species which appear to be reduced in a simultaneous process.

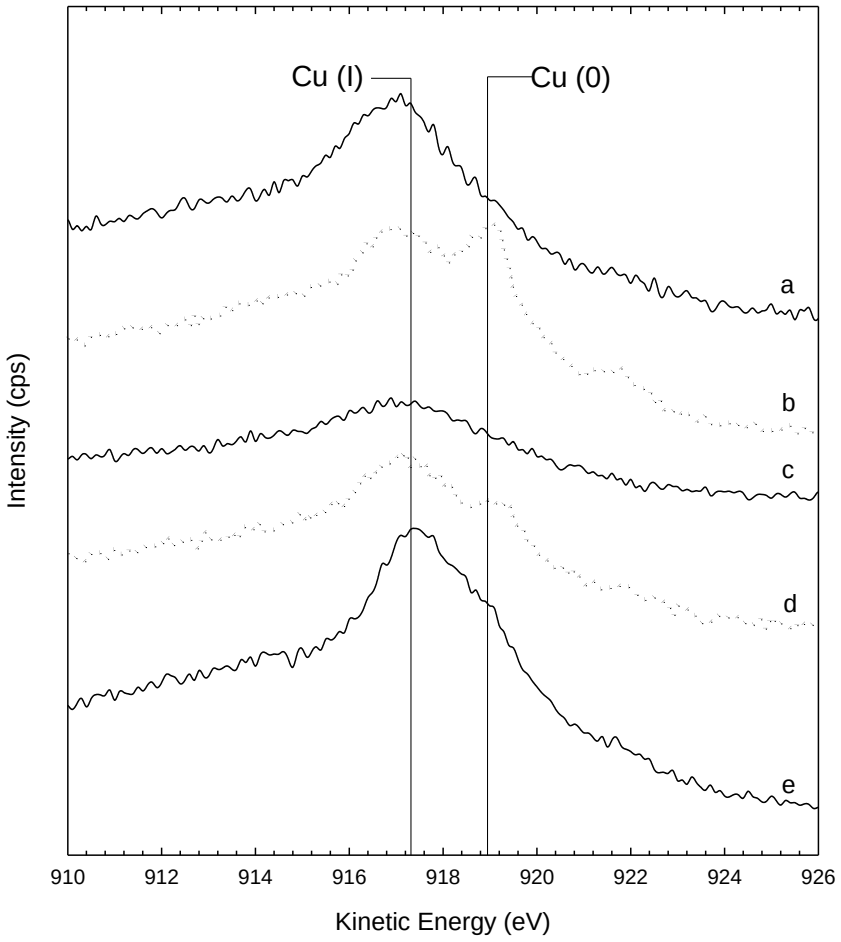


Figure 3.7. Auger spectra (a), air-oxidized Cu before reaction, and (b), after reaction; (c) anodized Cu before reaction, and (d), after reaction; (e), electrodeposited cuprous oxide film before reaction.

### 3.3.6 Cyclic Voltammetry

Cyclic voltammetry shows oxide reduction behavior depends on the method of preparation. As seen in Figure 7, the anodized Cu electrode shows a significant increase in

cathodic current at near –0.7 V (SCE) which diminishes on the reverse scan. Several large reduction peaks from –1.0 V to –2.0 V (SCE) overlapping in the anodized Cu scan suggest copper oxides created in this method are relatively easy to reduce at potentials positive of $CO_2$ reduction. Voltammetric behavior of the air-oxidized Cu and electrodeposited cuprous oxide film shows relatively little hysteresis with an onset reduction potential near –1.2 V (SCE) and –1.0 V (SCE) respectively. This behavior indicates the air-oxidized and cuprous oxide film may be relatively more stable in these electrolytes. Further, while both cuprous and cupric oxides are p-type semiconductors ($E_g$ = 2.1, 1.2 eV respectively) voltammetric analysis did not show any measurable photocurrents under UV or laboratory lighting. The lack of any appreciable photocurrents suggests surfaces are non-homogeneous (including metallic Cu) or include high levels of defects which cause degenerate/metallic behavior.

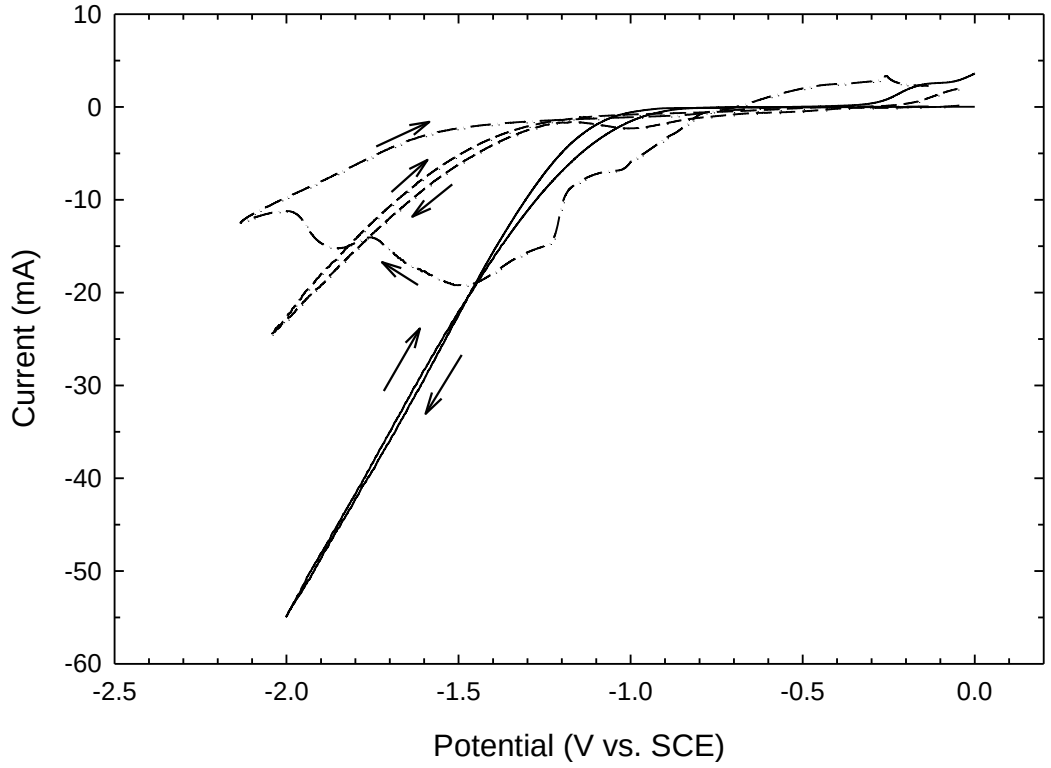


Figure 3.8. Cyclic voltammetry of – –, air-oxidized Cu; –·–·–, anodized Cu; ─, electrodeposited cuprous oxide film.

### 3.4 Discussions

Cu(I) active sites have been proposed in several electrochemical, photoelectrochemical and chemical routes (Chinchen et al., 1986; Chinchen et al., 1987; Frese, 1991; Joo et al., 1999; Nakatsuji et al., 2000; Wu et al., 2001; Tseng et al., 2002; Liu et al., 2003; Saito et al., 2004; Wu et al., 2005; Slamet et al., 2009). Frese suggests the oxides at the surfaces of GaAs, InP, and Mo in aqueous solutions act in a similar fashion as the Cu(I) species allowing improved CO adsorption and may also affect selectivity to $CH_3OH$. Based on the voltage independence of $CH_3OH$ rates and Faradaic efficiencies greater than unity, the author also suggests an initial chemical (nonfaradaic) step involving the formation of adsorbed CO and $O^-$ species. Cu(I) sites were considered to allow the valance band electrons to participate in CO adsorption and formyl (HCO) species are presumably formed by the dissociation of water followed by hydrogenation via adsorbed hydrogen. Unfortunately, the nature of the selectivity to $CH_3OH$ rather than $CH_4$ at copper oxides was not explicitly considered and hydrogen dissociation at metallic Cu is known to be relatively slow (Sheffer et al., 1989; Szanyi et al., 1991; Yang et al., 2010).

Although there is no general consensus on the mechanism for hydrogenation at Cu/ZnO catalysts, Cu(I) sites are thought to promote catalytic activity and selectivity toward $CH_3OH$ (Herman et al., 1979; Chinchen et al., 1986; Chinchen et al., 1987; Sheffer et al., 1989; Szanyi et al., 1991; Bailey et al., 1995; Sahibzada et al., 1998; Liu et al., 2003; Nakamura et al., 2003; Ozawa et al., 2007). While Cu-Zn alloys are considered active sites for $CO_2$ reduction, Cu(I) sites are considered key species for CO adsorption in hydrogenation reactions (Herman et al., 1979). Further, Cu(I) sites are believed to stabilize reaction intermediates such as carbonates ($CO_3^{2-}$-), formates ($HCOO^-$-) and methoxy adsorbates ($H_3CO^-$-) due to their higher heats of adsorption (Bailey et al., 1995). Further, Cu / ZnO hydrogenation catalysts rely on the addition

of oxidizers ($H_2O$, $O_2$, and $CO_2$) to retain Cu(I) sites and promote CO adsorption by decreasing the reduction potential of the $CO/H_2$ feed (Herman et al., 1979; Sahibzada et al., 1998; Nakamura et al., 2003; Ozawa et al., 2007). Sheffer et al. showed alkali metals help stabilize Cu(I) active sites and increase Cu(I) concentrations which significantly improve $CH_3OH$ yield (Sheffer et al., 1989). Similarly, Cu(I) species are considered as the active sites in $CH_3OH$ oxidation reactions at copper oxide surfaces. Oxidation studies at single crystal Cu(I) shows $H_3CO$ adsorbed at (111) surfaces (with Cu(I) atoms at the second atomic layer) allows coordinately unsaturated oxygen anions to act as hydrogen abstraction sites for dehydrogenation (Cox et al., 1990). In this case, it is possible the unsaturated oxygen atoms at the (111) surfaces of the cuprous oxide film (Figure 3.3) act as a hydrogen donors sites in the reduction reaction.

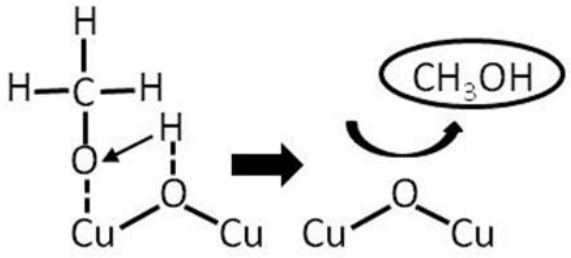


Figure 3.9. Hydrogenation of methoxy adsorbates at $Cu_2O$ (111) surfaces.

A recent theoretical report by Peterson et al. describes a pathway for the electrochemical reduction of $CO_2$ to $CH_4$ at Cu electrodes based on Density Functional Theory (DFT) and Computational Hydrogen Electrode (CHE) models applied to Hori's experimental data (Peterson et al., 2010). In that work, the authors indicate that the carbon atom of CO adsorbates may be hydrogenated via proton transfer to form HCO at -0.74 V (RHE). Hydrogenation of an adsorbed CO species is proposed to occur directly via proton addition from solution since their availability is significantly greater than hydrogenation from adsorbed hydrogen. Accordingly, once the HCO species is formed, the carbon atom continues proton and electron transfer reactions to form

$H_3CO$ adsorbates. Following this pathway, the last proton transfer to the $H_3CO$ species (on Cu (211) surfaces) favors $CH_4$ formation by 0.27 eV. In the case of cuprous oxide electrodes as described here, the reduction reaction may benefit from both improved intermediate stability and the ability of $H^+$ species coordinated with surface bound oxygen. This surface would allow hydrogen addition to the oxygen atom of the $H_3CO$ adsorbate rather than the carbon atom as shown in Figure 3.9.

While these results show copper oxides are reduced along with $CO_2$, it is interesting to consider Cu(I) stability relative to photoelectrochemical or hydrogenation conditions. In contrast with $CH_3OH$ generation via electrochemical reduction processes where oxidation and reduction reactions are spatially separated, photoelectrochemical and hydrogenation reactions may benefit from relatively stable Cu(I) species. In fact, the photoelectrochemical process with Cu-loaded titania may follow a similar mechanism as the electrochemical case; however, there is no net charge difference at the electrode and the titania may help maintain Cu in the Cu(I) state. Likewise, the water and zinc oxides used in hydrogenation reactions may help promote stable Cu(I) species and reaction intermediates while allowing hydrogenation of oxygen atoms by adsorbed hydrogen as described in the model by Peterson.

**3.5 Conclusions**

This chapter successfully proves the direct relationship between methanol formation rate and Cu(I) intensity on the catalysts' surface. $CH_3OH$ formation rates increase with increasing Cu(I) intensity as determined by NEXAFS and Auger analysis. Electrodeposited cuprous films with a strong crystal orientation in the (100) orientation showed the greatest $CH_3OH$ formation rate (up to 43 μmol $cm^{-2}$ $hr^{-1}$) and Faradaic efficiencies up to 38%. Faradaic efficiencies diminish significantly at potentials more cathodic of –1.5 V (SCE) due to the hydrogen evolution reaction.

While Cu electrodes yield $CH_4$ as the primary product, Cu(I) species may show selectivity toward $CH_3OH$ formation by enabling hydrogenation of oxygen atoms from $H_3CO$ adsorbates. All SEM, NEXAFS, and Auger data suggests $CH_3OH$ yields are dynamic and copper oxide ($Cu_2O$, $Cu_4O_3$ and CuO) are reduced to metallic Cu in a simultaneous process at potential required for $CO_2$ reduction. These results indicate the loss in selectivity towards $CH_3OH$ is associated with reduction of copper oxide species rather than contamination. Chapter 4 will continue this study by introducing a new designed catalyst (Cu, $Cu_xO$ supported on ZnO substrates) with the hope of forming a more stable electrocatalyst for the direct $CO_2$ reduction.

# CHAPTER 4. REDUCTION OF $CO_2$ AT CU/ZNO AND $CU_XO$/ZNO SURFACES

## 4.1 Introduction

As Cu(I) species have demonstrated greater activity and selectivity toward $CH_3OH$ formation as shown in Chapter 3, copper oxides are reduced in a simultaneous process during the $CO_2$ reduction reaction. A more stable catalyst in terms of activity, selectivity, and stability is essential. Since the active sites appear to be associated with Cu(I), a first approach would focus on stabilizing copper oxide surface sites. While ZnO and $TiO_2$ have been demonstrated as essential support for Cu catalyst in both hydrogenation and photoelectrochemical reduction process for methanol formation (Tseng et al., 2002; Liu et al., 2003; Wu et al., 2005), these oxides have not been used as electrocatalysts in purely electrochemical reduction process. Since only specific sites on ZnO faces are active in methanol formation (Wilmer et al., 2003), and $CO_2$ electrochemical reduction is a highly surface sensitive reaction, using polycrystalline ZnO samples with mixed crystal planes would be difficult to fully understand the catalytic active sites. In this work, we examine the surface chemistry and $CO_2$ reduction reaction behavior of Cu and $Cu_xO$ nanoclusters supported on ZnO (10-10) single crystals.

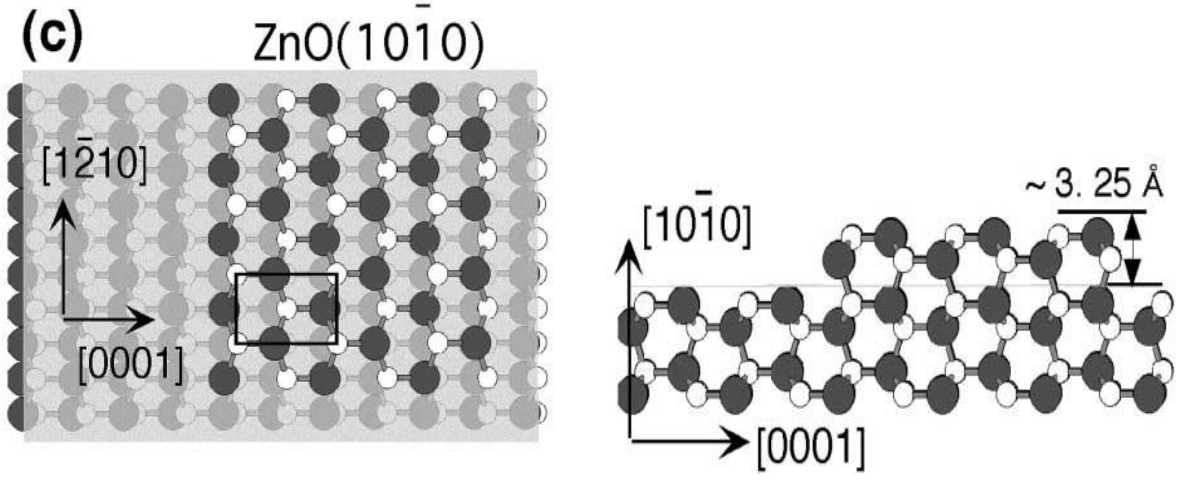


Figure 4.1. The (a), top; and (b), bottom views of ZnO (10-10) surface (reprinted from (Dulub et al., 2002))

The ZnO (10-10) surface is the most stable face with the lowest surface cleavage energies (2.32 J $m^{-2}$) compared to others ((0001)-Zn: 4 J $m^{-2}$, (000-1)-O: 4 J $m^{-2}$, (11-20): 4.1 J $m^{-2}$) (Wander et al., 2001). This surface does not exhibit any reconstruction and is autocompensated since it consists of equal number of Zn and O atoms per unit area and the same number of Zn and O bonds are broken when the surface is formed. The ZnO (10-10) surface has a perfect flat structure with rectangular terraces separated by single step edges along the (1-210) and (0001) directions as shown in Figure 4.1 (Dulub et al., 2002). With such a stable and well-defined structure, the ZnO (10-10) face may provide an electrostatically stable support for the Cu(I) surface in the $CO_2$ reduction reaction. Besides, using a single crystal platform allows improved collaboration between simulation, materials characterization, and catalyst evaluation. Therefore, a better understanding of how surface chemistry affects catalyst performance at an atomic level and possible reaction mechanism can be established to achieve the ultimate goal: "electrocatalysts by design" for $CO_2$ reduction.

## 4.2 Experimental

### 4.2.1 Fabrication of Electrodes

Electrodes for $CO_2$ reduction are fabricated via non polar ZnO (10-10) single crystals (MTI Corporation). After cleaning in a sequence of de-ionized $H_2O$, acetone, methanol, de-ionized $H_2O$, ZnO substrates are ready to be transferred into an ultra high vacuum (UHV) chamber for the sputter – anneal and copper deposition processes. The chamber's pressure is kept below 1E-9 Torr. For the sputtering process, the chamber is filled with $Ar^+$ as inert gas up to 5E-5 Torr and surface atoms are bombarded with ionized $Ar^+$. Typical beam voltage and emission current for the sputtering process are 1.0 kV and 15-20 mA, respectively. The samples are heat treated by annealing up to 700 ˚C and 5E-9 Torr for surface recovery from the sputtering

process. In this chamber, each ZnO crystal goes through at least five sputter – anneal cycles to eliminate any adsorbed substances, as well as to obtain a smooth surface. Auger Electron Spectroscopy (AES) or low-energy electron diffraction (LEED) is used to analyze the surface cleanliness by bombardment with a collimated beam of low energy electrons (20-200eV), and diffracted electrons were observed as spots on a fluorescent screen. After obtaining a clean, purified ZnO single crystal, the sample's surface is evaporated with copper (Alfa Ltd) via an E-beam evaporator. In this physical vapor deposition process, copper is bombarded with an electron beam from a charged tungsten filament (20 – 40 V) to precipitate onto the ZnO substrates. Then, the samples are either annealed up to 150 → 200 ˚C to form Cu clusters (Cu/ZnO) or exposed to $O_2$ at 400 → 450 ˚C and 1E-7 Torr to form copper oxide nanoclusters on ZnO ($Cu_xO$/ZnO).

### 4.2.2 Electrochemical Reduction Reactions and Electrode Characterization

The $CO_2$ reduction experiments are performed in a typical three electrode cell (30 mL volume) at potentials of –1.4 V, –1.5 V, –1.6 V (Ag/AgCl) for 10 to 35 minutes. Typical cathode areas range from 0.4 to 0.8 $cm^2$. An aqueous electrolyte (0.5 M $KHCO_3$) is saturated with ultrapure $CO_2$ (99.9999%, Airgas, USA) by bubbling for 30 minutes (298 K, pH 7.6). An Ag/AgCl electrode saturated with NaCl is selected as the reference electrode along with a Pt wire as the counter electrode. A Princeton Applied Research Model 263A potentiostat is used in all electrochemical experiments. Liquid and gas phase samples are taken from the sealed reactor via a syringe septum, and reaction products are analyzed by Gas Chromatography-Flame Ionization and Thermal Conductivity Detector (GC-FID&TCD) (Shimadzu, GC 2014).

A UHV Scanning Tunneling Microscope (STM) is used to image electrodes' surfaces at the atomic level. The electrodes' microstructure and morphology are analyzed using an Agilent

5500 Atomic Force Microscopy (AFM) equipped with a Picoscan software. Non-conductive silicon nitride probes (Model: MSCT-AUNM) (Veeco Probes) with spring constant of 0.5 N $m^{-1}$ are used for imaging experiments. The tip speed for approaching to or withdrawing from the surface is 10 nm $s^{-1}$, and the scan rate is 3 nm $s^{-1}$. A Nicolet 6700 In-situ Fourier Transform Infrared Spectroscopy (FTIR) is used to identify possible intermediates and predict mechanism model. The IR experiment is conducted with 64 scans, 4 $cm^{-1}$ resolution, and a MCTA detector. A full integration OMNIC software is used for analysis. A reactor is specifically designed to be used in this in-situ FTIR experiment with a $CaF_2$ IR transparent window between the electrode surface and the beam contacting area. This window allows IR beam to pass through a thin layer of electrolyte to reach the electrode's surface and be reflected with an incidence angle of 65˚.

### 4.3 Results

#### 4.3.1 Scanning Tunneling Microscope (STM)

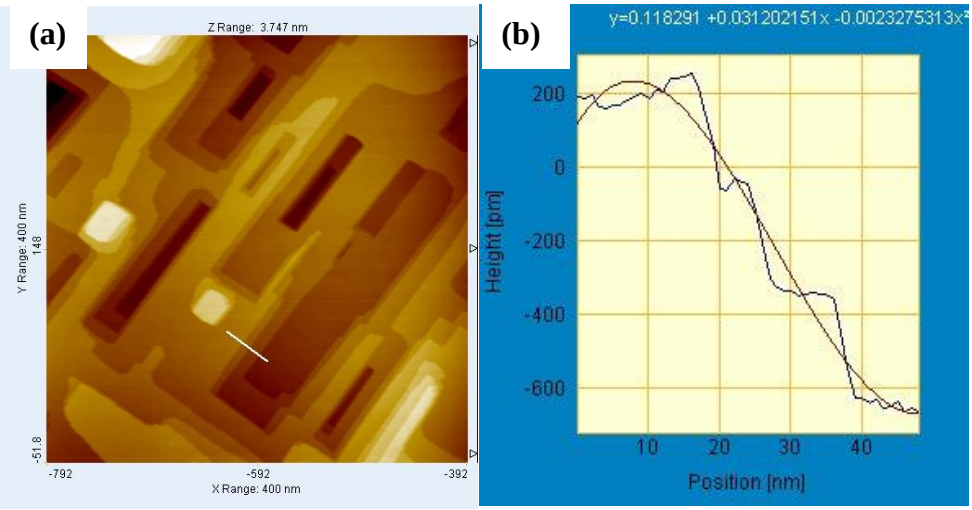


Figure 4.2. (a), STM image of ZnO (10-10); (b), STM depth profile of ZnO (10-10) (Zhang et al. to be published) .

The geometric model and electronic structure of Cu based ZnO (10-10) is studied with Scanning Tunneling Microscope (STM). The STM images reveal a smooth and well defined structure of the pure non polar ZnO(10-10) substrate as seen in Figure 4.2(a). The defect free

surface allows high quality copper film growth and represents a good model system for surface chemistry experiment. Figure 4.2(b) shows a depth profile of the ZnO substrate with three layers approximately 200 pm in height per layer creating numerous step edges on the surface. These step edges may provide active sites for copper and copper oxide nanoclusters deposition and increase Cu-O-Zn interactions.

### 4.3.2 Electrochemical Reduction Reaction

Initial $CO_2$ electrochemical reduction experiments at Cu/ZnO and $Cu_xO$/ZnO electrodes show $CH_3OH$ formation rates ranging from 1.11 μmol $cm^{-2}$ $hr^{-1}$ to 86.7 μmol $cm^{-2}$ $hr^{-1}$. For each sample, $CO_2$ reduction reactions are attempted at least two times and repeatability for $CH_3OH$ yields is difficult. Table 4.1 lists reaction conditions and results for four Cu/ZnO and $Cu_xO$/ZnO samples which yield $CH_3OH$. The experimental potential ranges from –1.4 V to –1.6 V (Ag/AgCl), and reaction time ranges from 10 to 35 minutes. The greatest $CH_3OH$ yield (86.7 μmol $cm^{-2}$ $hr^{-1}$) is obtained from Sample 1, a copper oxide nanoclusters on ZnO single crystal sample. This remarkably high $CH_3OH$ yield of Sample 1 leads to a Faradaic efficiency greater than 100 % suggesting both electrochemical and chemical steps are involved in the $CH_3OH$ production. No liquid phase products other than $CH_3OH$ are detected, and gas phase analysis shows only $H_2$ with formation rate at 0.22 μmol $cm^{-2}$ $hr^{-1}$. The four samples are prepared from the same method introduced in section 4.2; however, their copper evaporating time and annealing temperature are different, which results in different surface structures (Figure 4.3). It is observed that as the potential becomes more cathodic to –1.6 V (Ag/AgCl), the electrodes change to a darker, smoky black color, which may lead to deactivation, while a potential anodic to –1.4 V (Ag/AgCl) have not yet shown any $CH_3OH$ activity. Therefore, $CH_3OH$ formation may only occur in a small window from –1.4 V to –1.6 V (Ag/AgCl).

Table 4.1. Experiment parameters and results for $CO_2$ reduction experiments at Cu/ZnO and $Cu_xO$/ZnO experiments.

| | Sample 1 ($CuO_x$/ZnO) | Sample 2 (Cu/ZnO) | Sample 3 ($CuO_x$/ZnO) | Sample 4 ($CuO_x$/ZnO) |
|---|---|---|---|---|
| Potential (V vs. Ag/AgCl) | –1.4 to –1.5 | –1.5 to –1.6 | –1.6 | –1.5 |
| Current density (mA $cm^{-2}$) | 2.7 | 1.3 | 4.6 | 0.36 |
| Reaction time (minutes) | 10 - 15 | 10 - 35 | 35 | 10 |
| $CH_3OH$ yield (µmol $cm^{-2}$ $hr^{-1}$)* | 4.19 - 86.7 | 1.11 - 15.2 | 9.64 | 1.84 |
| $F_{CH3OH}$ (%) | 33.8 - 516 | 10.0 - 188 | 40.4 | 65.7 |
| $H_2$ yield (µmol $cm^{-2}$ $hr^{-1}$) | 0.22 | 0.29 | 11.83 | NR |
| $F_{H2}$ (%) | 0.43 | 1.20 | 13.78 | NR |

NR: not recorded

* These are ranges of $CH_3OH$ yields observed at Sample 1 – 4. $CO_2$ reduction at each sample is performed at least two times and $CH_3OH$ yield reproducibility is difficult.

### 4.3.3 Atomic Force Microscopy (AFM)

In order to correlate the surface chemistry of Cu/ZnO and $Cu_xO$/ZnO electrodes with their dynamic reaction behavior, AFM images are used to examine the surface morphology, and structure of each sample after the $CO_2$ reduction reaction (Figure 4.3). Dispersed nanoclusters with 50-100 nm diameter and 20 nm in height are observed on Sample 1 as seen in Figure 4.3(a). Figure 4.3(b) and 4.3(c) show similar surface morphology of Cu/ZnO and $Cu_xO$/ZnO with larger clusters: ~500-1000 nm in diameter, except the clusters's height in Figure 4.3(c) ($Cu_xO$/ZnO) are taller than those in Figure 4.3(b) (Cu/ZnO): 30 nm versus 15 nm. Figure 4.3(d) reveals islands and elongated clusters of copper oxide on ZnO surface with ~2.5 nm in height and 300-800 nm in diameter.

$CH_3OH$ yields from Sample 1 are an order of magnitude greater than Sample 2 and 3, and two orders of magnitude greater than Sample 4 based on apparent (geometric) electrode area. Unlike others, sample 1 has completely different surface structure with approximately ~20-40 times smaller clusters than other samples which may increase more ZnO surface exposure and Cu-ZnO interfaces. If yields are normalized based on Cu-ZnO interfaces, $CH_3OH$ yields can be thousands of times higher. $CH_3OH$ yields from Sample 2 and Sample 3 are in the same order of magnitude even though sample 2 is metallic Cu/ZnO and sample 3 is $Cu_xO$/ZnO. Since the electrodes are exposed to atmosphere before the $CO_2$ reaction, all sample surfaces are expected to be oxidized to some degree.

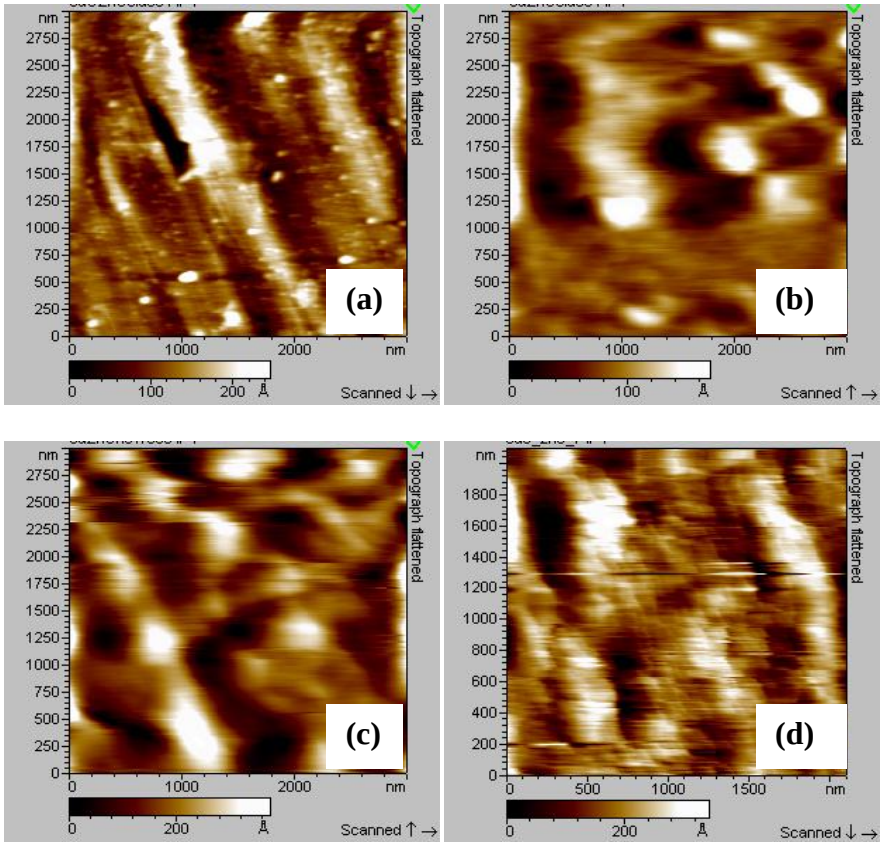


Figure 4.3. AFM images of (a), sample 1 ($CuO_x$/ZnO); (b), sample 2 (Cu/ZnO); (c), sample 3 ($Cu_xO$/ZnO); (d), sample 4 ($Cu_xO$/ZnO) after reaction.

Figure 4.4 compares surface structure and morphology of single crystal ZnO (Figure

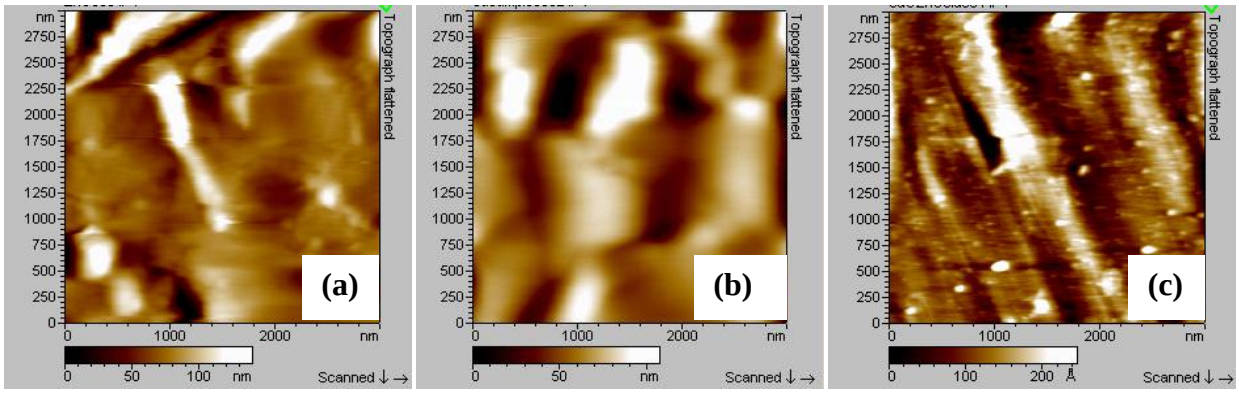


Figure 4.4. AFM images of (a), ZnO (10-10); (b), cuprous oxide thin flim; (c), $CuO_x$/ZnO electrode

4.4(a)), cuprous oxide thin film (Figure 4.4(b)), and nanocluster $Cu_xO$/ZnO (Figure 4.4(c)) surfaces. While ZnO shows no $CH_3OH$ activity, $Cu_xO$/ZnO shows $CH_3OH$ yields up to 86.7 μmol $cm^{-2}$ $hr^{-1}$ at –1.4 V (Ag/AgCl) indicates the presence of copper oxide and Cu-ZnO interface enhances methanol formation in the $CO_2$ reduction reaction. Compared with cuprous oxide thin films from Chapter 3, $CH_3OH$ yield from nanocluster $CuO_x$/ZnO electrode is much higher (86.7 μmol $cm^{-2}$ $hr^{-1}$ versus 43 μmol $cm^{-2}$ $hr^{-1}$), noted yields are calculated based on apparent (planar) 2D surface areas in each case. Although the actual active sites on nanocluster $CuO_x$/ZnO samples are still unknown, oxidized Cu nanoclusters always show improvement in $CH_3OH$ yield compared to metallic Cu/ZnO. Enhancement mechanism may be related to cluster Cu(I) surfaces, interfaces, charge, or stained surfaces. Yields normalized to Cu(I) surfaces or Cu-O-Zn interfaces would be significantly higher. Understanding the effects of surface structure and morphology on $CH_3OH$ yields and the active sites activity in the molecular mechanism will allow us to form a basis for catalyst by design.

### 4.3.4 Fourier Transform Infrared Spectroscopy (FTIR)

In-situ reaction is performed to monitor the reduction reaction behavior over time and detect intermediates via a Nicolet 6700 FTIR spectroscopy. The reaction is performed using

$Cu_xO$ nanoclusters on ZnO (10-10) electrode at -1.5 V vs. Ag/AgCl for 10 minutes. Figure 4.5 reveals the AFM image of the $Cu_xO$/ZnO electrode before reaction with larger clusters (~100 nm in height, and ~200-600 nm in diameter) compared to the four samples shown in section 4.3.3. In-situ FTIR spectra for the $CO_2$ reduction at 1.22 and 9.77 reaction minutes are shown in Figure 4.6.

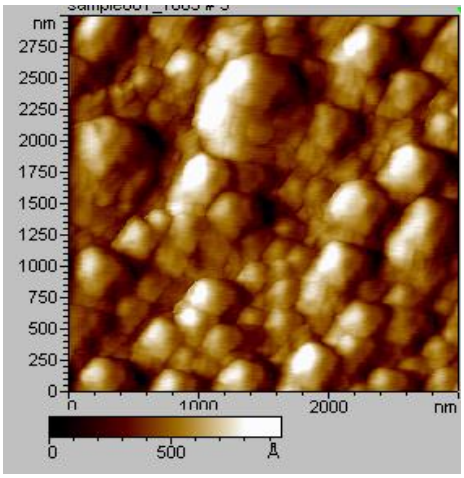


Figure 4.5. AFM of $CuO_x$/ZnO sample (Sample 5)

The background used in this FTIR experiment is a $KHCO_3$ saturated with $CO_2$ solution. The peak for adsorption of $CO_2$ on the sample surface at 2350 $cm^{-1}$ which is clearly shown in the background fully disappears in the IR spectra. This observation confirms the IR spectra are completely subtracted from the background. The intermediate from the first hydrogenation (O=C–OH) doesn't show up in the spectra because its adsorption is similar to that of $HCO_3^-$ which is a major species in the electrolyte background. Although the C≡O band is not detected as adsorbate, the C=O stretching band is shown at 1750 $cm^{-1}$ (Millar et al., 1995; Fisher et al., 1997; Slamet et al., 2009). This C=O stretching band indicates the presence of either formyl (HC=O) or formaldehyde ($H_2C$=O) intermediate or both. Since the 1750 $cm^{-1}$ peak has a considerably broad shape and the signal is relatively strong, C=O stretching band for both formyl and formaldehyde can overlap.

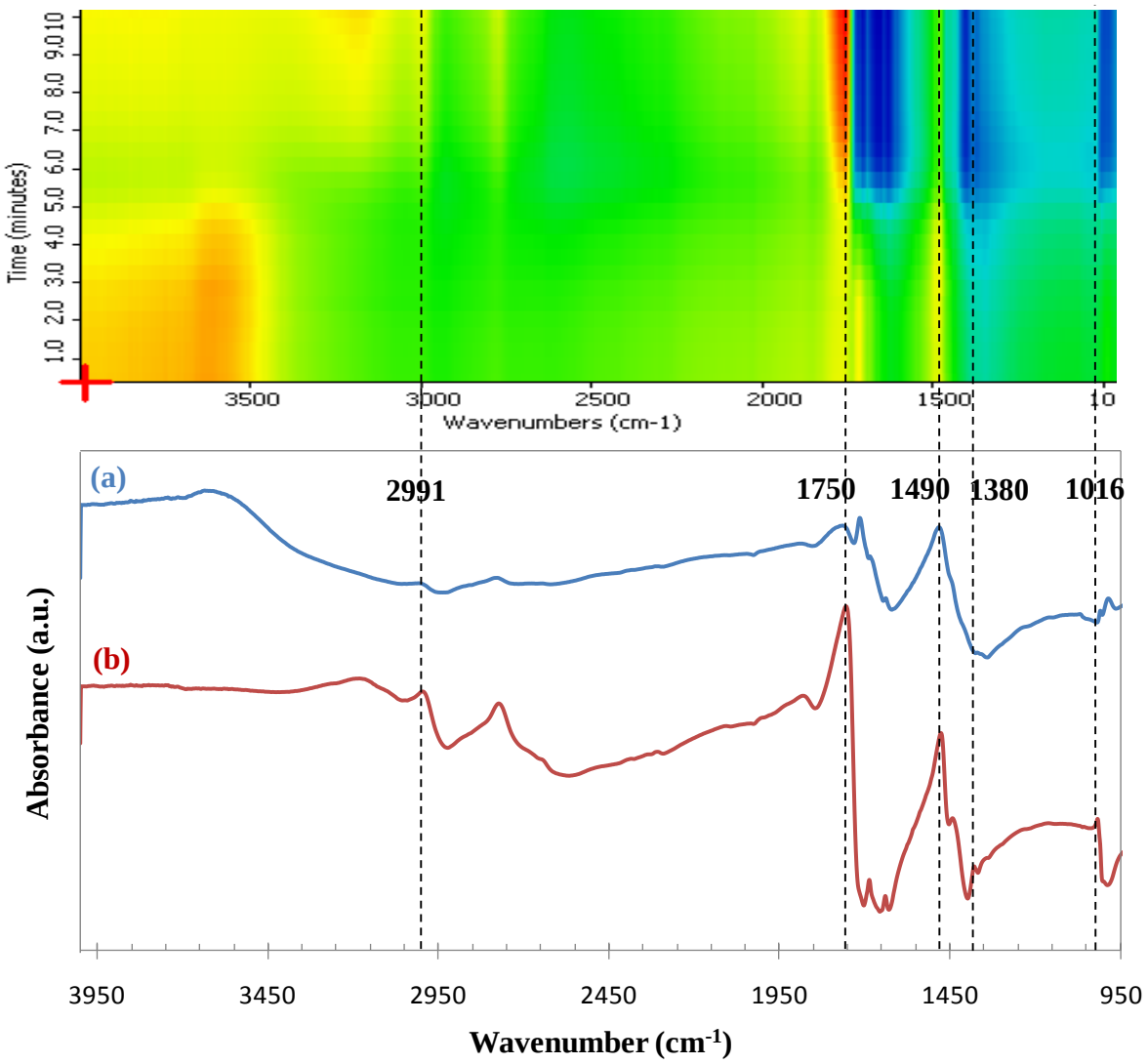


Figure 4.6. In-situ FTIR spectra of $CO_2$ reduction at $Cu_xO$/ZnO electrode (Sample 5) after (a), 1.22 reaction minutes; (b), 9.77 reaction minutes.

The peak observing at 1380 $cm^{-1}$ represents the C–H stretching band for formic acid (HCOOH). Similarly, an FTIR study of formic acid adsorption on potassium – promoted $Cu/SiO_2$ catalyst show infrared band positions of formic acid adsorbing on K/ $SiO_2$, reduced K/Cu/ $SiO_2$ and oxidized K/Cu/ $SiO_2$ surfaces have C–H stretching band positioning at 1376, 1380, and 1377 $cm^{-1}$, respectively (Millar et al., 1995; Fisher et al., 1997; Slamet et al., 2009). While Peterson et al. reports HCOOH is the dead-end product in the electrochemical reduction of $CO_2$ to $CH_4$ at Cu surfaces since experiments starting with HCOOH showed no detectable

products (Hori et al., 1989), Yang et al. claims the main pathway for methanol synthesis from $CO_2$ hydrogenation is via HCOOH intermediate (Peterson et al., 2010; Yang et al., 2010). Although it is not clear at this point whether HCOOH would involve in the mechanism for $CO_2$ electrochemical reduction to methanol at copper oxide surfaces, IR data suggests the presence of HCOOH species.

The C–O stretching band at 1016 $cm^{-1}$ suggests the adsorption of methoxy ($H_3CO$) species on the $Cu_xO$/ZnO electrode surface. Compared to the C–O stretching band in $CH_3OH$ (1030 $cm^{-1}$), the C–O stretching band from our electrode shows an 11 $cm^{-1}$ red shift. As seen in Figure 4.7, our C–O stretching band exhibits a red shift similar to the behavior of methoxy adsorption on Cu (100), Ru (001), Ni (100) and Ni (111) surfaces (Zenobi et al., 1993; Huberty et al., 1996; Andersson et al., 2002; de Barros et al., 2003). A larger anharmonic shift for C–O dissociation energies in methanol compared to that of methoxy chemisorbed (12.5 $cm^{-1}$ versus 8.5 $cm^{-1}$) indicates C–O dissociation energy of methanol is higher (Zenobi et al., 1993). Likewise, a strong interaction between the O atom of $H_3CO$ and electrode surfaces can also weaken the C–O bond and increase its wavelength. This information would lead to a lower stretching frequency for $H_3CO$ adsorbate compared to that of $CH_3OH$. Further, an ab initio calculation on Ni (100) surface show the presence of a coadsorbed hydrogen can raise the vibrational frequency of the neighboring C–O bond; therefore, the addition hydrogen bond in methanol contributes to a higher C–O stretching frequency (Huberty et al., 1996; Yang et al., 1997). The $CH_3$ stretching band at 3000 $cm^{-1}$ also supports the existence of the $H_3CO$ adsorbates. The increase of C=O, C–O and $CH_3$ adsorption bands with increasing reaction time confirms the $CO_2$ reduction activity toward $CH_3OH$ at the $Cu_xO$/ZnO surface. While methoxy is predicted as the last intermediate for $CO_2$ reduction to $CH_4$ at Cu surface by a computational model, this is

the first time methoxy is shown as intermediate for $CO_2$ electrochemical reduction to $CH_3OH$ from an experimental perspective. Table 4.2 lists known adsorption bands observed in this in-situ FTIR assignment.

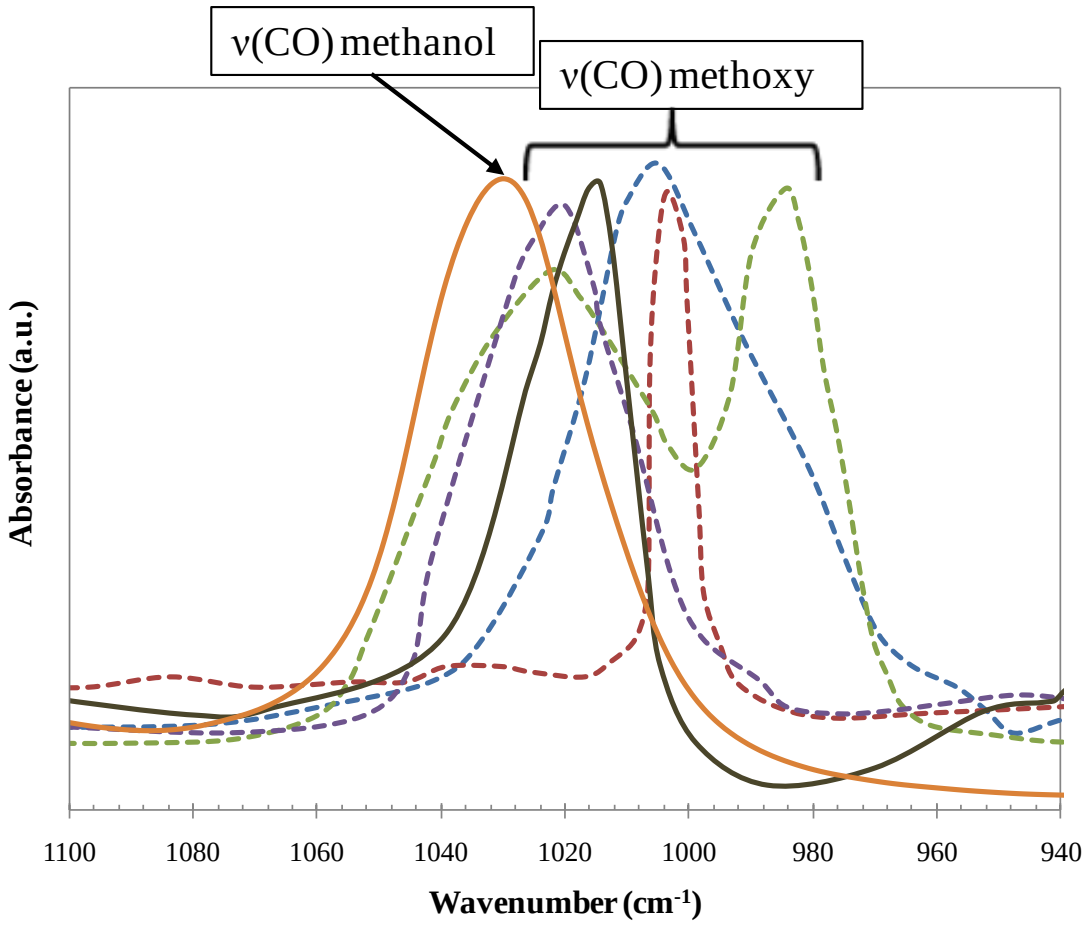


Figure 4.7. IR spectra for C–O stretching band of methanol standard, methoxy adsorbed on $Cu_xO$/ZnO (our results), methoxy adsorbed on Ru (001), methoxy adsorbed on Cu (100), methoxy adsorbed on Ni (100), methoxy adsorbed on Ni (111) (reproduced from (Zenobi et al., 1993; Huberty et al., 1996; Andersson et al., 2002; de Barros et al., 2003)).

The 3D plot in Figure 4.6 illustrates the IR adsorption peak's intensities as a function of time. All peaks appear after the reaction has proceeded for about 5 minutes and remains throughout the 10 minute reaction verifying $CO_2$ reduction activity. Although $H_3CO^-$ adsorbate is detected in the IR spectra, $CH_3OH$ is not detected from the GC since the reaction may be

desorption limited. Similar to a photoelectrochemical reduction study at $TiO_2$ surface, $CH_3OH$ once formed can possibly absorb on the electrode's surface and cover the active sites (Wu et al., 2010). This phenomenon may result in high $CH_3OH$ concentration on the electrode's surface, while the amount of $CH_3OH$ concentration in the bulk electrolyte solution is limited. In addition, the surface morphology of Sample 5 as seen in Figure 4.5 shows bulk copper on ZnO, while other samples with reported $CH_3OH$ yields discussed in the previous section have much smaller copper clusters on the surfaces. Likewise, $CH_3OH$ formation may center on nanocluster of Cu supported on ZnO, and Cu-O-Zn interface may be associated with active sites.

Table 4.2. FTIR adsorption bands observed in the $CO_2$ reduction reaction at $Cu_xO$/ZnO electrode

| Wavenumber ($cm^{-1}$) | Assignment | References |
|---|---|---|
| 2991 | $CH_3$ asymmetric stretching | (Andersson et al., 2002) |
| 1750 | C=O stretching of HCO or $H_2CO$ | (Millar et al., 1995; Williams et al., 2004) |
| 1490 | $CH_3$ asymmetric deformation | (Andersson et al., 2002) |
| 1380 | $CH_3$ symmetric deformation or CH stretching for HCOOH | (Millar et al., 1995; Fisher et al., 1997) |
| 1016 | C–O stretching of $H_3CO$ | (Andersson et al., 2002) |

### 4.3.5 Near Edge X-Ray Absorption Fine Structure (NEXAFS)

The O K-edge NEXAFS spectra of the $Cu_xO$/ZnO electrode before and after the $CO_2$ reduction reaction is shown in Figure 4.7. The O-K edge for $Cu_2O$ and CuO standards are characterized by relatively intense features at 533.5 eV and 530.8 eV, respectively. As seen in the spectra, Cu(II) peak is not observed on any sample. The peak at ~533.5 eV occur at both before and after reaction indicates the presence of Cu(I) nanoclusters on the ZnO surfaces. The

sample after reaction has been through several runs at -1.4 V to -1.6 V (Ag/AgCl) for over 2 hours. Although the Cu(I) peak intensity decrease after reaction, $Cu_xO$/ZnO surfaces are still considerably more stable than the copper oxide surfaces discussed in Chapter 3.

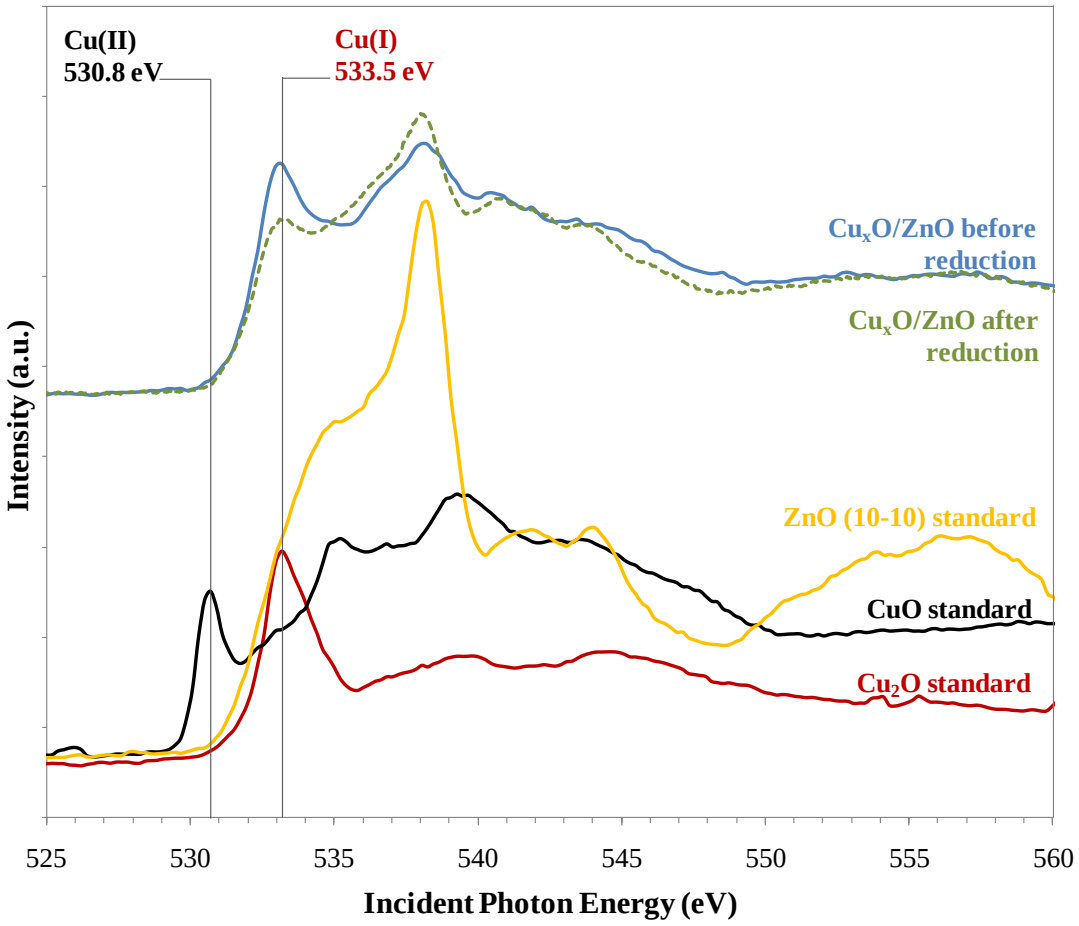


Figure 4.8. NEXAFS spectra of O-K edge regions of $Cu_xO$/ZnO electrode before and after the $CO_2$ reduction.

**4.4 Discussion**

Generally, a clean ZnO (10-10) surface is autocompensated which makes it easier to predict the step edges' stability (Diebold et al., 1998). As shown in Figure 4.1, the (10-10) surface is relatively flatter and has rectangular terraces separated with step edges along the non polar (1-210) and polar (0001) planes. An STM study of Cu deposition on ZnO (10-10) surfaces shows Cu clusters preferentially grow three-dimensionally along the (1-210) direction instead of

on the terraces or (0001) direction (Dulub et al., 2002). However, on slightly contaminated surface with residual gas (CO, $CO_2$, $H_2O$, $H_2$) from the UHV chamber, these 3D Cu clusters can be distributed on the entire surface. Numerous researches have reported ZnO–CO bond is much weaker than Cu–CO bond and Cu(I) is the active site for CO adsorption and methanol synthesis (Waugh, 1992; Harikumar et al., 1998; Casarin et al., 1999).

Studies have shown transition metals with high pseudocapacity or the ability of weakly adsorbed $CO_2$ such as Cu, Zn, Au and Ag would have good electrocatalytic activity towards $CO_2$ reduction (Bandi et al., 1993). The d-orbitals in these metals may be responsible for a covalent bond with $CO_2$ in which the first electron transfer may serve as the rate determining step to form a $CO^{2-}$• anion radical. Cu is unique among others with the ability to break the C–O bond and proceed further though the hydrogen addition process. While a metal such as Cu may act as a Lewis base adsorbing hydrogen to form C-H bond for $CH_4$ and $C_2H_4$ formation, an oxide may behave as a Lewis acid attracting hydroxide for $CH_3OH$ formation. Adsorption of OH groups on ZnO has demonstrated significant roles throughout methanol synthesis process from synthetic gas (Kurtz et al., 2005). In particular, formyl adsorbate may attract the proton of the neighboring OH group to become formaldehyde intermediate followed by hydrogen addition to form methoxy species. The final step for methanol formation would be the proton transfer from another neighboring OH group to methoxy adsorbate. Vibrational data from High Resolution Electron Energy Loss Spectroscopy (HREELS) and Thermal Desorption Spectroscopy (TDS) technique have identified the presence of O–H stretching mode on various ZnO surface indicating the formation of OH species when ZnO is exposed to $H_2O$ at room temperature (Wang et al., 2005; Wang et al., 2006). Since adsorption of OH groups on electrode's surface may be the key to methanol selectivity, increasing binding sites for OH species would be essential. By using

Cu/ZnO electrodes for $CO_2$ reduction, both metal and oxide properties toward methanol formation can be utilized. While Cu increases the electrode's conductivity, ZnO may provide the preferred sites for OH adsorption and create Cu–O–Zn active interface to promote stable Cu(I) species or make Cu(0) behave as Cu(I) for the $CO_2$ reduction to methanol.

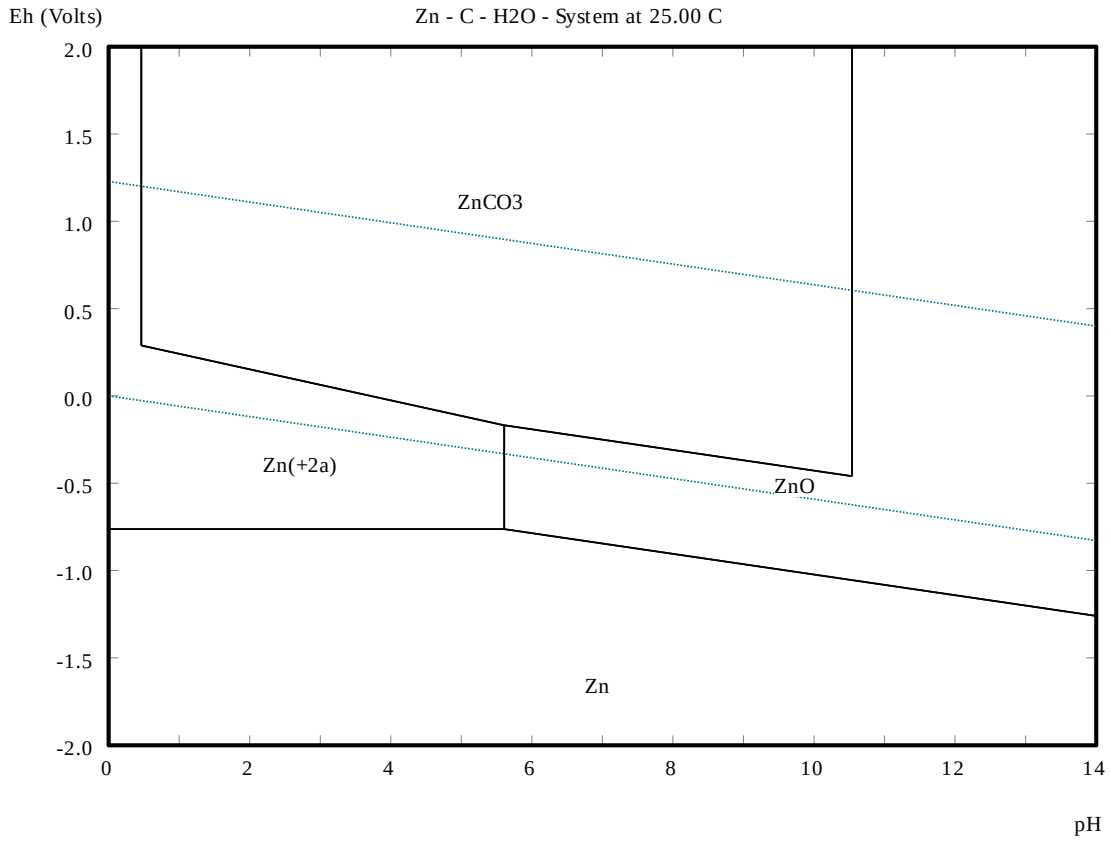


Figure 4.9. Pourbaix diagram for ZnO at 25˚C

Although Cu/ZnO and $Cu_xO$/ZnO electrodes have shown remarkable $CH_3OH$ yields, reproducibility remains a challenge. The equilibrium potential for ZnO as a function of pH is given in Figure 4.8. ZnO is easily reduced to Zn either in an acidic environment or in negative cathodic potential: $ZnO + 2e^- \rightleftharpoons Zn$ ($E_o$ = -0.76 V vs. SHE). With hydrogen overpotentials, ZnO is expected to be reduced at lower potential, which is consistent with our experimental results

that Cu/ZnO and $Cu_xO$/ZnO electrodes start losing activity at potential cathodic to -1.6 V (Ag/AgCl). Besides, $Zn^+$ concentration in the electrolyte solution is analyzed using an Inductively Coupled Plasma Mass Spectroscopy (ICP-MS). ZnO crystal is immersed in 0.5 M $KHCO_3$ solution for 20 hours and this solution is compared with the original solution. The test finds higher $Zn^+$ concentration in the ZnO-immersed electrolyte compared to the original solution (16.4 ± 2.7 ppm versus 12.7 ± 2.4 ppm) indicating $Zn^+$ can dissolve in an neutral-acidic solution environment.

Futhermore, it is important to consider the effect of local pH at the electrode surface on the $CO_2$ reduction. Athough $CO_2$ can serve as a buffer for the bicarbonate system, the generation of $OH^-$ species or consumption of $H^+$ on the electrode surface can lead to an increase in local electrolyte's pH by one order of magnitude near the electrode surface (Gupta et al., 2006). Since potential of $CO_2$ reduction occurs in proximity with water reduction, a change in local pH on the electrode surface can quickly drive the electrolyte more alkaline leading to hydrogen revolution as shown in the $CO_2$ Pourbaix diagram (Figure 1.1).

**4.5 Conclusions**

Electrochemical reduction of $CO_2$ at copper and copper oxide nanosclusters on ZnO electrodes (up to 87 μmol $cm^{-2}$ $hr^{-1}$) yields higher $CH_3OH$ rates than cuprous oxide thin films (up to 43 μmol $cm^{-2}$ $hr^{-1}$) from Chapter 3. Because yields are normalized to apparent (planar) 2D surface areas in each case, yields normalized to actual Cu(I) surface areas would be significantly higher. Oxidized Cu nanoclusters on ZnO show a 4-6 times improvement in $CH_3OH$ yield compared to metallic Cu on ZnO indicating the importance of an oxide surface in $CH_3OH$ formation. An in-situ FTIR reactor is designed to verify $CO_2$ reduction activity, as well as

evaluate possible intermediate and predict model from a theoretical perspective. Formyl or formaldehyde and methoxy adsorbates are detected after 5 minute reaction via IR spectra.

Experimental results show Cu/ZnO and $Cu_xO$/ZnO electrodes are reusable, and their surfaces are relatively more stable than cuprous oxide thin films during reaction. Benefiting from both metal and oxide properties, Cu/ZnO and $Cu_xO$/ZnO electrodes may inherit full functional aspects toward methanol selectivity such as the ability of breaking C–O bond of Cu followed by hydrogen addition and the ability of attracting OH group of ZnO. While the direct reduction of $CO_2$ to $CH_3OH$ at Cu/ZnO, $Cu_xO$/ZnO surfaces has shown very appealing results, the reproducibility puzzle needs to be solved. More experiments are required to overcome this critical problem, and hopefully with collaboration between experiment and simulation, a molecular pathway for direct $CO_2$ reduction to methanol at the atomic level can be developed.

# CHAPTER 5. MECHANISM PATHWAYS

## 5.1 Proposed Mechanism Pathways

As seen in the IR spectra (Figure 4.6), C=O and C–O stretching bands are observed on $Cu_xO$/ZnO (10-10) electrode's surface. While the presence of $H_3CO^-$ adsorbate is clearly confirmed by the C–O and $CH_3$ stretching bands, it is difficult to distinguish the $HCO^-$ and $H_2CO^-$ adsorbates since their C=O stretching bands are in the same regions. Since the formation of $HCO^-$ intermediate has been reported as rate determining step in $CO_2$ reduction to $CH_4$, and $H_2CO^-$ intermediate is detected in both hydrogenation and photoelectrocatalytic process for $CH_3OH$ formation (Slamet et al., 2009; Peterson et al., 2010; Yang et al., 2010), this C=O stretching is likely to represent both intermediates. Two possible mechanism pathways (A and B) for the direct electrochemical reduction of $CO_2$ to $CH_3OH$ are proposed in Figure 4.9. While mechanism A proceeds through CO pathway, mechanism B undergoes formate ($HCOO^-$) intermediate. The last four steps in both A and B mechanism pathways are the same with HCO adsorbate formation, $H_2CO$ adsorbate formation, $H_3CO$ adsorbate formation and hydrogenation of $H_3CO$ adsorbate to $CH_3OH$.

Similar to Peterson and Gattrell's mechanisms for $CO_2$ reduction at Cu surfaces, pathway A proceeds via CO intermediate (Gattrell et al., 2006; Peterson et al., 2010). The first electron and proton transfer may be associated with the formation of dioxymethylene ($HOCO^-$). When another electron and proton are added to the OH group of the $HOCO^-$ adsorbate, the C–$OH_2$ bond is broken to desorb a $H_2O$ molecule and leave CO adsorbate on the surface. The reaction is continued with the formation of HCO species by H addition to the C atom. Once the HCO species are formed, the carbon atom continues proton and electron transfer reactions to form $H_2CO$ and $H_3CO$ adsorbates. Although it is not clear whether these adsorbates would attach to

the Cu, Zn, or O bond, ZnO (10-10) surface would promote $CH_3OH$ formation by drawing OH adsorption and allowing the H atom to attach to the O atom of the $H_3CO$ species.

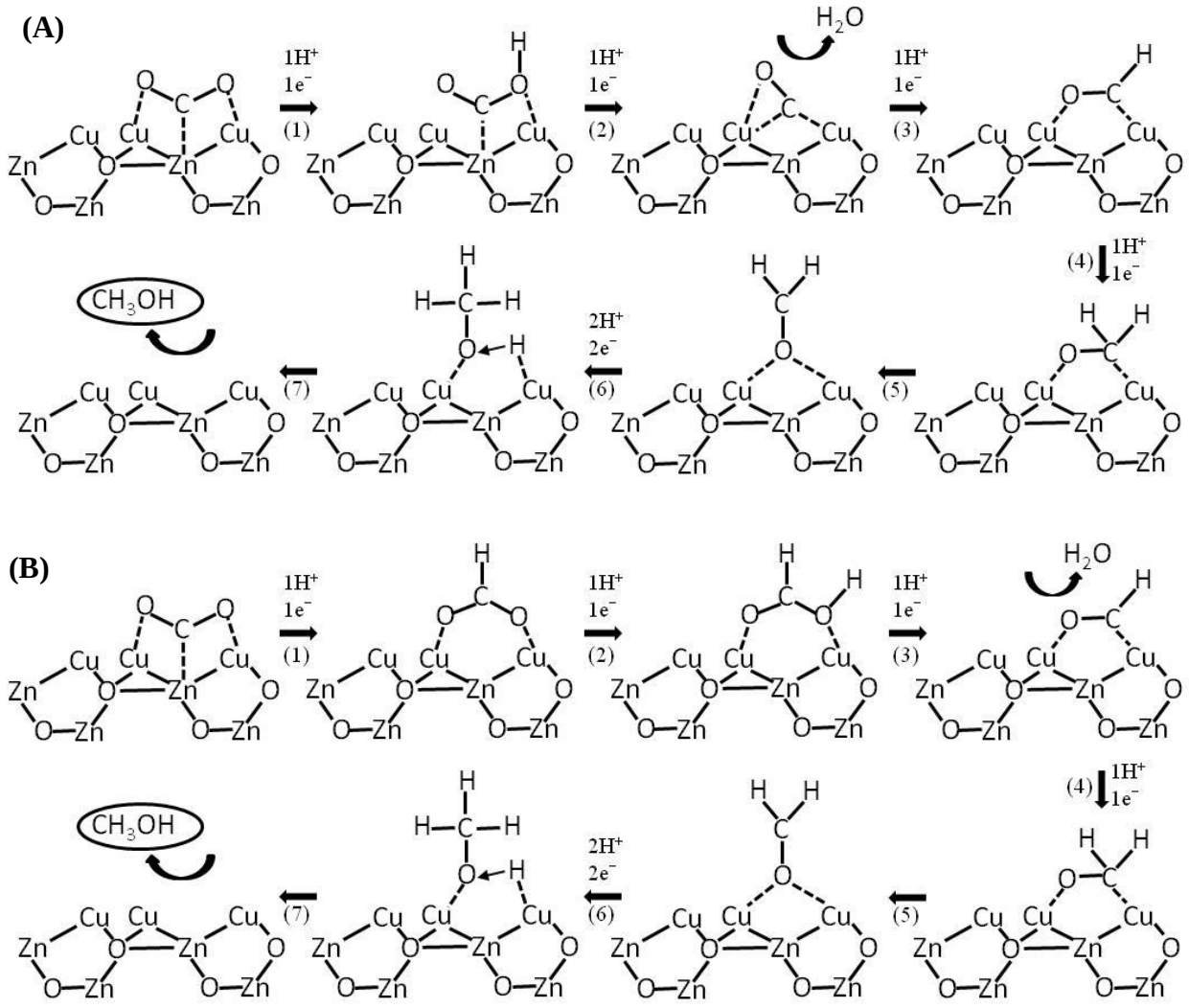


Figure 4.10. Proposed mechanism pathways for electrochemical reduction of $CO_2$ to $CH_3OH$

Since the C≡O band is not observed in the IR spectra (Figure 4.6), it is possible that the mechanism proceeds through formate ($HCOO^-$) intermediate as shown via pathway B. Numerous papers on $CO_2$ hydrogenation at Cu/ZnO catalyst have reported $HCOO^-$ as the main pathway to methanol synthesis (Bailey et al., 1995; Nakamura et al., 2003; Yang et al., 2010). The H attaches to the C atom instead of the O atom on $CO_2$ adsorbate; hence, $HCOO^-$ is formed rather than $HOCO^-$. This formate pathway may be verified by the presence of the CH stretching

band at 1380 $cm^{-1}$ from the IR spectra. Although this is in conflict with Peterson work as formate is reported to be the dead-end product (Peterson et al., 2010), it could explain the formation of $CH_3OH$ instead of $CH_4$ at copper oxide surfaces. The mechanism proceeds with H additions to the O atom of the formate (HCOO) species first to form HCO after a $H_2O$ molecule dissociates from the surface. Similar to mechanism A, once HCO species are formed, the reaction continues electron and proton transfer until $CH_3OH$ is desorbed from the surface. These two mechanism pathways are proposed based on our FTIR results and comparison with other scientists' work. Future Density Functional Theory work will help confirm these results.

**5.2 Summary/Conclusions**

This study successfully explores the relationship between surface chemistry and reaction behavior of several types of copper oxide in $CO_2$ electrochemical reduction to methanol. Direct reduction of $CO_2$ to $CH_3OH$ at electrodeposited cuprous oxide thin films is demonstrated at rates up to 43 μmol $cm^{-2}$ $hr^{-1}$ and Faradaic efficiencies up to 38%. These rates and efficiencies are remarkably higher than either air-oxidized or anodized Cu electrodes prepared in this study and suggests Cu(I) species may play a critical role in electrode activity and selectivity to $CH_3OH$. Surface analysis of the oxides before and after the reaction show mixed oxidation states ($Cu_2O$, $Cu_4O_3$, and CuO) depending on the method of preparation and $CH_3OH$ yields qualitatively follow Cu(I) concentrations. Experimental results also indicate $CH_3OH$ yields are dynamic, and copper oxides are reduced to metallic Cu in a simultaneous process at the potentials required for $CO_2$ reduction. In order to improve methanol activity and electrode surface's stability, we continue this study by examining the conversion of $CO_2$ to methanol at Cu/ZnO(10-10) and $Cu_xO$/ZnO(10-10) electrodes from a unified theoretical and experimental perspective. $CH_3OH$ rates observed at these copper based surfaces were up to 87 μmol $cm^{-2}$ $hr^{-1}$, and Faradaic

efficiencies greater than 100 % suggesting both electrochemical and chemical steps are involved in the mechanism. Focusing on simple molecules ($CO_2$, $H_2O$ and $CH_3OH$) and using single crystal metal oxide such as ZnO(10-10) gives the potential to unify simulation and experiment to guide the design of new highly efficient electrocatalysts.

In contrast with Cu electrodes, where $CH_4$ is the preferred reduction product, Cu(I) species may improve the stability of intermediates and alter selectivity towards $CH_3OH$ by enabling hydrogenation of oxygen atoms from $H_3CO$ adsorbates. While more experimental and computational work is needed, these results suggest Cu(I) species may play a critical role in selectivity towards $CH_3OH$ and their stability may be a key factor for maintaining catalytic activity in other (photoelectrochemical or hydrogenation) methanol generation reactions.

**5.3 Recommendations**

Experimental data at different conditions are necessary to correlate surface properties with yields and selectivity. A new designed reactor allowing high pressure reaction conditions could be built in order to increase $CO_2$ solubility in the electrolyte. High pressure would allow higher current density, and high $CO_2$ concentration would guarantee to provide abundant sources for methanol conversion. An electrochemical synthesis of methanol from $CO_2$ was succeeded by using Cu electrode in the high pressure ethanol – water system (Li et al., 1997). Li et al. reported current density for methanol formation up to 40% after 8 hours of electrolysis at 70 atm, and 80 ˚C.

In general, ZnO (10-10) surface is autocompensated and has the lowest energy plane. The (10-10) face is expected to provide an energetically favorable surface for Cu, $Cu_xO$ clusters growth to be used as electrocatalyst in $CO_2$ reduction to methanol. Although other ZnO faces ((0001), (1-210), (000-1)) are known to be less stable and more complicated surfaces, their

stability mechanism are strongly influenced by the Cu clusters' geometric and electronic structure. Therefore, it is worthwhile to consider these surfaces as potential supports for $CO_2$ electrocatalytic reduction.

Since ZnO surface can be reduced to Zn in neutral-acid solution, $TiO_2$ surface may be the answer for a more stable support because of its larger window for reduction potential and its well known effect as a support in photoelectrochemical reaction. Experiment on $CO_2$ adsorption behavior and vibrational frequencies such as UPS, EELS, or TDS technique can be used to evaluate the band gap energy, binding energy and adsorption energy. Recognizing how surface chemistry affects reaction behavior helps explore potential routes for improving selectivity and yield based on theoretical predictions. More experimental and computational work is needed to leverage a fundamental understanding of electrocatalytic mechanisms and create "electrocatalysts by design".

## REFERENCES


M. P. Andersson, P. Uvdal,A. D. MacKerell (2002). "Fundamental, binary combination, and overtone modes in methoxy adsorbed on Cu(100): Infrared spectroscopy and ab initio calculations." Journal of Physical Chemistry B **106**(20): 5200-5211.

T. S. Askgaard, J. K. Norskov, C. V. Ovesen,P. Stoltze (1995). "A kinetic model of methanol synthesis." Journal of Catalysis **156**(2): 229-242.

M. Azuma, K. Hashimoto, M. Hiramoto, M. Watanabe,T. Sakata (1990). "Electrochemical reduction of carbon dioxide on various metal electrodes in low temperature aqueous KHCO3 media." Journal of the Electrochemical Society **137**(6): 1772-1778.

S. Bailey, G. F. Froment, J. W. Snoeck,K. C. Waugh (1995). "A DRIFTS study of the morphology and surface adsorbate composition of an operating methanol synthesis catalyst." Catalysis Letters **30**(1-4): 99-111.

A. Bandi (1990). "Electrochemical reduction of carbon dioxide on conductive metallic oxides." Journal of the Electrochemical Society **137**(7): 2157-2160.

A. Bandi, J. Schwarz,C. U. Maier (1993). "ADSORPTION OF CO2 ON TRANSITION-METALS AND METAL-OXIDES." Journal of the Electrochemical Society **140**(4): 1006-1008.

G. Broden, T. N. Rhodin, C. Brucker, R. Benbow,Z. Hurych (1976). "Synchrotron radiation study of chemisorptive bonding of CO on transition - metals - polarization effect on IR(100)." Surface Science **59**(2): 593-611.

D. Canfield,K. W. Frese (1983). "Reduction of carbon dioxide to methanol on n-GaAs and p-GaAs and p-InP. Effect of crystal face, electrolyte and current density." Journal of the Electrochemical Society **130**(8): 1772-1773.

M. Casarin, C. Maccato,A. Vittadini (1999). "A theoretical investigation of the relaxation effects induced on the ZnO(10(1)over-bar0) surface by the chemisorption of H-2 and CO." Applied Surface Science **142**(1-4): 192-195.

T. Y. Chang, R. M. Liang, P. W. Wu, J. Y. Chen,Y. C. Hsieh (2009). "Electrochemical reduction of CO2 by Cu2O-catalyzed carbon clothes." Materials Letters **63**(12): 1001-1003.

G. C. Chinchen, M. S. Spencer, K. C. Waugh,D. A. Whan (1987). "Promotion of methanol synthesis and the water gas shift reactions by adsorbed oxygen on supported copper catalysts." Journal of the Chemical Society-Faraday Transactions I **83**: 2193-2212.

G. C. Chinchen, K. C. Waugh,D. A. Whan (1986). "The activity and state of the copper surface in methanol synthesis catalysts." Applied Catalysis **25**(1-2): 101-107.

Y. Choi, K. Futagami, T. Fujitani,J. Nakamura (2001). "The role of ZnO in Cu/ZnO methanol synthesis catalysts - morphology effect or active site model?" Applied Catalysis a-General **208**(1-2): 163-167.

G. M. Chow, L. K. Kurihara, D. Ma, C. R. Feng, P. E. Schoen,L. J. MartinezMiranda (1997). "Alternative approach to electroless Cu metallization of AlN by a nonaqueous polyol process." Applied Physics Letters **70**(17): 2315-2317.

A. Coehn,S. Jahn (1904). "Electrolytic Reduction of carbon dioxide." Berichte der Deutschen Chemischen Gesellschaft **37**.

J. J. Conti, L. E. Doman, K. A. Smith, L. D. Mayne, E. M. Yucel, J. L. Barden, A. M. Fawzi, P. D. Martin, V. V. Zaretskaya, M. L. Mellish, D. R. Kearney, B. T. Murphy, K. R. Vincent, P. M. Lindstrom, M. T. Leff, A. Geagla, J. Holte, B. Kapilow-Cohen, M. LaRiviere, C. L. Smith, J. Staub, G. Sweetnam,P. Wells (2010). International Energy Outlook 2010. DOE/EIA-0484(2010). Washington, DC, The U.S. Energy Information Administration (EIA), U.S. Department of Energy**:** 1-338.

R. L. Cook, R. C. Macduff,A. F. Sammells (1987). "Efficient high rate carbon dioxide reduction to methane and ethylene at in situ electrodeposited copper electrode." Journal of the Electrochemical Society **134**(9): 2375-2376.

D. F. Cox,K. H. Schulz (1990). "Methano decompostion on single crystal Cu2O." Journal of Vacuum Science & Technology a-Vacuum Surfaces and Films **8**(3): 2599-2604.

R. B. de Barros, A. R. Garcia,L. M. Ilharco (2003). "Reactivity of methanol on clean Ru(001) studied by RAIRS: effect of deuterium substitution." Surface Science **532**: 185-190.

J. F. Deng, Q. Sun, Y. L. Zhang, S. Y. Chen,D. Wu (1996). "A novel process for preparation of a Cu/ZnO/Al2O3 ultrafine catalyst for methanol synthesis from CO2+H-2: Comparison of various preparation methods." Applied Catalysis a-General **139**(1-2): 75-85.

U. Diebold, J. Lehman, T. Mahmoud, M. Kuhn, G. Leonardelli, W. Hebenstreit, M. Schmid,P. Varga (1998). "Intrinsic defects on a TiO2(110)(1x1) surface and their reaction with oxygen: a scanning tunneling microscopy study." Surface Science **411**(1-2): 137-153.

O. Dulub, L. A. Boatner,U. Diebold (2002). "STM study of Cu growth on the ZnO(1010) surface." Surface Science **504**(1-3): 271-281.

O. Dulub, L. A. Boatner,U. Diebold (2002). "STM study of the geometric and electronic structure of ZnO(0001)-Zn, (000(1)over-bar)-O, (10(1)over-bar0), and (11(2)over-bar0) surfaces." Surface Science **519**(3): 201-217.

M. Estrella, L. Barrio, G. Zhou, X. Q. Wang, Q. Wang, W. Wen, J. C. Hanson, A. I. Frenkel,J. A. Rodriguez (2009). "In Situ Characterization of CuFe2O4 and Cu/Fe3O4 Water-Gas Shift Catalysts." Journal of Physical Chemistry C **113**(32): 14411-14417.

F. Fischer,O. Prziza (1914). "Electrolytic Reduction of Carbon Oxides Dissolved Under Pressure." Berichte der Deutschen Chemischen Gesellschaft **47**.

I. A. Fisher,A. T. Bell (1997). "In-situ infrared study of methanol synthesis from H-2/CO2 over Cu/SiO2 and Cu/ZrO2/SiO2." Journal of Catalysis **172**(1): 222-237.

K. W. Frese (1991). "Electrochemical reduction of CO2 at intentionally oxidized copper electrodes." Journal of the Electrochemical Society **138**(11): 3338-3344.

K. W. Frese,S. Leach (1985). "Electrochemical reduction of carbon dioxide to methane, methanol, and CO on Ru electrodes." Journal of the Electrochemical Society **132**(1): 259-260.

A. Fujishima, K. Kohayakawa,K. Honda (1975). "Hydrogen production under sunlight with an electrochemical photocell." Journal of the Electrochemical Society **122**(11): 1487-1489.

T. Fujitani,J. Nakamura (2000). "The chemical modification seen in the Cu/ZnO methanol synthesis catalysts." Applied Catalysis a-General **191**(1-2): 111-129.

M. Gattrell, N. Gupta,A. Co (2006). "A review of the aqueous electrochemical reduction of CO2 to hydrocarbons at copper." Journal of Electroanalytical Chemistry **594**(1): 1-19.

T. D. Golden, M. G. Shumsky, Y. C. Zhou, R. A. VanderWerf, R. A. VanLeeuwen,J. A. Switzer (1996). "Electrochemical deposition of copper(I) oxide films." Chemistry of Materials **8**(10): 2499-2504.

N. Gupta, M. Gattrell,B. MacDougall (2006). "Calculation for the cathode surface concentrations in the electrochemical reduction of CO2 in KHCO3 solutions." Journal of Applied Electrochemistry **36**(2): 161-172.

M. Halmann (1978). "Photoelectrochemical reduction of aqueous carbon dioxide on p-type gallium phosphide in liquid junction solar cells." Nature **275**(5676): 115-116.

K. R. Harikumar,C. N. R. Rao (1998). "Interaction of CO with Cu/ZnO catalyst surfaces prepared in situ in the electron spectrometer: evidence for CO2- and related species relevant to methanol synthesis." Applied Surface Science **125**(2): 245-249.

J. C. Hemminger, R. Carr,G. A. Somorjai (1978). "Photoassised reaction of gaseous water and carbon dioxide adsorbed on SrTiO2 (111) crystal face to form methane." Chemical Physics Letters **57**(1): 100-104.

R. G. Herman, K. Klier, G. W. Simmons, B. P. Finn, J. B. Bulko,T. P. Kobylinski (1979). "Catalytic synthesis of methanol from CO-H2. 1. Phase composition, electronic properties, and activities of the Cu/ZnO/M2O3 catalysts." Journal of Catalysis **56**(3): 407-429.

K. Hirano, K. Inoue,T. Yatsu (1992). "Photocatalyzed reduction of CO2 in aqueous TiO2 suspension mixed with copper powder." Journal of Photochemistry and Photobiology a-Chemistry **64**(2): 255-258.

Y. Hori (2008). Electrochemical CO2 reduction on Metal Electrodes. Springer, New York.

Y. Hori, K. Kikuchi, A. Murata,S. Suzuki (1986). "PRODUCTION OF METHANE AND ETHYLENE IN ELECTROCHEMICAL REDUCTION OF CARBON-DIOXIDE AT COPPER ELECTRODE IN AQUEOUS HYDROGENCARBONATE SOLUTION." Chemistry Letters(6): 897-898.

Y. Hori, K. Kikuchi,S. Suzuki (1985). "Production of CO and CH4 in electrochemical reduction of CO2 at metal electrodes in aqueous hydrogencarbonate solution." Chemistry Letters(11): 1695-1698.

Y. Hori, H. Konishi, T. Futamura, A. Murata, O. Koga, H. Sakurai,K. Oguma (2005). ""Deactivation of copper electrode" in electrochemical reduction of CO2." Electrochimica Acta **50**(27): 5354-5369.

Y. Hori, A. Murata,R. Takahashi (1989). "Formation of hydrocarbons in the electrochemical reduction of carbon dioxide at a copper electrode in aqueous solution." Journal of the Chemical Society-Faraday Transactions I **85**: 2309-2326.

Y. Hori, A. Murata,Y. Yoshinami (1991). "Adsorption of CO, intermediately formed in electrochemical reduction of CO2 at copper electrode." Journal of the Chemical Society-Faraday Transactions **87**(1): 125-128.

Y. Hori,S. Suzuki (1982). "Electrolytic reduction of carbon dioxde at mercury electrode in aqueous solution." Bulletin of the Chemical Society of Japan **55**(3): 660-665.

Y. Hori, H. Wakebe, T. Tsukamoto,O. Koga (1995). "Adsorption of CO accompanied with simutaneous charge transfer on copper single crystal electrodes related with electrochemical reduction of CO2 to hydrocarbons." Surface Science **335**(1-3): 258-263.

J. S. Huberty,R. J. Madix (1996). "An FTIR study of the bonding of methoxy on Ni(100): Effects of coadsorbed sulfur, carbon monoxide and hydrogen." Surface Science **360**(1-3): 144-156.

T. Inoue, A. Fujishima, S. Konishi,K. Honda (1979). "Photelectrocatalytic reduction of carbon dioxide in aqueous suspensions of semiconductor powders." Nature **277**(5698): 637-638.

M. Jayamurthy,S. Vasudevan (1996). "Methanol-to-gasoline (MTG) conversion over ZSM-5. A temperature programmed surface reaction study." Catalysis Letters **36**(1-2): 111-114.

O. S. Joo, K. D. Jung, I. Moon, A. Y. Rozovskii, G. I. Lin, S. H. Han,S. J. Uhm (1999). "Carbon dioxide hydrogenation to form methanol via a reverse - water - gas - shift reaction (the

CAMERE process)." Industrial & Engineering Chemistry Research **38**(5): 1808-1812.

K. Kabra, R. Chaudhary,R. L. Sawhney (2004). "Treatment of hazardous organic and inorganic compounds through aqueous-phase photocatalysis: A review." Industrial & Engineering Chemistry Research **43**(24): 7683-7696.

S. Kaneco, N. Hiei, Y. Xing, H. Katsumata, H. Ohnishi, T. Suzuki,K. Ohta (2003). "High-efficiency electrochemical CO2-to-methane reduction method using aqueous KHCO3 media at less than 273 K." Journal of Solid State Electrochemistry **7**(3): 152-156.

S. Kaneco, K. Iiba, N. Hiei, K. Ohta, T. Mizuno,T. Suzuki (1999). "Electrochemical reduction of carbon dioxide to ethylene with high Faradaic efficiency at a Cu electrode in CsOH/methanol." Electrochimica Acta **44**(26): 4701-4706.

S. Kaneco, K. Iiba, K. Ohta,T. Mizuno (1999). "Electrochemical CO2 reduction on a copper wire electrode in tetraethylammonium perchlorate plus methanol at extremely low temperature." Energy Sources **21**(7): 643-648.

S. Kaneco, H. Katsumata, T. Suzuki,K. Ohta (2006). "Electrochemical reduction of carbon dioxide to ethylene at a copper electrode in methanol using potassium hydroxide and rubidium hydroxide supporting electrolytes." Electrochimica Acta **51**(16): 3316-3321.

J. J. Kim, D. P. Summers,K. W. Frese (1988). "Reduction of CO2 and CO to methane on Cu foil electrodes." Journal of Electroanalytical Chemistry **245**(1-2): 223-244.

D. S. King,R. M. Nix (1996). "Thermal stability and reducibility of ZnO and Cu/ZnO catalysts." Journal of Catalysis **160**(1): 76-83.

K. Klier (1982). Advances in Catalysis. New York.

K. Klier, V. Chatikavanij, R. G. Herman,G. W. Simmons (1982). "Catalytic syntheis of methanol from CO/H2. IV. The effects of carbon dioxide." Journal of Catalysis **74**(2): 343-360.

M. Kurtz, J. Strunk, O. Hinrichsen, M. Muhler, K. Fink, B. Meyer,C. Woell (2005). "Active sites on oxide surfaces: ZnO-catalyzed synthesis of methanol from CO and H-2." Angewandte Chemie-International Edition **44**(18): 2790-2794.

J. S. Lee, K. H. Lee, S. Y. Lee,Y. G. Kim (1993). "A comparative study of methanol synthesis from CO2/H2 and CO/H2 over a Cu/ZnO/Al2O3 catalyst." Journal of Catalysis **144**(2): 414-424.

S. Lee, M. Gogate,C. J. Kulik (1995). "Methanol - to - gasoline vs. DME - to - gasoline. II. Process comparison and analysis." Fuel Science & Technology International **13**(8): 1039-1057.

J. W. Li,G. Prentice (1997). "Electrochemical synthesis of methanol from CO2 in high-pressure

electrolyte." Journal of the Electrochemical Society **144**(12): 4284-4288.

X. M. Liu, G. Q. Lu, Z. F. Yan,J. Beltramini (2003). "Recent advances in catalysts for methanol synthesis via hydrogenation of CO and CO2." Industrial & Engineering Chemistry Research **42**(25): 6518-6530.

T. Mahalingam, J. S. P. Chitra, S. Rajendran,P. J. Sebastian (2002). "Potentiostatic deposition and characterization of Cu2O thin films." Semiconductor Science and Technology **17**(6): 565-569.

G. J. Millar, C. H. Rochester,K. C. Waugh (1995). "AN FTIR STUDY OF THE ADSORPTION OF FORMIC-ACID AND FORMALDEHYDE ON POTASSIUM-PROMOTED CU/SIO2 CATALYSTS." Journal of Catalysis **155**(1): 52-58.

J. Nakamura, Y. Choi,T. Fujitani (2003). "On the issue of the active site and the role of ZnO in Cu/ZnO methanol synthesis catalysts." Topics in Catalysis **22**(3-4): 277-285.

H. Nakatsuji,Z. M. Hu (2000). "Mechanism of methanol synthesis on Cu(100) and Zn/Cu(100) surfaces: Comparative dipped adcluster model study." International Journal of Quantum Chemistry **77**(1): 341-349.

K. Ogura, R. Oohara,Y. Kudo (2005). "Reduction of CO2 to ethylene at three-phase interface effects of electrode substrate and catalytic coating." Journal of the Electrochemical Society **152**(12): D213-D219.

K. Ogura, H. Yano,F. Shirai (2003). "Catalytic reduction of CO2 to ethylene by electrolysis at a three-phase interface." Journal of the Electrochemical Society **150**(9): D163-D168.

S. Ohya, S. Kaneco, H. Katsumata, T. Suzuki,K. Ohta (2009). "Electrochemical reduction of CO2 in methanol with aid of CuO and Cu2O." Catalysis Today **148**(3-4): 329-334.

G. A. Olah, A. Goeppert,G. K. S. Prakash (2006). Beyond Oil and Gas: The Methanol Economy. Weinhein, Wiley-VCH.

K. Ozawa, Y. Oba,K. Edamoto (2007). "Oxidation of copper clusters on ZnO (10(1)over-bar0): Effect of temperature and preadsorbed water." Surface Science **601**(14): 3125-3132.

W. Paik, T. N. Andersen,H. Eyring (1969). "Kinetic studies of electrolytic reduction of carbon dioxide on mercury electrode." Electrochimica Acta **14**(12): 1217-1232.

W. X. Pan, R. Cao, D. L. Roberts,G. L. Griffin (1988). "Methanol synthesis activity of Cu/ZnO catalysts." Journal of Catalysis **114**(2): 440-446.

A. A. Peterson, F. Abild-Pedersen, F. Studt, J. Rossmeisl,J. K. Norskov (2010). "How copper catalyzes the electroreduction of carbon dioxide into hydrocarbon fuels." Energy & Environmental Science **3**(9): 1311-1315.

J. P. Popic, M. L. AvramovIvic,N. B. Vukovic (1997). "Reduction of carbon dioxide on ruthenium oxide and modified ruthenium oxide electrodes in 0.5 M NaHCO3." Journal of Electroanalytical Chemistry **421**(1-2): 105-110.

J. P. Qu, X. G. Zhang, Y. G. Wang,C. X. Xie (2005). "Electrochemical reduction of CO2 on RuO2/TiO2 nanotubes composite modified Pt electrode." Electrochimica Acta **50**(16-17): 3576-3580.

P. B. Rasmussen, P. M. Holmblad, T. Askgaard, C. V. Ovesen, P. Stoltze, J. K. Norskov,I. Chorkendorff (1994). "Methanol synthesis on Cu(100) from a binary gas mixture of CO2 and H2." Catalysis Letters **26**(3-4): 373-381.

P. B. Rasmussen, M. Kazuta,I. Chorkendorff (1994). "Synthesis of methanol from a mixture of H2 and CO2 on Cu (100)." Surface Science **318**(3): 267-380.

P. G. Russell, N. Kovac, S. Srinivasan,M. Steinberg (1977). "Electrochemical reduction of carbon dioxide, formic acid, and formaldehyde." Journal of the Electrochemical Society **124**(9): 1329-1338.

M. Sahibzada, I. S. Metcalfe,D. Chadwick (1998). "Methanol synthesis from CO/CO2/H-2 over Cu/ZnO/Al2O3 at differential and finite conversions." Journal of Catalysis **174**(2): 111-118.

M. Saito,K. Murata (2004). "Development of high performance Cu/ZnO-based catalysts for methanol synthesis and the water-gas shift reaction." Catalysis Surveys from Asia **8**(4): 285-294.

T. Schedel-Niedrig, T. Neisius, N. Bottger, E. Kitzelmann, G. Weinberg, D. Demuth,R. Schlogl (2000). "Copper (sub)oxide formation: a surface sensitive characterization of model catalysts." Physical Chemistry Chemical Physics **2**(10): 2407-2417.

G. R. Sheffer,T. S. King (1989). "Potassium promotional effect of unsupported copper catalysts for methanol synthesis." Journal of Catalysis **115**(2): 376-387.

Slamet, H. W. Nasution, E. Purnama, K. Riyani,J. Gunlazuardi (2009). "Effect of Copper Species in a Photcatalytic Synthesis of Methanol from Carbon Dioxide over Copper-doped Titania Catalysts." World Applied Sciences Journal **6**(1).

N. Spataru, K. Tokuhiro, C. Terashima, T. N. Rao,A. Fujishima (2003). "Electrochemical reduction of carbon dioxide at ruthenium dioxide deposited on boron-doped diamond." Journal of Applied Electrochemistry **33**(12): 1205-1210.

D. P. Summers, S. Leach,K. W. Frese (1986). "The electrochemical reduction of aqueous carbon dioxide to methanol at molybdenum electrodes with low overpotentials." Journal of Electroanalytical Chemistry **205**(1-2): 219-232.

J. Szanyi,D. W. Goodman (1991). "Methanol synthesis on a Cu(100) catalyst." Catalysis Letters **10**(5-6): 383-390.

P. Tans (2009). Trends in Carbon Dioxide. NOAA/ESRL.

T. E. Teeter,P. Van Rysselberghe (1954). "Reduction of carbon dioxide on mercury cathodes." Journal of Chemical Physics **22**.

Y. Terunuma, A. Saitoh,Y. Momose (1997). "Relationship between hydrocarbon production in the electrochemical reduction of CO2 and the characteristics of the Cu electrode." Journal of Electroanalytical Chemistry **434**(1-2): 69-75.

I. H. Tseng, W. C. Chang,J. C. S. Wu (2002). "Photoreduction of CO2 using sol-gel derived titania and titania-supported copper catalysts." Applied Catalysis B-Environmental **37**(1): 37-48.

M. V. Twigg,M. S. Spencer (2001). "Deactivation of supported copper metal catalysts for hydrogenation reactions." Applied Catalysis a-General **212**(1-2): 161-174.

K. S. Udupa, G. S. Subramanian,H. V. K. Udupa (1971). "Electrolytic reduction of carbon dioxide to formic acid." Electrochimica Acta **16**(9): 1593-&.

A. Wander, F. Schedin, P. Steadman, A. Norris, R. McGrath, T. S. Turner, G. Thornton,N. M. Harrison (2001). "Stability of polar oxide surfaces." Physical Review Letters **86**(17): 3811-3814.

X. Q. Wang, J. C. Hanson, A. I. Frenkel, J. Y. Kim,J. A. Rodriguez (2004). "Time-resolved studies for the mechanism of reduction of copper oxides with carbon monoxide: Complex behavior of lattice oxygen and the formation of suboxides." Journal of Physical Chemistry B **108**(36): 13667-13673.

Y. Wang, B. Meyer, X. Yin, M. Kunat, D. Langenberg, F. Traeger, A. Birkner,C. Woll (2005). "Hydrogen induced metallicity on the ZnO(10(1)over-bar0) surface." Physical Review Letters **95**(26).

Y. Wang, M. Muhler,C. Woll (2006). "Spectroscopic evidence for the partial dissociation of H2O on ZnO(1010)." Physical Chemistry Chemical Physics **8**(13): 1521-1524.

K. C. Waugh (1992). "METHANOL SYNTHESIS." Catalysis Today **15**(1): 51-75.

S. M. Williams, K. R. Rodriguez, S. Teeters-Kennedy, A. D. Stafford, S. R. Bishop, U. K. Lincoln,J. V. Coe (2004). "Use of the extraordinary infrared transmission of metallic subwavelength arrays to study the catalyzed reaction of methanol to formaldehyde on copper oxide." Journal of Physical Chemistry B **108**(31): 11833-11837.

H. Wilmer, M. Kurtz, K. V. Klementiev, O. P. Tkachenko, W. Grunert, O. Hinrichsen, A. Birk-

-ner, S. Rabe, K. Merz, M. Driess, C. Woll,M. Muhler (2003). "Methanol synthesis over ZnO: A structure-sensitive reaction?" Physical Chemistry Chemical Physics **5**(20): 4736-4742.

J. C. S. Wu, H. M. Lin,C. L. Lai (2005). "Photo reduction of CO2 to methanol using optical-fiber photoreactor." Applied Catalysis a-General **296**(2): 194-200.

J. G. Wu, M. Saito, M. Takeuchi,T. Watanabe (2001). "The stability of Cu/ZnO-based catalysts in methanol synthesis from a CO2-rich feed and from a CO-rich feed." Applied Catalysis a-General **218**(1-2): 235-240.

Z. Yan, S. Chinta, A. A. Mohamed, J. P. Fackler,D. W. Goodman (2006). "CO oxidation over Au/TiO2 prepared from metal-organic gold complexes." Catalysis Letters **111**(1-2): 15-18.

H. Yang, J. L. Whitten, J. S. Huberty,R. J. Madix (1997). "Coadsorption of CO and CH3O on Ni(100)." Surface Science **375**(2-3): 268-280.

Y. X. Yang, J. Evans, J. A. Rodriguez, M. G. White,P. Liu (2010). "Fundamental studies of methanol synthesis from CO2 hydrogenation on Cu(111), Cu clusters, and Cu/ZnO(000(1)over-bar)." Physical Chemistry Chemical Physics **12**(33): 9909-9917.

H. Yano, T. Tanaka, M. Nakayama,K. Ogura (2004). "Selective electrochemical reduction of CO2 to ethylene at a three-phase interface on copper(I) halide-confined Cu-mesh electrodes in acidic solutions of potassium halides." Journal of Electroanalytical Chemistry **565**(2): 287-293.

R. Zenobi, J. Z. Xu, J. T. Yates, B. N. J. Persson,A. I. Volokitin (1993). "FTIR OVERTONE SPECTROSCOPY ON SURFACES - THE C-O MODE IN CHEMISORBED METHOXY ON NI(111)." Chemical Physics Letters **208**(5-6): 414-419.

## APPENDIX: APPROVED PERMISSION FOR REUSE OF PUBLISHED MATERIALS

**Anne Clementson**

**From:** Minh Le [mle5@tigers.lsu.edu]
**Sent:** Monday, April 25, 2011 11:19 AM
**To:** Copyright
**Subject:** Request for Permission to Reproduce or Re-Publish ECS Material

Dear,

My name is Minh T. H. Le, a graduate student from Louisiana State University. I am preparing a thesis entitled "Electrochemical Reduction of CO2 to Methanol" to be completed by August 2011.

I would like to request permission to reprint "M. Le, M. Ren, Z. Zhang, P. T. Sprunger, R. L. Kurtz, and J. C. Flake, "Electrochemical Reduction of $CO_2$ to $CH_3OH$ at Copper Oxide Surfaces", *Journal of The Electrochemical Society*, **158** (5), E45-E49 (2011)" in my thesis, and request nonexclusive rights for all the subsequent editions for distribution throughout the world. I am the first author in this paper.

My contact information is:
Name: Minh T. H. Le
Address: 12231 Mollylea Drive
Baton Rouge, LA 70815
Telephone: (225)288 0509
Email: mle5@tigers.lsu.edu

Thank you!

--
Minh T. H. Le
Graduate Assistant
Department of Chemical Engineering
Louisiana State University
Baton Rouge, LA 70803
U.S.A

Permission is granted to include the above-referenced paper in your thesis, provided that you obtain permission of the other individual authors. In the thesis, please acknowledge the authors and the citation given above, and include the words: "Reproduced by permission of ECS — The Electrochemical Society."

April 26, 2011
Date

Ann F. Goedkoop, Director of Publications

**Anne Clementson**

**From:** Minh Le [mle5@tigers.lsu.edu]
**Sent:** Thursday, March 24, 2011 2:19 PM
**To:** Copyright
**Subject:** Request for Permission to Reproduce or Re-Publish ECS Material

**Follow Up Flag:** Follow up
**Flag Status:** Flagged

Dear,

My name is Minh T. H. Le, a graduate student from Louisiana State University. I am preparing a thesis entitled "Electrochemical Reduction of CO2 to Methanol" to be completed by August 2011.

I would like to request permission to use the following material in my thesis, and request nonexclusive rights for all the subsequent editions for distribution throughout the world.

I wish to use table 2, table 3 and figure 8 in "Electrochemical reduction of carbon dioxide on various metal electrodes in low temperauter aqueous KHCO3 media". Below is the source publication:

M. Azuma, K. Hashimoto, M. Hiramoto, M. Watanabe,T. Sakata (1990). "Electrochemical reduction of carbon dioxide on various metal electrodes in low temperature aqueous KHCO3 media." Journal of the Electrochemical Society **137**(6): 1772-1778.

My contact information is:
Name: Minh T. H. Le
Address: 12231 Mollylea Drive
Baton Rouge, LA 70815
Telephone: (225)288 0509
Email: mle5@tigers.lsu.edu

Thank you!

--
Minh T. H. Le

Permission is granted to reproduce the above-referenced material. Please acknowledge the author(s) and publication title of the original material, and include the words: "Reproduced by permission of ECS — The Electrochemical Society."

March 30, 2011
Date

Ann F. Goedkoop, Director of Publications

**SPRINGER LICENSE**
**TERMS AND CONDITIONS**

Mar 24, 2011

This is a License Agreement between Minh T.H. Le ("You") and Springer ("Springer") provided by Copyright Clearance Center ("CCC"). The license consists of your order details, the terms and conditions provided by Springer, and the payment terms and conditions.

**All payments must be made in full to CCC. For payment instructions, please see information listed at the bottom of this form.**

| | |
|---|---|
| License Number | 2635561348864 |
| License date | Mar 24, 2011 |
| Licensed content publisher | Springer |
| Licensed content publication | Journal of Applied Electrochemistry |
| Licensed content title | Calculation for the cathode surface concentrations in the electrochemical reduction of $CO_2$ in $KHCO_3$ solutions |
| Licensed content author | N. Gupta |
| Licensed content date | Feb 1, 2006 |
| Volume number | 36 |
| Issue number | 2 |
| Type of Use | Thesis/Dissertation |
| Portion | Figures |
| Author of this Springer article | No |
| Order reference number | |
| Title of your thesis / dissertation | Electrochemical Reduction of CO2 to Methanol |
| Expected completion date | Aug 2011 |
| Estimated size(pages) | 80 |
| Total | 0.00 USD |
| Terms and Conditions | |

## AMERICAN CHEMICAL SOCIETY LICENSE TERMS AND CONDITIONS

Mar 24, 2011

This is a License Agreement between Minh T.H. Le ("You") and American Chemical Society ("American Chemical Society") provided by Copyright Clearance Center ("CCC"). The license consists of your order details, the terms and conditions provided by American Chemical Society, and the payment terms and conditions.

**All payments must be made in full to CCC. For payment instructions, please see information listed at the bottom of this form.**

| | |
|---|---|
| License Number | 2635470275728 |
| License Date | Mar 24, 2011 |
| Licensed content publisher | American Chemical Society |
| Licensed content publication | Industrial & Engineering Chemistry Research |
| Licensed content title | Treatment of Hazardous Organic and Inorganic Compounds through Aqueous-Phase Photocatalysis: A Review |
| Licensed content author | Kavita Kabra et al. |
| Licensed content date | Nov 1, 2004 |
| Volume number | 43 |
| Issue number | 24 |
| Type of Use | Thesis/Dissertation |
| Requestor type | Not specified |
| Format | Print |
| Portion | Table/Figure/Micrograph |
| Number of Table/Figure/Micrographs | 1 |
| Author of this ACS article | No |
| Order reference number | |
| Title of the thesis / dissertation | Electrochemical Reduction of CO2 to Methanol |
| Expected completion date | Aug 2011 |
| Estimated size(pages) | 80 |
| Billing Type | Invoice |
| Billing Address | 12231 Mollylea Drive<br>Baton Rouge, LA 70815<br>United States |
| Customer reference info | |
| Total | 0.00 USD |

**ELSEVIER LICENSE**
**TERMS AND CONDITIONS**

Mar 24, 2011

This is a License Agreement between Minh T.H. Le ("You") and Elsevier ("Elsevier") provided by Copyright Clearance Center ("CCC"). The license consists of your order details, the terms and conditions provided by Elsevier, and the payment terms and conditions.

**All payments must be made in full to CCC. For payment instructions, please see information listed at the bottom of this form.**

| | |
|---|---|
| Supplier | Elsevier Limited<br>The Boulevard,Langford Lane<br>Kidlington,Oxford,OX5 1GB,UK |
| Registered Company Number | 1982084 |
| Customer name | Minh T.H. Le |
| Customer address | 12231 Mollylea Drive<br>Baton Rouge, LA 70815 |
| License number | 2635460975030 |
| License date | Mar 24, 2011 |
| Licensed content publisher | Elsevier |
| Licensed content publication | Applied Catalysis A: General |
| Licensed content title | The role of ZnO in Cu/ZnO methanol synthesis catalysts — morphology effect or active site model? |
| Licensed content author | Y. Choi, K. Futagami, T. Fujitani, J. Nakamura |
| Licensed content date | 14 February 2001 |
| Licensed content volume number | 208 |
| Licensed content issue number | 1-2 |
| Number of pages | 5 |
| Start Page | 163 |
| End Page | 167 |
| Type of Use | reuse in a thesis/dissertation |
| Intended publisher of new work | other |
| Portion | figures/tables/illustrations |
| Number of figures/tables/illustrations | 1 |
| Format | print |
| Are you the author of this Elsevier article? | No |

**ELSEVIER LICENSE**
**TERMS AND CONDITIONS**

Mar 24, 2011

This is a License Agreement between Minh T.H. Le ("You") and Elsevier ("Elsevier") provided by Copyright Clearance Center ("CCC"). The license consists of your order details, the terms and conditions provided by Elsevier, and the payment terms and conditions.

**All payments must be made in full to CCC. For payment instructions, please see information listed at the bottom of this form.**

| | |
|---|---|
| Supplier | Elsevier Limited<br>The Boulevard,Langford Lane<br>Kidlington,Oxford,OX5 1GB,UK |
| Registered Company Number | 1982084 |
| Customer name | Minh T.H. Le |
| Customer address | 12231 Mollylea Drive<br>Baton Rouge, LA 70815 |
| License number | 2635461292766 |
| License date | Mar 24, 2011 |
| Licensed content publisher | Elsevier |
| Licensed content publication | Applied Catalysis B: Environmental |
| Licensed content title | Photoreduction of $CO_2$ using sol–gel derived titania and titania-supported copper catalysts |
| Licensed content author | I-Hsiang Tseng, Wan-Chen Chang, Jeffrey C. S. Wu |
| Licensed content date | 8 April 2002 |
| Licensed content volume number | 37 |
| Licensed content issue number | 1 |
| Number of pages | 12 |
| Start Page | 37 |
| End Page | 48 |
| Type of Use | reuse in a thesis/dissertation |
| Intended publisher of new work | other |
| Portion | figures/tables/illustrations |
| Number of figures/tables/illustrations | 2 |
| Format | print |
| Are you the author of this Elsevier article? | No |

# SPRINGER LICENSE
# TERMS AND CONDITIONS

Mar 24, 2011

This is a License Agreement between Minh T.H. Le ("You") and Springer ("Springer") provided by Copyright Clearance Center ("CCC"). The license consists of your order details, the terms and conditions provided by Springer, and the payment terms and conditions.

**All payments must be made in full to CCC. For payment instructions, please see information listed at the bottom of this form.**

| | |
|---|---|
| License Number | 2635460457053 |
| License date | Mar 24, 2011 |
| Licensed content publisher | Springer |
| Licensed content publication | Topics in Catalysis |
| Licensed content title | On the Issue of the Active Site and the Role of ZnO in Cu/ZnO Methanol Synthesis Catalysts |
| Licensed content author | J. Nakamura |
| Licensed content date | Apr 1, 2003 |
| Volume number | 22 |
| Issue number | 3 |
| Type of Use | Thesis/Dissertation |
| Portion | Figures |
| Author of this Springer article | No |
| Order reference number | |
| Title of your thesis / dissertation | Electrochemical Reduction of CO2 to Methanol |
| Expected completion date | Aug 2011 |
| Estimated size(pages) | 80 |
| **Total** | **0.00 USD** |
| Terms and Conditions | |

**ELSEVIER LICENSE**
**TERMS AND CONDITIONS**

Mar 24, 2011

This is a License Agreement between Minh T.H. Le ("You") and Elsevier ("Elsevier") provided by Copyright Clearance Center ("CCC"). The license consists of your order details, the terms and conditions provided by Elsevier, and the payment terms and conditions.

**All payments must be made in full to CCC. For payment instructions, please see information listed at the bottom of this form.**

| | |
|---|---|
| Supplier | Elsevier Limited<br>The Boulevard,Langford Lane<br>Kidlington,Oxford,OX5 1GB,UK |
| Registered Company Number | 1982084 |
| Customer name | Minh T.H. Le |
| Customer address | 12231 Mollylea Drive<br>Baton Rouge, LA 70815 |
| License number | 2635470045519 |
| License date | Mar 24, 2011 |
| Licensed content publisher | Elsevier |
| Licensed content publication | Applied Catalysis A: General |
| Licensed content title | Photo reduction of $CO_2$ to methanol using optical-fiber photoreactor |
| Licensed content author | Jeffrey C.S. Wu, Hung-Ming Lin, Chao-Ling Lai |
| Licensed content date | 12 December 2005 |
| Licensed content volume number | 296 |
| Licensed content issue number | 2 |
| Number of pages | 7 |
| Start Page | 194 |
| End Page | 200 |
| Type of Use | reuse in a thesis/dissertation |
| Intended publisher of new work | other |
| Portion | figures/tables/illustrations |
| Number of figures/tables/illustrations | 1 |
| Format | print |
| Are you the author of this Elsevier article? | No |

**ELSEVIER LICENSE**
**TERMS AND CONDITIONS**

May 23, 2011

This is a License Agreement between Minh T.H. Le ("You") and Elsevier ("Elsevier") provided by Copyright Clearance Center ("CCC"). The license consists of your order details, the terms and conditions provided by Elsevier, and the payment terms and conditions.

**All payments must be made in full to CCC. For payment instructions, please see information listed at the bottom of this form.**

| | |
|---|---|
| Supplier | Elsevier Limited<br>The Boulevard,Langford Lane<br>Kidlington,Oxford,OX5 1GB,UK |
| Registered Company Number | 1982084 |
| Customer name | Minh T.H. Le |
| Customer address | 12231 Mollylea Drive<br>Baton Rouge, LA 70815 |
| License number | 2674921239628 |
| License date | May 23, 2011 |
| Licensed content publisher | Elsevier |
| Licensed content publication | Surface Science |
| Licensed content title | STM study of the geometric and electronic structure of ZnO(0 0 0 1)-Zn, ()-O, (), and () surfaces |
| Licensed content author | Olga Dulub, Lynn A. Boatner, Ulrike Diebold |
| Licensed content date | 10 November 2002 |
| Licensed content volume number | 519 |
| Licensed content issue number | 3 |
| Number of pages | 17 |
| Start Page | 201 |
| End Page | 217 |
| Type of Use | reuse in a thesis/dissertation |
| Intended publisher of new work | other |
| Portion | figures/tables/illustrations |
| Number of figures/tables/illustrations | 1 |
| Format | both print and electronic |
| Are you the author of this Elsevier article? | No |

## VITA

Minh T. H. Le was born in December 1987, to Tuan H. Le and Trang T. T. To, in Ho Chi Minh City, Vietnam. She graduated from Clarke County High School in Grove Hill, Alabama, in May 2005 and enrolled at Louisiana State University in August 2005. She obtained her Bachelor of Science in Chemical Engineering degree in May 2009 from Louisiana State University. Upon graduation, she decided to pursue the Master of Science in Chemical Engineering degree at Louisiana State University. She has been working under Dr. John C. Flake and this thesis will complete her requirements to receive the degree of Master of Science in Chemical Engineering.